Physics of Particles and Nuclei, Vol. 36, No. 4, 2005, pp. 378–426. Translated from Fizika Elementarnykh Chastits i Atomnogo Yadra, Vol. 36, No. 4, 2005, pp. 712–800.

Dedicated to the memory of Petr Alekseevich Cherdantsev

Multidimensional Stochastic Approach to the Fission Dynamics of Excited Nuclei

G. D. Adeev*, A. V. Karpov, P. N. Nadtochii*, and D. V. Vanin****

** Omsk State University, pr. Mira 55, Omsk, 644077 Russia*
*** Joint Institute for Nuclear Research, Dubna, Moscow oblast, 141980 Russia*

Abstract—The purpose of this review is to discuss the results obtained over the last five years from calculations of the mass–energy, charge, and angular distributions of fragments formed during the fission of excited nuclei. The calculations are performed within the stochastic approach to fission dynamics, which is based on a multidimensional Langevin equation, and carried out for a wide range of fissility parameters and excitation energies of compound nuclei. A temperature-dependent finite-range liquid-drop model, taking into account a diffuse nuclear surface, is used in a consistent way to calculate the potential energy and level-density parameter. In order to describe the dissipation of collective motion, a modified one-body mechanism of nuclear viscosity including a reduction coefficient of the contribution made by the "wall" formula is used. The evaporation of light prescission particles is taken into account on the basis of a statistical model combined with Langevin dynamics. Calculations performed in multidimensional Langevin dynamics satisfactorily reproduce all the parameters of experimentally observed distributions of fission fragments and the prefission neutron multiplicity as a function of compound-nucleus parameters. In order to attain a simultaneous reproduction of the mass–energy distribution of fission fragments and the prefission neutron multiplicity, the reduction coefficient needs to be half or less of the total one-body viscosity. In this review, problems that need to be solved to facilitate further development of the multidimensional stochastic approach to fission dynamics are discussed.

CONTENTS

INTRODUCTION 379
1. MODEL 380
1.1. Shape Parametrization and Collective Coordinates 380
1.2. Equations of Motion 383
1.3. Initial and Final Conditions 383
1.4. Conservative Force: The Level-Density Parameter 386
1.5. Inertia and Friction Tensors 389
1.6. Statistical Model of Excited-Nucleus Decay 391
2. MASS–ENERGY DISTRIBUTION (MED) OF FISSION FRAGMENTS 393
2.1. Two-Dimensional MEDs of Fission Fragments 394
2.2. One-Dimensional Mass and Energy Distributions of Fragments 395
2.3. Mechanisms of Nuclear Viscosity and MEDs of Fission Fragments 397
2.4. Correlation Dependences of MED Parameters 399
3. NEUTRON MULTIPLICITIES AND FISSION TIMES 399
3.1. Introduction 399
3.2. Prescission Neutron Multiplicities and Fission Times 400
3.3. Dependence of Prescission Neutron Multiplicity on the Mass and Kinetic Energy of Fragments 400
3.4. Postscission and Total Neutron Multiplicities 403
3.5. Fission Probability 407
4. CHARGE DISTRIBUTION OF FISSION FRAGMENTS 408
4.1. Features of the Model Describing Charge Fluctuations 409
4.1.1. Potential energy 409
4.1.2. Inertial parameter of the charge mode 410
4.1.3. Friction parameter of the charge mode 410
4.2. Relaxation Times of the Charge Mode: The Statistical Limit at the Scission Point 411
4.3. Variance of the Charge Distribution 413
4.4. Determination of the Two-Body Viscosity Coefficient from Study of Charge Mode Fluctuations 414
5. ANGULAR DISTRIBUTION (AD) OF FISSION FRAGMENTS 415
5.1. Transition-State Model 417
5.1.1. The effect of prescission neutron evaporation on AD anisotropy 418
5.1.2. The effect of model dimension on AD 419
5.2. *K*-Mode Relaxation Time 420
CONCLUSIONS 421
REFERENCES 422

INTRODUCTION

Stochastic methods are widely used in the natural sciences (physics, chemistry, astronomy, and biology) and in technical applications of radiophysics and quantum optics [1]. Interest in random fluctuations, as well as their description via stochastic methods, has greatly increased in the last two decades, as is reflected by [2–4] and the references therein.

Since the mid-1980s, when deep inelastic transfer reactions were first discovered [5], stochastic methods have also been widely used in nuclear physics. It should be noted that the use of stochastic equations in nuclear physics began with Kramers' classical study [6]. Using an approach that he named the diffusion model, Kramers proposed describing nuclear fission with a small number of degrees of freedom, which would then interact with a thermostat formed by all the other single-particle degrees of freedom. Under these circumstances, the collective-variable dynamics becomes similar to Brownian-particle dynamics, since the collective subsystem energy varies only slightly during one act of interaction with a single-particle subsystem. The motion in such a physical model is adequately described by the Fokker–Planck equation (FPE), introduced for the distribution function of collective coordinates and their conjugate momenta, or by physically equivalent Langevin equations.

Using the analogy between nuclear-fission dynamics and Brownian-particle motion, Kramers calculated the diffusion rate of Brownian particles, which are initially located in a potential well, through a potential barrier separating the initial and final states of a system. With this approach, Kramers refined the Bohr and Wheeler equation [7] for fission width obtained one year earlier. The Kramers' refining factor takes into account the effect of nuclear viscosity on the fission rate (the fission width). It is interesting to note that, although much research has been devoted to the problem of calculating the barrier-reaction rate (see, for example, [8, 9]), this problem still remains unsolved. In the general case, the problem has a multidimensional nature and involves complex relief of the potential-energy surface and deformation dependence of transport coefficients in the FPE and Langevin equations. It is also concerned with calculating the induced-fission width, which can be considered, at the present time, as an open problem (for more details, see Section 1.6 of this review).

The FPE-based stochastic approach has been successfully applied to many problems related to collective nuclear dynamics: theories of deep inelastic transfers [10], induced fission [11–13], and description of prescission neutron multiplicity [14]. Nevertheless, in recent years, preference has been given to the Langevin equations, since an exact solution to the FPE is possible only for a limited number of low-dimensional model cases [11] and generally requires the use of various approximations. The Langevin equations, in contrast, can be solved on the basis of numerical methods and without additional simplifications for a multidimensional case. However, even using the Langevin equations involves serious difficulties at the current level of computer engineering. In order to describe a large number of experimentally observed fission characteristics, it is necessary to introduce a possibly very large number of collective coordinates. The introduction of each new coordinate considerably increases the volume of calculations. Therefore, it is natural that one-dimensional Langevin calculations are performed first and, only then, two-dimensional calculations. One-dimensional calculations make it possible to calculate the fission probability and multiplicities of evaporating prescission particles. Two-dimensional models provide the additional possibility of calculating either the fragment-mass distribution corresponding to the most probable kinetic energy of fragments or the energy distribution corresponding to a preset ratio between fragment masses.

The experimentally observed two-dimensional mass–energy distribution cannot be obtained in terms of either one-dimensional or two-dimensional Langevin calculations. In this case, it is necessary to have at least three collective coordinates. For a simultaneous description of the charge distribution, it is inevitably necessary to introduce a fourth collective coordinate so as to determine the charge distribution between fragments.

Results from the first estimative three-dimensional calculations of the parameters of the distribution of fission fragments over kinetic energy and the mean prescission neutron multiplicity [15] were published only in 1995. Since 2000–2001, the results of systematic four-dimensional [16] and three-dimensional [17–24] Langevin calculations have begun appear regularly in publications.

At the present time, the theoretical basis of the stochastic approach to collective nuclear dynamics based on the Langevin equations and the results of one-dimensional and two-dimensional calculations are adequately described in the published reviews of Abe *et al.* [25] and Fröbrich and Gontchar [26, 27], and in the book by Fröbrich and Lipperheide [28]. For this reason, we mostly omit the fundamentals of the stochastic approach in this review and focus our attention on clarification and discussion of the most important results obtained in last five years within the multidimensional stochastic approach. We place particular emphasis on the specific problems and difficulties resulting from the multidimensionality of the approach developed and used in the calculations.

The stochastic approach to the description of large-amplitude collective nuclear motion is dynamic. Therefore, the model intended for realization of this approach in calculations of experimentally observed values inevitably involves the following development stages [29]: the choice of parametrization for the nuclear shape and

collective coordinates, which are considered as classical generalized coordinates satisfying the Fokker–Planck stochastic equations of motion or the physically equivalent Langevin equations. Phenomenological equations of motion introduced in this way are completely specified by their transport coefficients: the conservative force and the inertia, friction, and diffusion tensors.

Integration of the equations of motion in the Langevin description determines the stochastic trajectory of a fissile system in the collective-coordinate space. It is necessary to consider the evaporation of light particles (neutrons, γ quanta, and light charged particles) along each Langevin trajectory. Thus, a statistical model of particle evaporation should be combined with dynamics, i.e., with integration of the equations of motion. Naturally, when considering the evolution of a fissile system, it is necessary, as in the case of any dynamic problem, to impose conditions that initiate and accomplish the system's evolution.

The construction of collective nuclear dynamics within a microscopic approach [30, 31] is, on a technical level, extremely difficult to achieve at the present time; therefore, in most studies, the transport coefficients of the Langevin equations are determined within macroscopic models and approaches, which are known to viable in relation to fission theory, especially for excited nuclei. The first attempts to extend this approach to the case of low-energy fission are now being made [21]. By extending the stochastic approach to this energy range, it becomes possible to explain the observed multimodality of fission at low excitation energies.

In Section 1, we describe the model on which all the fundamental results obtained within the three-dimensional Langevin calculations, performed mainly by our group, are based.

In Section 2, we present and analyze results from calculations of two-dimensional and one-dimensional mass–energy distributions of fission fragments as a function of the fissility parameter and the excitation energy of a compound nucleus.

In Section 3, we present and analyze results from calculations of the mean prescission neutron multiplicity and fission times. The dependences of prescission neutron multiplicity on the mass and the kinetic energy of fragments are also discussed.

In Sections 4 and 5, we present results on the charge and angular distributions of fission fragments obtained within the three-dimensional Langevin approach.

Finally, we present a summary of our main conclusions and discuss the prospects for future application of the multidimensional stochastic approach for describing the dynamics of nuclear fusion and fission reactions.

This work is a continuation of investigations into the characteristics of excited-nuclei fission in terms of the stochastic approach, whose stages were initially described in [13, 32].

1. MODEL

1.1. Shape Parametrization and Collective Coordinates

The study of fission reactions is conventionally limited by axially symmetric shapes. In this case, a nuclear shape can be described in cylindrical coordinates by the profile function $\rho_s(z)$, whose rotation around the symmetry axis decides the nuclear surface. The most frequently used parameterizations are the $\{c, h, \alpha\}$ [33], Trentalange [34], Cassini ovaloid [35–37], and two-center parametrizations [38, 39].

The use of a particular nuclear-shape parametrization is closely connected to the problem of choosing collective coordinates. All the possible collective coordinates can be conditionally divided into coordinates describing a nuclear shape and coordinates setting collective degrees of freedom not associated with nuclear-shape variation. For an adequate description of nuclear fission, it is necessary that the chosen parametrization involves at least three parameters and allows introduction of the following shape coordinates: nuclear elongation, a coordinate determining neck evolution in a nuclear shape, and a mirror-asymmetry coordinate. Such a minimal set of collective coordinates permits calculation of the two-dimensional mass–energy distributions (MEDs) of fission fragments. Among the collective coordinates not associated with nuclear shape, we mention, for example, the charge-asymmetry coordinate specifying the charge distribution between formed fragments.

A successful choice of collective coordinates provides for the convenience of the dynamic-calculation procedure and, frequently, the accuracy of the obtained results. In this context, we now discuss the introduction of collective shape coordinates using the well-known $\{c, h, \alpha\}$ parametrization [33]. In [33, 40], it was shown that, in terms of this parametrization, it is possible to accurately reproduce the characteristics of nuclear saddle configurations obtained on the basis of variational calculations [41, 42] in the sharp-edge liquid-drop model.

This parametrization has also been used for static calculations performed with the Strutinsky shell-correction method [33], dynamic calculations of MEDs in the diffusion model [13, 43], and for calculating a large number of different fission characteristics in the Langevin approach [18, 19, 44–48]. This parametrization sets a three-parameter family of shapes and is therefore reasonably convenient for performing three-dimensional Langevin calculations. The parameter c describes nuclear elongation (the nuclear length, in units of the initial-sphere radius R_0, is equal to $2c$), the parameter h defines neck-thickness variation for a given elongation, and the coordinate α sets the ratio between

the masses of future fragments. In the chosen shape parametrization, the nuclear-surface equation is written as

$$\rho_s^2(z) = \begin{cases} (c^2 - z^2)(A_s + Bz^2/c^2 + \alpha z/c), & \text{if } B \geq 0 \\ (c^2 - z^2)(A_s + \alpha z/c)\exp(Bcz^2), & \text{if } B < 0, \end{cases} \quad (1)$$

where ρ_s is the polar radius and z is the coordinate along the nuclear symmetry axis. The factor B is expressed by nuclear-shape parameters (c, h, α) [33]:

$$B = 2h + \frac{c-1}{2}. \quad (2)$$

The parameter A_s is determined from the condition of conservation of nuclear volume and, for continuous nuclear shapes, has the form

$$A_s = \begin{cases} c^{-3} - \dfrac{B}{5}, & \text{if } B \geq 0 \\ -\dfrac{4}{3}\dfrac{B}{\exp(Bc^3) + \left(1 + \dfrac{1}{2Bc^3}\right)\sqrt{-\pi Bc^3}\,\mathrm{erf}(\sqrt{-Bc^3})}, & \\ \text{if } B < 0. & \end{cases} \quad (3)$$

Nuclear shapes in the $\{c, h, \alpha\}$ parametrization are enclosed within $z_{\min} = -c$ and $z_{\max} = c$. If the function $\rho_s^2(z)$ vanishes within these limits only at $z = \pm c$, we have continuous nuclear shapes. If there are two more roots at the interval $[z_{\min}, z_{\max}]$, such shapes are interpreted as being discontinuous. Other cases (with an odd number of roots within $[z_{\min}, z_{\max}]$) cannot be considered as nuclear shapes and are frequently referred to as forbidden or "nonphysical" shapes (for a more detailed discussion of such shapes, see [49]).

We now introduce the neck concept. The coordinate z for which the function $\rho_s^2(z)$ reaches a minimum is defined as the neck coordinate z_N. The neck coordinate is determined from the condition

$$\frac{\partial \rho_s^2}{\partial z} = 0, \quad (4)$$

which results in an algebraic equation. If there are three real roots lying within $[z_{\min}, z_{\max}]$), one of them (a minimum) is the neck coordinate z_N and other two (maxima) are coordinates of the thickest cross sections of a compound-nuclear shape. These maxima determine the coordinates of formed fragments.

When choosing the collective shape coordinates, the following conditions should be taken into account:

(i) Collective coordinates are functions of the nuclear-shape parameters. Therefore, the simpler the form of these functions, the more convenient it is to use various coordinates. By simplicity, we also refer to the possibility of finding analytical inverse functions for the dependence of the shape parameters on the collective coordinates.

(ii) The mesh for dynamic calculations should involve the largest possible variety of nuclear shapes that can be given by the chosen parametrization and no forbidden shapes. In addition, if nuclear fission is studied from the fusion instant to the neck rupture, it is desirable to exclude unconsidered discontinuous nuclear shapes.

(iii) The choice of collective coordinates is closely related to boundary conditions at the mesh edges. In the available publications, only one boundary condition, specifically, the rupture condition, has been discussed. However, if there is an unsuccessful choice of collective coordinates or of their variation limits at the mesh, a Brownian particle can hit the boundaries, which is equivalent to introducing physically unjustified infinite forces restricting nuclear evolution. In order to prevent such an event, the mesh boundaries should be "inaccessible," either due to high values of potential energy (in comparison with the total nuclear excitation energy) or due to the behavior of inertial and friction coefficients.

Usually, collective coordinates are chosen by two methods:

(1) Physical values describing nuclear shape, for example, the spacing R between the mass centers of fragments (elongation coordinate), neck thickness r_N, and ratio of the difference between the masses of formed fragments and the total nuclear mass η_A (the mass-asymmetry coordinate)

$$\eta_A = \frac{A_R - A_L}{A_R + A_L} = \frac{3}{4R_0^3}\left(\int_{z_N}^{z_{\max}} \rho_s^2(z)dz - \int_{z_{\min}}^{z_N} \rho_s^2(z)dz\right), \quad (5)$$

where A_R and A_L are the mass numbers of the formed fragments (here and below, the subscripts R and L designate right-hand and left-hand fragments, respectively).

In addition to the fact that the coordinates (R, r_N, η_A) have a clear physical meaning, there is a further advantage to be gained in their use: All the allowed values of the coordinates η_A introduced by Strutinsky lie in the interval –1 to 1 (in [50], the definition of the coordinate η_A differs from that given in Eq. (5) by a factor of two), and the minimal value of the coordinate $r_N = 0$. This makes such a choice of collective coordinates successful from the standpoint of the second and third conditions outlined above.

We tested the above choice of collective coordinates using well-known Lawrence forms [51]. The profile function was taken to be

$$\rho_s^2(z) = az^4 + bz^3 + cz^2 + dz + e, \quad (6)$$

where we considered not only symmetric nucleus configurations ($b = 0$ and $d = 0$) but also asymmetric ones. Thus, we have five unknown coefficients (a, b, c, d, and e) in Eq. (6).

The neck concept, connecting two future fragments, has a physical meaning only under severe nuclear-shape deformation [37]. Therefore, it is also necessary to extend this concept to weakly deformed shapes so as to be able to define the collective coordinates R and η_A for every nuclear configuration, including those that have no pronounced bridge. In this case, the neck also has a coordinate defined by Eq. (4) and located at a point where the function $\rho_s^2(z)$ has only an extremum (a maximum) at the interval $[z_{\min}, z_{\max}]$. Thus, the neck is always at $(\partial\rho_s^2/\partial z)_{z=z_N} = 0$.

Then, assuming that the reference point coincides with the neck coordinate z_N, we find that the coefficient d is equal to zero $[(\partial\rho_s^2/\partial z)_{z=z_N=0} = 0 \Rightarrow d = 0]$. Thus, there remain only four unknown coefficients (a, b, c, and e) in Eq. (6). The coefficient e unambiguously defines the neck thickness for $z = z_N = 0$. As was mentioned above, we can choose it in the form of an independent parameter determining nuclear shape (we denote this coordinate as r_N^2; i.e., $e = r_N^2$). In addition, by imposing a constant-volume condition (in an approximation of nuclear-matter incompressibility) and using two free parameters (elongation and asymmetry), we can determine the coefficients a, b, and c. For this purpose, we use Eq. (5) and the following equations:

$$V = \frac{4}{3}\pi R_0^3, \quad R = \frac{\int_{z_N}^{z_{\max}} z\rho_s^2(z)dz}{\int_{z_N}^{z_{\max}} \rho_s^2(z)dz} - \frac{\int_{z_{\min}}^{z_N} z\rho_s^2(z)dz}{\int_{z_{\min}}^{z_N} \rho_s^2(z)dz}. \quad (7)$$

Because the neck position coincides with the origin of the coordinates ($z_N = 0$), many calculations using Eqs. (5) and (7) can be performed analytically. Naturally, nonlinear equations require the use of numerical methods to find the coefficients a, b, and c. In this study, we used the iteration method.

By applying the definition of the coordinate R and the condition of conservation of nucleus volume, it is possible to show how the maximal values of the coordinates r_N and R are related: $r_N^2 = R_0^3/R$. In this context, the most convenient coordinates from a technical point of view (the possibility of constructing a rectangular mesh) seem to be $(R, \eta_A, g = r_N^2 R)$. Thus, the limits on variation of the collective coordinates are $R \in [0, \infty]$, $\eta_A \in [-1, 1]$, and $g \in [0, 1]$.

We can ascribe the use of multipole nuclear-density moments [52] to the same method of choosing collective parameters. It should be noted that (R, η_A) are the first two collective coordinates for large R in this scheme for introducing the coordinates.

(2) Collective coordinates are nuclear-shape parameters. These particular collective coordinates are convenient from the standpoint of satisfying the first condition mentioned above and frequently extremely inconvenient according to the second and third conditions. Below, we explain this tendency and propose our own method of introducing the collective coordinates using the $\{c, h, \alpha\}$ parametrization.

First of all, we discuss the problem of forbidden shapes. It should be noted that forbidden shapes exist only for $\alpha \neq 0$. In addition, for each c and h, it is possible to find $\alpha_{\max}$ such that nuclear shapes lie only in the region of $|\alpha| \leq \alpha_{\max}$ and forbidden shapes lie in the remaining region.

We note that the ultimate values of the parameter η_A (± 1) are attained when the mass of one of the fragments is equal to zero. This condition can be written as

$$\left(\frac{\partial\rho_s^2(z)}{\partial z}\right)_{z=z_{\min}(z_{\max})} = 0. \quad (8)$$

Condition (8) means that the minimum (the neck) is at one of the extreme points ($z_{\min}$ or $z_{\max}$) of a nuclear shape. Using Eq. (8) and taking into account that the function $\rho_s^2(z)$ vanishes at the extreme points, we obtain, for the $\{c, h, \alpha\}$ parametrization,

$$\alpha_{\max} = \begin{cases} (A_s + B), & B \geq 0 \\ A_s, & B < 0. \end{cases} \quad (9)$$

It can clearly be seen that $\alpha_{\max}$ essentially depends on c and h. It is precisely this dependency that creates the problem of constructing a mesh with the use of the shape parameter α as the mass-asymmetry coordinate.

The new parameter α', which was introduced in [18, 49], is related to α by the scale transformation

$$\alpha' = \alpha c^3. \quad (10)$$

In part, this introduction solved the problem under consideration: for $|\alpha'| \leq 1$, there are no forbidden shapes. In addition, the dependence of $\alpha'_{\max} = \alpha_{\max} c^3$ on c and h is much weaker than the similar dependence of $\alpha_{\max}$. However, not all the possible asymmetries are given by a fall in the parametrization in the region $|\alpha'| \leq 1$. In particular, it becomes impossible to consider fission dynamics from the entrance reaction channel when there is a large difference between the masses of the target nucleus and an impinging ion.

We propose a new method of introducing the mass-asymmetry coordinate:

$$q_3 = \frac{\alpha}{\alpha_{\max}} = \begin{cases} \alpha/(A_s + B), & B \geq 0 \\ \alpha/A_s, & B < 0. \end{cases} \quad (11)$$

For such a choice, the problem of forbidden shapes is completely solved: all the possible asymmetric

nuclear shapes (for given c and h) are enclosed within $|q_3| \le 1$.

It is convenient to choose the collective parameter responsible for formation of the neck in a nuclear shape so that the condition of zero neck thickness is satisfied for the same (or nearly the same) value of this parameter. In the case of $\alpha = 0$, zero neck thickness is attained for

$$h = h_{sc} = \frac{5}{2c^3} + \frac{1-c}{4}. \quad (12)$$

From Eq. (12), it follows that the value h_{sc} essentially varies depending on c. We introduce the collective neck coordinate in the following form:

$$q_2 = \frac{h + 3/2}{h_{sc} + 3/2}. \quad (13)$$

The coordinate q_2 has the following properties: if $q_2 = 0$, $h = -3/2$ (which guarantees reasonably high values of potential energy for eliminating a Brownian particle hit in this area); if $q_2 = 1$, the neck thickness is equal to zero for symmetric shapes. For asymmetric nuclear shapes, the neck thickness vanishes for somewhat smaller, but close to unity, values of q_2.

Thus, in our opinion, the collective coordinates $\mathbf{q} = (q_1 = c, q_2, q_3)$ are optimal when using the $\{c, h, \alpha\}$ parametrization. We use these coordinates with the following variation ranges: $q_1 \in [0.5, 4.5]$, $q_2 \in [0, 1]$, and $q_3 \in [-1, 1]$. When studying the charge mode, it is convenient to additionally introduce a charge-asymmetry coordinate in the form of $q_4 = \eta_Z = (Z_R - Z_L)/(Z_R + Z_L)$, where Z_R and Z_L are the charges of the formed right-hand and left-hand fragments.

1.2. Equations of Motion

In the stochastic approach [6, 25, 53], the evolution of collective degrees of freedom of a fissile nucleus is considered by analogy with the motion of a Brownian particle placed in a thermostat formed by all the other nuclear degrees of freedom. In calculations, a set of Langevin equations is usually used. For the case of N collective coordinates, this set, in the difference form, is written as

$$p_i^{(n+1)} = p_i^{(n)} - \left(\frac{1}{2}p_j^{(n)}p_k^{(n)}\left(\frac{\partial \mu_{jk}(\mathbf{q})}{\partial q_i}\right)^{(n)} - K_i^{(n)}(\mathbf{q}) - \gamma_{ij}^{(n)}(\mathbf{q})\mu_{jk}^{(n)}(\mathbf{q})p_k^{(n)}\right)\tau + \theta_{ij}^{(n)}\xi_j^{(n)}\sqrt{\tau}, \quad (14)$$

$$q_i^{(n+1)} = q_i^{(n)} + \frac{1}{2}\mu_{ij}^{(n)}(\mathbf{q})(p_j^{(n)} + p_j^{(n+1)})\tau.$$

Here, q_i is the set of collective coordinates, p_i are the momenta conjugate to q_i, m_{ij} ($\|\mu_{ij}\| = \|m_{ij}\|^{-1}$) is the inertia tensor, γ_{ij} is the friction tensor, K_i is the conservative force, $\theta_{ij}\xi_j$ is the random force, θ_{ij} is the random-force amplitude, and ξ_j is a random variable with the following statistical properties:

$$\langle \xi_i^{(n)} \rangle = 0,$$
$$\langle \xi_i^{(n_1)}\xi_j^{(n_2)} \rangle = 2\delta_{ij}\delta_{n_1 n_2}. \quad (15)$$

The superscript n in Eqs. (14) and (15) indicates that the corresponding value is calculated at the instant of time $t_n = n\tau$, where τ is the time step in the integration of the Langevin equations. The angular brackets in Eq. (15) denote averaging over the statistical ensemble. In Eqs. (14) and (15), the repeating indices assume summation from 1 to N. The stochastic Langevin trajectory characterized by the shapes that a nucleus acquires during fission is obtained by numerically solving set of Eqs. (14) in the collective-coordinate space.

Random-force amplitudes are related to the diffusion tensor D_{ij} in the following way:

$$D_{ij} = \theta_{ik}\theta_{kj}. \quad (16)$$

In turn, the diffusion tensor satisfies the Einstein relation

$$D_{ij} = T\gamma_{ij}. \quad (17)$$

From these equations, we found the random-force amplitudes.

The thermostat temperature T used in calculations can be determined within the Fermi-gas model:

$$T = (E_{int}/a(\mathbf{q}))^{1/2}. \quad (18)$$

Here, E_{int} is the excitation energy of the internal degrees of freedom of a compound nucleus (the internal energy) and $a(\mathbf{q})$ is the level-density parameter, whose explicit form is discussed in Section 1.4.

When a nucleus moves to the rupture surface along an entire stochastic Langevin trajectory in the collective-coordinate space, it is necessary to verify that the law of conservation of energy is satified:

$$E^* = E_{int} + E_{coll}(\mathbf{q}, \mathbf{p}) + V(\mathbf{q}) + E_{evap}(t). \quad (19)$$

Here, E^* is the total excitation energy of a compound nucleus determined from the impinging-ion energy and the difference between the masses of colliding nuclei and the compound system in the entrance reaction channel, $E_{coll}(\mathbf{q}, \mathbf{p}) = \frac{1}{2}\mu_{ij}(\mathbf{q})p_i p_j$ is the kinetic energy of collective motion of a nucleus, and $E_{evap}(t)$ is the nuclear excitation energy carried away by particles that evaporate at the instant of time t.

1.3. Initial and Final Conditions

In the most general case, the initial collective coordinates $\mathbf{q}_0$, momenta $\mathbf{p}_0$, and total compound-nucleus

momentum I can be sampled by the Neumann method using the generating function

$$P(\mathbf{q}_0, \mathbf{p}_0, I, t = 0) \sim P(\mathbf{q}_0, \mathbf{p}_0)\sigma_{\text{fus}}(I). \quad (20)$$

The function $\sigma_{\text{fus}}(I)$ describes the initial momentum distribution of compound nuclei and is frequently approximated by the expression

$$\sigma_{\text{fus}}(I) = \frac{2\pi}{k^2}(2I + 1)T(I), \quad (21)$$

where $k^2 = 2\mu E_{\text{l.s}}/\hbar^2$, μ is the reduced mass of the impinging-ion–target system, and $T(I)$ is the penetrability coefficient, which is defined within a model reproducing experimental fusion cross sections. When performing Langevin calculations, the difference between the total nuclear spin $I = |\mathbf{l} + \mathbf{s}_t + \mathbf{s}_p|$ ($\mathbf{s}_p$ and $\mathbf{s}_t$ are the impinging-ion and target-nucleus eigenmomenta, respectively) and the angular momentum $\mathbf{l}$ is usually disregarded. In this case, Eq. (22) describes the initial angular-momentum distribution of nuclei.

In our calculations, the following form of the function $T(I)$ was used:

$$T(I) = \frac{1}{1 + \exp[(I - I_c)/\delta I]}. \quad (22)$$

The parameters I_c and δI were determined using the method described in [26], where expressions approximating the results of dynamic calculations [54] were given according to the surface-friction model [55] for two-ion fusion.

The problem of initial spin distribution has been widely discussed in the literature (frequently in the context of studying the angular distributions of fission fragments); however, it remains an open problem in modern nuclear physics. The majority of distributions contain two or more varied parameters. It is difficult to determine these parameters because direct experimental data can only be derived from the fusion cross section, and only one parameter can be fixed in this way. The other parameters must be determined from certain theoretical model representations. The angular distribution (AD) of fragments is affected by the second moment of the spin $\langle I^2 \rangle$ distribution of nuclei. It is obvious that various theoretical approximations can give values of $\langle I^2 \rangle$ that differ dramatically from each other, whereas they all correctly reproduce the fusion cross section. The only suitable approximation for one-parameter partial fusion cross sections is the triangular distribution (the varied parameter is the maximal momentum at which fusion takes place). However, the triangular distribution can be considered only as a zero approximation of a real situation.

When studying the fission of excited compound nuclei, the initial values of the collective coordinates are frequently chosen for use as the compound-nucleus ground (spherical) state. In this case, the initial momentum distribution is chosen as the equilibrium value. Then,

$$P(\mathbf{q}_0, \mathbf{p}_0) \sim \exp\left\{-\frac{V(\mathbf{q}_0, l) + E_{\text{coll}}(\mathbf{q}_0, \mathbf{p}_0)}{T}\right\}\delta(\mathbf{q}_0 - \mathbf{q}_{\text{gs}}), \quad (23)$$

where $\mathbf{q}_{\text{gs}}$ are the coordinates of the nuclear ground state.

The choice of initial conditions in the form of Eqs. (20)–(23) means that we begin the Langevin calculations with a completely statistically equilibrium state of a compound nucleus for a fixed initial excitation energy. It should be noted that such a choice of initial conditions can be considered only as an approximation to a real and more complicated situation. Fusion–fission reactions can be divided into two stages: a fast pre-equilibrium stage and a slower stage of decay of a residual statistically equilibrium compound nucleus. Their thermalization phase can be described in the intranuclear-cascade model [56]. After the thermalization stage is accomplished, compound nuclei are formed as a result of fluctuations in the cascade. All their characteristics have a wide distribution: the number of protons and neutrons, excitation energy, and linear or angular momenta. The intranuclear-cascade model is the only model in which it is possible to take into account these fluctuations and to determine the total distribution of the parameters describing a compound nucleus. Consideration of the pre-equilibrium reaction stage is necessary for comparison of the calculated fission characteristics at high excitation energies $E^* > 150$–200 MeV. At energies $E^* < 100$ MeV, the concept of a statistically equilibrium nucleus is a quite satisfactory approximation of the initial conditions for simulating fission dynamics.

The most natural choice of initial conditions can be obtained from consideration of the dynamics in the entrance reaction channel. Initial conditions chosen in the spherical momentum–equilibrium nuclear state are unsuitable for describing the quasifission process and deep inelastic transfer reactions. It should be emphasized that the conventional concept of a compound nucleus becomes a rough idealization of the real and complicated situation that exists for large angular momenta.

Now, we discuss the final conditions under which the simulation of compound-nucleus evolution is accomplished in our calculations. There are two such conditions: the formation of an evaporation residue and nuclear fission into fragments.

Evaporation residue is detected when, as a result of light-particle and γ-quanta emission, the nuclear excitation energy is reduced to the values $E_{\text{int}} + E_{\text{coll}}(\mathbf{q}, \mathbf{p}) < \min(B_f, B_n)$, where B_f and B_n are the fission barrier and the neutron binding energy, respectively.

When performing calculations in the multidimensional Langevin dynamics, the choice of rupture surface in the collective-coordinate space is important, as, by its intersection, it is possible to ascertain that a compound nucleus has disintegrated into fragments. The rupture surface is the locus of discontinuous nuclear configurations. In the case of N collective coordinates, the rupture surface is an $N-1$-dimensional hypersurface.

The choice of the rupture condition dramatically affects important fission characteristics such as the mean values and variances of the energy distributions of fission fragments. The cause of this sensitivity of the energy-distribution parameters is obvious: the kinetic energy of fragments predominantly depends on the energy of their interaction at the instant of scission.

At present, there is no known unambiguous approach to the choice of rupture criterion. However, it is possible to note several of the most frequently used criteria:

(i) Equality of the neck thickness to zero. At first, this rupture criterion seems a natural choice. However, it has an essential disadvantage and, therefore, can be considered only as a zero approximation of the problem. In fact, if the neck radius is comparable with the nucleon size, the description of a nucleus within the liquid-drop model becomes meaningless. Usually, the fission of a nucleus into fragments is assumed to occur with a rather thick neck [33, 41, 57].

(ii) From a physical standpoint, a rupture criterion in which a nucleus is disintegrated due to the loss of stability with respect to the neck-thickness variation [13, 33] seems to be more attractive. Mathematically, this condition can be written as

$$\left(\frac{\partial^2 V}{\partial q_2^2}\right)_{q_1, q_3} = 0. \tag{24}$$

If this condition is averaged over the ensemble of Langevin trajectories, it corresponds to nuclear shapes with a neck radius of $0.3R_0$ [33, 41, 44].

(iii) Another physically acceptable rupture criterion is based on the assumption that a nucleus becomes unstable relative to the neck scission at the instant when the forces of Coulomb repulsion and nuclear attraction between the formed fragments are balanced. In [58], it was shown that, in the actinide region, this condition corresponds to shapes that also have a neck radius approximately equal to $0.3R_0$.

(iv) The most flexible condition is the stochastic nuclear-rupture condition. For example, in [59], nuclear fission into fragments was considered as a fluctuation that could occur for arbitrary nuclear shapes with a neck. The rupture probability was determined from the relation $P_{\text{rup}} \sim \exp(-\Delta E/T)$, where ΔE is the change in the system energy under a deformed-nucleus rupture into two fragments. In [60], it was shown that, if this criterion is used, a rupture under deformations corresponding to nuclear shapes with $r_N \simeq 0.24R_0$ is highly probable.

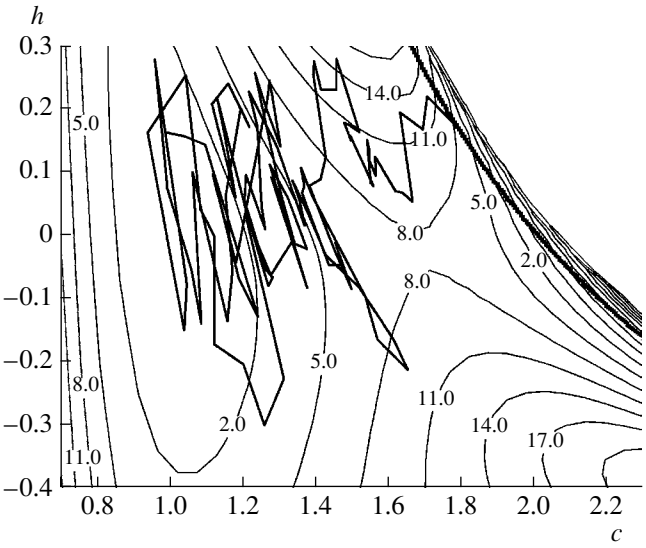

Fig. 1. Example of a stochastic Langevin trajectory in the collective coordinates (c, h) ($\alpha = 0$) shown against the potential-energy background. The numbers at the isolines specify values of the potential energy in MeV. The solid thick line corresponds to scission. The trajectory given in this figure represents a fission event.

In view of the above consideration, we consider that the fission of a nucleus into fragments occurs for a neck radius equal to $0.3R_0$, since this condition is in good agreement with the last three rupture criteria. The equation for the rupture surface can be written as

$$\rho_s(z_N) = r_N, \tag{25}$$

where r_N is the neck radius corresponding to prescission shapes. The case $\rho_s(z_N) = 0$ corresponds to the rupture condition under which a zero neck radius is attained.

Examples of Langevin trajectories are shown in Figs. 1 and 2. As can be seen from these figures, a spherical nuclear shape is chosen as the initial deformation, and numerical integration of the Langevin equations stops when a nucleus reaches the scission configuration. The observed quantities were calculated by simulating the ensemble of Langevin trajectories, with subsequent statistical averaging over this ensemble.

We now introduce the concept of a mean trajectory. The mean dynamic trajectory is that obtained in dynamic Langevin calculations by averaging over an ensemble of stochastic trajectories. In this case, the Langevin equations coincide with generalized Hamiltonian equations [61] because the term responsible for fluctuations (the random force) disappears after such averaging. In order to calculate the mean trajectory, the initial values of the mass-asymmetry coordinate q_3 and momentum p_3 are set equal to zero. It is obvious that the mean trajectory lies in the plane $q_3 = 0$. In Fig. 3, we show the potential energy in the coordinates q_1 and q_2 for the case of $q_3 = 0$. The dashed line in this figure rep-

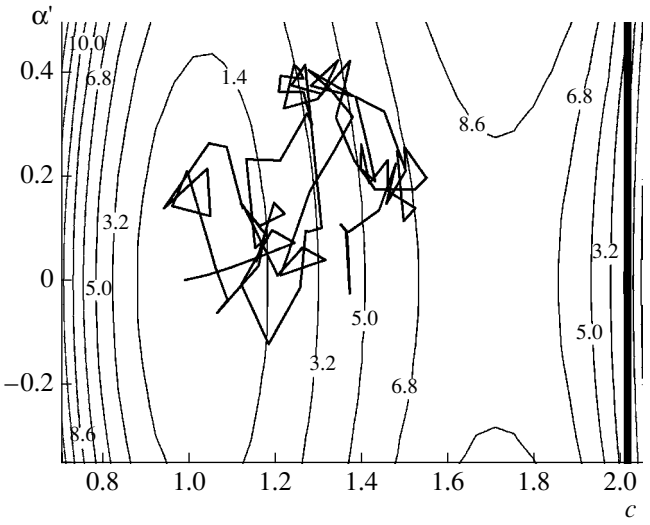

Fig. 2. The same as in Fig. 1 but in the collective coordinates (c, α') at $h = 0$. The trajectory shown in this figure represents evaporation residue.

resents the mean trajectory calculated under the assumption of a one-body mechanism of nuclear viscosity with $k_s = 0.25$ (see Section 1.5), and the crosses mark the saddle point and nuclear ground state. In addition, this figure shows examples of nuclear shapes in the $\{c, h, \alpha\}$ parametrization. The calculations are performed using the ^{224}Th nucleus as an example. One more important concept is the mean scission point, i.e., the point of intersection between the mean dynamic trajectory and the rupture surface. The mean scission point determines the mean values of the observed quantities (for example, the mean kinetic energy or average charge of fission fragments). The spread in scission configurations with respect to the mean scission point determines the variances of the observed quantities (for example, the width of the energy or charge distributions of fragments).

1.4. Conservative Force: The Level-Density Parameter

Heated rotating compound nuclei formed in reactions with heavy ions represent a thermodynamic system. As is known, the conservative force operating in such a system should be determined by part of its thermodynamic potential (for example, the free energy [62] or entropy [26]).

The expression for conservative force $K(\mathbf{q})$ can be written as [26, 29]

$$K_i = -\left(\frac{\partial F}{\partial q_i}\right)_T = T\left(\frac{\partial S}{\partial q_i}\right)_E. \quad (26)$$

It should be noted that both the given definitions of conservative force are equivalent. The choice of a certain thermodynamic potential depends on its convenience with respect to the calculations, since they are related in the following way:

$$F(\mathbf{q}, T) = E^*(\mathbf{q}, T) - TS. \quad (27)$$

In the Fermi-gas model, the entropy and level-density parameter can be calculated from the known free energy

$$S(\mathbf{q}, T) = -\left(\frac{\partial F(\mathbf{q}, T)}{\partial T}\right)_V, \quad a(\mathbf{q}, T) = \frac{S(\mathbf{q}, T)}{2T}. \quad (28)$$

Moreover, within the Fermi-gas model, the following relation is valid:

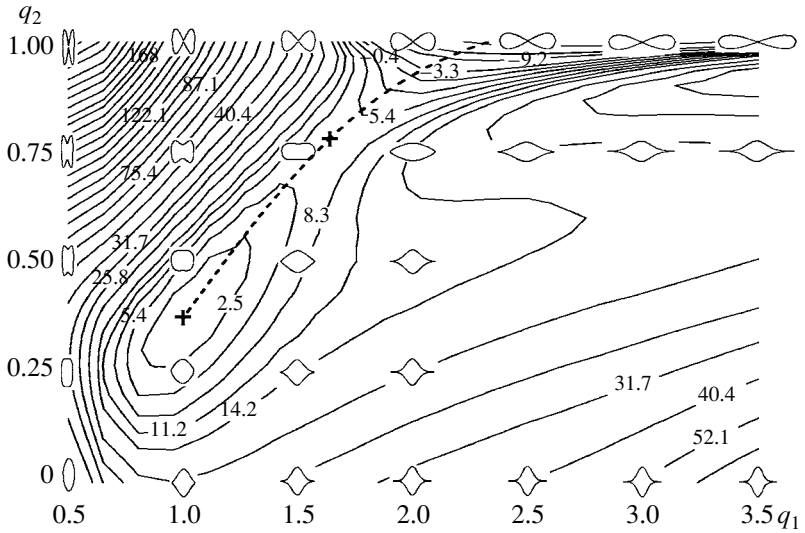

Fig. 3. Potential-energy map in the coordinates q_1 and q_2 for the ^{224}Th nucleus ($q_3 = 0$) and the corresponding set of nuclear shapes. The crosses denote the ground state and the saddle point. The dashed line is the mean trajectory calculated under the assumption of the one-body mechanism of viscosity with $k_s = 0.25$. The numbers at the isolines correspond to the potential energy in MeV.

Table 1. Coefficients of Eq. (32)

	r_0	a	a_d	a_v	k_v	a_s	k_s
$a_i(0)$	1.16	0.68	0.7	16.0	1.911	21.13	2.3
$10^3 x_i$ (MeV^{-2})	–0.736	–7.37	–7.37	–3.22	5.61	4.81	–14.79

Note: The first row represents values at zero temperature and the second row gives the thermal coefficients x_i.

$$E_{\text{int}}(\mathbf{q}, T) = E^*(\mathbf{q}, T) - E^*(\mathbf{q}, T = 0) = a(\mathbf{q})T^2, \quad (29)$$

where $E_{\text{int}}(\mathbf{q}, T)$ and $E^*(\mathbf{q}, T)$ are the internal and total excitation energy of the system, respectively, and $a(\mathbf{q})$ is the level-density parameter. The following temperature dependence of the free energy follows from Eqs. (28) and (29):

$$F(\mathbf{q}, T) = V(\mathbf{q}) - a(\mathbf{q})T^2, \quad (30)$$

where $V(\mathbf{q})$ is the nuclear potential energy at the temperature $T = 0$ $\{V(\mathbf{q}) = F(\mathbf{q}, T = 0)\}$, and $a(\mathbf{q})$ is the level-density parameter of an excited nucleus.

From the first part of Eq. (26), it can be seen that the conservative force in the Fermi-gas model is

$$K_i = -\frac{\partial V(\mathbf{q})}{\partial q_i} + \frac{\partial a(\mathbf{q})}{\partial q_i}T^2. \quad (31)$$

We use this expression for calculating the conservative force involved in the Langevin equations.

The current preference is to calculate the nuclear potential energy in the liquid-drop model (LDM), taking into account the finite range of nuclear forces and diffuse nuclear surface [63, 64] with the aid of Sierk parameters [64]. In this model, it is assumed that nuclear forces have a finite range of action. For nucleon–nucleon interaction, the Yukava-plus-exponential double-folding potential is selected [63]. Its use, as opposed to the simple Yukava potential, in calculations of the potential energy improves description of experimental data [64] on the fission barriers and yields a more realistic surface energy for strongly deformed nuclei [63]. Moreover, for two fragments of nuclear matter, the interaction potential reaches its lowest value when the fragments are in mutual contact, which follows from the property of saturation of nuclear forces.

In [62], a free-energy formula based on the finite-range LDM was proposed. The nuclear free energy as a function of the mass number $A = N + Z$, neutron excess (isotopic number) $I = (N - Z)/A$, and collective coordinates $\mathbf{q}$ describing nuclear shape has the form [62]

$$\begin{aligned} &F(A, Z, \mathbf{q}, T, L) \\ &= -a_v(1 - k_v I^2)A + a_s(1 - k_s I^2)B_n(\mathbf{q})A^{2/3} + c_0 A^0 \\ &+ a_c\frac{Z^2}{A^{1/3}}B_c(\mathbf{q}) - a_c\frac{5}{4}\left(\frac{3}{2\pi}\right)^{2/3}\frac{Z^{4/3}}{A^{1/3}} + \frac{\hbar^2 L(L+1)}{2J_\perp(\mathbf{q})}, \end{aligned} \quad (32)$$

where a_v, a_s, and a_c are the parameters of volume, surface, and Coulomb energies, respectively, in the LDM when the diffuse edge is at zero temperature, and k_v and k_s are the corresponding volume and surface parameters of the symmetry energy.

The deformation dependence enters Eq. (32) via the functionals $B_n(\mathbf{q})$ and $B_c(\mathbf{q})$ of nuclear and Coulomb energies [64], respectively, and the moment of inertia $J_\perp(\mathbf{q})$ of a nucleus with respect to an axis perpendicular to the symmetry axis and passing through the nuclear center of mass. The latter term in Eq. (32) represents the rotational nuclear energy subject to the nuclear-density diffusivity [61].

The temperature dependence for the seven coefficients (a_v, a_s, k_v, k_s, r_0, a, and a_d) involved in Eq. (32) is parametrized in the form [62]

$$a_i(T) = a_i(T = 0)(1 - x_i T^2), \quad (33)$$

which can be considered as adequate for $T \le 4$ MeV [65]. Information on the temperature coefficients x_i was obtained in self-consistent microscopic calculations in terms of an extended form of the Thomas–Fermi method and the application of an SkM* interaction, which served as the effective interaction between nucleons [65, 66]. In [62], the results of these calculations for the Gibbs thermodynamic potential were used to derive Eq. (32). The values of the fourteen coefficients obtained in [62] are given in Table 1.

The microscopic calculations [65] performed in terms of the extended temperature-dependent Thomas–Fermi method showed that Eq. (30) for the free energy F is a reasonably exact approximation for $T \le 4$ MeV.

The level-density parameter $a(\mathbf{q})$ is an excited-nucleus characteristic when considered in terms of the Fermi-gas model. In [62, 67], the level-density parameter was calculated from Eqs. (28) and (32) within the finite-range LDM and taking into account the nuclear excitation. In [67], it was shown that, when the nuclear level-density parameter $a(\mathbf{q})$ is calculated in this approach, it depends only slightly on temperature. The same result was obtained in [62] for spherical nuclei. This fact means that it is possible to use the level-density parameter in the finite-range temperature-independent LDM.

At the same time, the deformation dependence of the level-density parameter is frequently represented by a leptodermic expansion [68–71] in the form

$$a(\mathbf{q}) = a_1 A + a_2 A^{2/3} B_s(\mathbf{q}). \quad (34)$$

Table 2. Values of the coefficients a_1 and a_2 obtained in [67, 71, 69]

	a_1 (MeV^{-1})	a_2 (MeV^{-1})
[67]	0.0598	0.1218
[69]	0.073	0.095
[71]	0.0685	0.274

Here, A is the mass number of a fissile nucleus, and the dimensionless factor $B_s(\mathbf{q})$ determines the surface area of a deformed nucleus in units of the equivalent spherical surface, i.e., the surface-energy functional in the sharp-edge LDM [72]. When parametrizing Eq. (34), the two sets of coefficients (a_1 and a_2) proposed by Ignatyuk *et al.* [69] and recommended by Töke and Swiatecki [71] are most frequently used.

In [67], the deformation dependence of the level-density parameter in the finite-range LDM was approximated by Eq. (34). The approximation was carried out for 70 nuclei along the beta-stability line [73], with the mass number Z ranging from 47 to 116. The results of the approximation are given in Table 2. In [67], it was shown that the accuracy of the performed approximation is reasonably high within the entire considered range of nuclei.

The coefficient a_2 determines the way in which the level-density parameter depends on deformation and, therefore, is of importance for statistical and dynamic models of nuclear fission. The value of this coefficient obtained in [67] is close to the Ignatyuk coefficient $a_2 = 0.095$ MeV^{-1} and over two times less than the value predicted by Töke and Swiatecki ($a_2 = 0.274$ MeV^{-1}). The second coefficient a_1 is approximately identical in all the sets under consideration. As a result, if we use the Ignatyuk coefficients for the level-density parameter, the results of the dynamic Langevin calculations virtually coincide with those obtained in the finite-range LDM but noticeably differ from the results obtained with the Töke and Swiatecki coefficients.

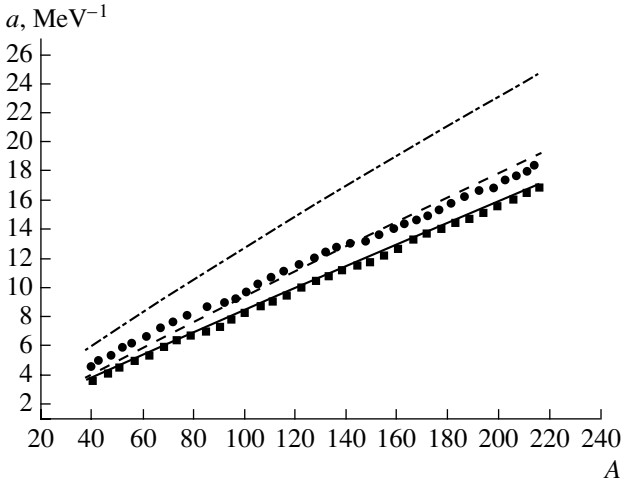

Fig. 4. Level-density parameter as a function of the mass number along the beta-stability line for the nuclear ground state. The solid curve is the level-density parameter in the finite-range LDM, the dashed line is the level-density parameter with the Ignatyuk coefficients [69], and the dashed and dotted line is the level-density parameter with the Töke and Swiatecki coefficients [71]. The squares show the dependence of the level-density parameter determined within the extended Tomas–Fermi method involving the Skyrme effective interaction SkM* [66], the circles indicate the results of consistent calculations in relativistic mean-field theory [75]. The figure is taken from [67].

In [74, 75], the level-density parameter was approximated by an expression similar to Eq. (34). The isotopic dependence of the level-density parameter and the Coulomb interaction were also taken into account:

$$a(\mathbf{q}) = a_{\rm vol}(1 + k_{\rm vol}I^2)A + a_{\rm surf}(1 + k_{\rm surf}I^2)A^{2/3}B_s(\mathbf{q}) + a_{\rm Coul}Z^2A^{-1/3}B_{\rm Coul}(\mathbf{q}). \quad (35)$$

Here, $B_{\rm Coul}(\mathbf{q})$ is a dimensionless functional of Coulomb energy in the sharp-edge LDM. In [75], the level-density parameter was estimated for a large number of spherical even–even nuclei in terms of relativistic mean-field theory and using Eq. (35).

When comparing the results obtained in [67, 74, 75], we can draw the following conclusions. First, in the studies under consideration, the level-density parameter and potential energy were calculated consistently. Clearly, the use of various model representations means that we obtain deformation dependences of the level-density parameter that are different from each other. Therefore, when analyzing various nuclear characteristics, it is necessary to place special emphasis on the consistency of the set of parameters in question. In particular, the fission barriers in statistical calculations, the conservative driving force in dynamic calculations, the nucleus temperature, and the level-density parameter should be determined under the same model assumptions (as occurred in [67, 74, 75]). Second, the level-density parameter obtained in the finite-range LDM can be approximated by Eq. (35). In [67], it was established that the contribution of the Coulomb term in Eq. (35) is relatively small, and the values (signs and magnitude) of the coefficients k_v and k_s strongly depend on the set of nuclei chosen for the approximation. Therefore, it makes sense to restrict the calculations to only two terms in expansion (34), which should not greatly affect the accuracy of the approximation.

In Fig. 4, we show a number of dependences of the level-density parameter on the mass number along the beta-stability line. The results are obtained for the nuclei ground state. It can clearly be seen that, when the level-density parameter is calculated with the Ignatyuk coefficients for the Woods–Saxon potential, it agrees with $a(\mathbf{q})$ obtained in the temperature-dependent LDM to within 10–15% and differs considerably from the dependence predicted by Töke and Swiatecki. The curve obtained with the Ignatyuk coefficients also

almost coincides with that for the dependence calculated in terms of relativistic mean-field theory [75]. Because, in [62], the temperature coefficients for the finite-range LDM were obtained from an approximation of the results of calculations within the extended Thomas–Fermi method and using the Skyrme effective interaction SkM* [65, 66], the curves corresponding to them on the plot superimpose onto each other.

1.5. Inertia and Friction Tensors

The so-called transport coefficients, i.e., the (inertial) mass and friction parameters, are an important component of dynamic models. As numerous calculations have shown, they generally define the character of the motion of a fissile system and directly influence both the MED parameters and the fission times, as well as the multiplicities of prescission and postscission particles. Thus, calculation of the transport coefficients is extremely important and, probably, a key factor in realizing a dynamic simulation.

The inertia and friction tensors are frequently calculated within the hydrodynamic approximation for incompressible vortex-free fluids. In this case, the mechanism of nuclear viscosity is a two-body one. In the hydrodynamic approximation, the Navier–Stokes equations for a viscous medium are usually solved on the basis of the Werner–Wheeler approximation [61, 76], which makes it possible to obtain reasonably simple expressions for the inertia and friction tensors. The Werner–Wheeler approximation is based on a representation in which a fluid flows in the form of cylindrical layers, with the fluid particles being unable to escape from their layer during motion. The accuracy of the Werner–Wheeler approximation in relation to calculation of the transport coefficients was investigated in [77, 78]. When calculating the mass tensor, it was found that the Werner–Wheeler approximation provides very high accuracy for the elongation degree of freedom. For example, when describing the nuclear shape using the Lawrence parametrization [51], mass-tensor components calculated from the elongation coordinate in the Werner–Wheeler approximation virtually coincide with the exact solution to the corresponding hydrodynamic Neumann problem [79], which was obtained by a method based on potential theory [80, 81]. For the Cassini ovaloid parametrization, there is a small distinction between the solutions only for shapes with an almost zero neck radius [77]. At the same time, for the collective coordinate determining evolution of the bridge in a nuclear shape, the difference between the solutions is more significant and can reach, for example, 10% in the case of the Lawrence parametrization [79]. In [61], it was shown that the difference between mass parameters determined by solving the corresponding Neumann problem and with the Werner–Wheeler method increased proportionally to the multipolarity of the vibrations near a spherical shape.

For the friction tensor, the Werner–Wheeler approximation of the collective coordinate associated with elongation is in good agreement with the result obtained for the exact solution to the corresponding Neumann problem [79], as in the case of the mass tensor. At the same time, for the coordinate related to bridge evolution, the Werner–Wheeler approximation for the Lawrence parametrization results in a 30–40% overestimation of the corresponding friction-tensor components.

In [79], an expression taking into account finite nuclear sizes was obtained for the two-body mechanism of nuclear viscosity. This expression differs from that obtained in [61] for an infinite medium by the dissipative-force work in displacing a fluid along the nuclear surface. The results of the calculations [79] showed that, when finite nuclear sizes are taken into account, much smaller values of the friction-tensor components are obtained for the two-body mechanism of nuclear viscosity than when the expressions given in [61] are applied.

In addition to the two-body mechanism of nuclear viscosity, the one-body mechanism [82–84] can also be used in calculations of the friction tensor. In this mechanism of nuclear viscosity, the authors take into account the fact that a nucleus is a fermion system involving Pauli blocking, which forbids nucleon scattering into occupied states. This circumstance imposes restrictions on the mean free path of particles (it increases up to the size of the system itself); therefore, the role of two-particle collisions decreases. Nucleons are kept within a nucleus due to the presence of a mean field; i.e., particles move almost freely within the nuclear shape and elastically hit only a "wall" simulating the nuclear surface, which itself has a certain velocity because the mean field in which nucleons move depends on the position of these nucleons, i.e., on the nuclear collective coordinates.

In [82–84], two formulas were obtained: The first, named the "wall" formula, describes the dissipation of nuclear shapes without a neck, and the second, called the "wall-plus-window" formula, was introduced for strongly extended nuclear shapes under conditions in which it is possible to detect formed fragments connected by a neck. A quantum consideration of one-body dissipation showed [85] that the nuclear viscosity amounts to only about 10% of the values calculated using the wall formula [82, 84], although the functional dependence of viscosity on nuclear shape is adequately reproduced by this formula. In this context, Nix and Sierk proposed a modified variant of one-body dissipation that led to the surface-plus-window formula. In this case, the contribution from the wall formula to the dissipation is reduced by almost four times. The reduction coefficient k_s was found from an analysis of the experimental width of giant resonances and amounted to $k_s = 0.27$. From a comparison of the calculated average values of the kinetic energy of fission fragments with the

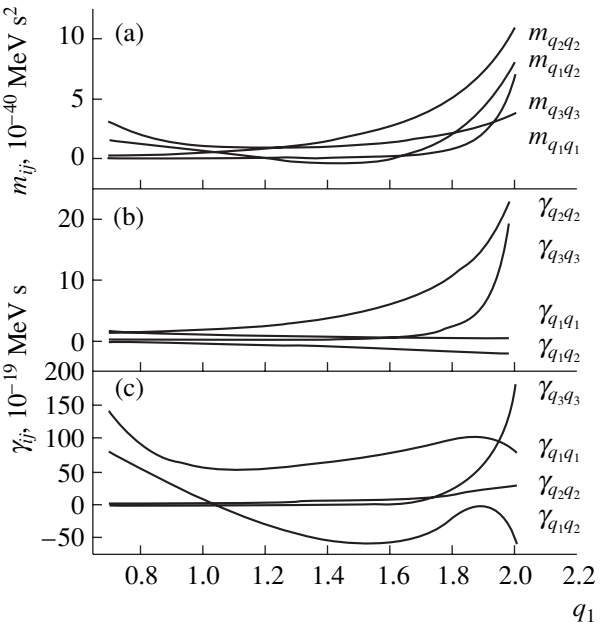

Fig. 5. Transport coefficients as functions of the coordinate q_1 ($h = \alpha = 0$): (a) the inertia tensor; (b) the friction tensor under the assumption of the two-body mechanism of nuclear viscosity $\nu_0 = 2 \times 10^{-23}$ MeV s fm^{-3}, and (c) the friction tensor under the one-body mechanism of viscosity with $k_s = 0.25$. The calculations are performed for the ^{224}Th nucleus.

experimental data, it was found [86] that k_s lies within $0.2 < k_s < 0.5$. The friction tensor corresponding to the surface-plus-window formula can be written in cylindrical coordinates as

$$\gamma_{ij}^{sw} = \frac{1}{2}\rho_m \overline{v}\left\{\frac{\partial R}{\partial q_i}\frac{\partial R}{\partial q_j}\Delta\sigma + \frac{32}{9}\frac{1}{\Delta\sigma}\frac{\partial V_1}{\partial q_i}\frac{\partial V_1}{\partial q_j}\right.$$

$$+ k_s\left[\pi\int_{z_{\min}}^{z_N}\left(\frac{\partial\rho_s^2}{\partial q_i} + \frac{\partial\rho_s^2}{\partial z}\frac{\partial D_L}{\partial q_i}\right)\left(\frac{\partial\rho_s^2}{\partial q_j} + \frac{\partial\rho_s^2}{\partial z}\frac{\partial D_L}{\partial q_j}\right)\right.$$

$$\times\left(\rho_s^2 + \left(\frac{1}{2}\frac{\partial\rho_s^2}{\partial z}\right)^2\right)^{-\frac{1}{2}}dz \qquad (36)$$

$$+ \pi\int_{z_N}^{z_{\max}}\left(\frac{\partial\rho_s^2}{\partial q_i} + \frac{\partial\rho_s^2}{\partial z}\frac{\partial D_R}{\partial q_i}\right)\left(\frac{\partial\rho_s^2}{\partial q_j} + \frac{\partial\rho_s^2}{\partial z}\frac{\partial D_R}{\partial q_j}\right)$$

$$\left.\left.\times\left(\rho_s^2 + \left(\frac{1}{2}\frac{\partial\rho_s^2}{\partial z}\right)^2\right)^{-\frac{1}{2}}dz\right]\right\},$$

where D_R and D_L are the positions of the centers of mass of future fragments and k_s is the reduction coefficient for the contribution made by the wall formula. If the coefficient $k_s = 1$ corresponds to the total one-body viscosity, then Eq. (36) corresponds to the wall-plus-window formula.

The two terms in square brackets in Eq. (36) correspond to the wall formula for the left-hand and right-hand fragments. We denote the friction-tensor components calculated from the wall formula as γ_{ij}^{w}. For neckless nuclear shapes, the friction tensor is usually calculated from the wall formula, and the surface-plus-window formula is applied to strongly deformed shapes with a thin neck. In order to describe the dissipation in an intermediate case, expressions of the type $\gamma_{ij} = k_s\gamma_{ij}^{w}f(r_N) + \gamma_{ij}^{sw}(1 - f(r_N))$ are usually used. The choice of the function $f(r_N)$ is quite arbitrary. As a rule, it is chosen so that it varies smoothly from $f(0) = 0$ to $f(1) = 1$. However, this choice is ambiguous [10, 87–89] and can affect the calculated characteristics [84].

In Fig. 5, we show components of the inertia and friction tensors calculated along the bottom of a fission valley under the assumption of one-body and two-body mechanisms of nuclear viscosity. As can be seen from this figure, the deformation dependence of various components of the friction tensor calculated with different mechanisms of viscosity essentially differ from each other. This brings about, in the scission for different mechanisms of viscosity, a different character in a fissile system's motion. It should be emphasized that it is difficult to compare these components of the inertia and friction tensors with the results of other studies. Even when using the same parametrization to describe nuclear shape, the qualitative behavior of the components depends on the chosen collective coordinates. For example, we used the $\{c, h, \alpha\}$ parametrization to describe nuclear shape and chose q_1, q_2, and q_3 as the collective coordinates, as they are convenient for use in dynamic calculations. Therefore, the components of the inertia and friction tensors shown in Fig. 5 do not coincide with the tensor components from other studies in which the $\{c, h, \alpha\}$ parametrization was used.

The reduced friction coefficient $\beta = \gamma/m$ is an important characteristic of the fission process and is frequently used during its analysis. In Fig. 6, we show the component $\beta_{q_2q_2} = \gamma_{q_2q_2}/m_{q_2q_2}$ calculated using the one-body and two-body mechanisms of nuclear viscosity. As our calculations show, this component generally defines the length of time and character of the motion of a fissile nucleus to scission, although the coordinate q_2 is not explicitly related to the elongation coordinate. From this figure, it can be seen that $\beta_{q_2q_2}$ amount to several units of 10^{21} s^{-1} at $k_s = 0.25$. Moreover, their order of magnitude is close to that of values calculated using the two-body mechanism of nuclear viscosity with $\nu_0 = 2 \times 10^{-23}$ MeV s fm^{-3}, but the deformation dependence is different.

In [82, 90–92], it was shown that the assumptions used in derivation of the wall formula do not apply

under certain conditions. For example, the assumption of the randomness of the particle motion inside a nuclear shape can not be applied to the motion of particles in integrable potentials such as an ellipsoidal rectangular well. In this case, the particle motion inside the nuclear shape is ordered. For this reason, the dissipation predicted by the wall formula is considerably overestimated. In this context, the authors of [93] proposed a deformation-dependent reduction coefficient in the wall formula reflecting the degree of particle motion randomization. However, it had already been shown in [82] that, even in integrable potentials, it is possible to obtain values close to those given by the wall formula if the particle motion is randomized. In [79], it was also shown that including collisions between particles in the consideration results in randomization of the particle motion, whose degree depends on the temperature and density of states near the Fermi energy.

In [94], the reduction coefficient of the contribution from the wall formula was defined through the measure of chaos in the single-particle motion of nucleons inside a nuclear shape. The measure of chaos (the randomness of nucleon motion) depends on the nuclear shape in question, i.e., on the collective coordinates. The degree of randomness was found to vary from zero to one during evolution of a nucleus from the spherical to scission configurations. Thus, the reduction coefficient explicitly depends on deformation, and this dependence is calculated on the basis of the general principles of chaos theory [95] instead of being introduced, as was done in [26, 27], ad hoc to explain experimental data. The first application of such an approach to describing fission widths, prescission neutron multiplicities, and cross sections for evaporation residues appeared to be reasonably successful, although the calculations were carried out in the one-dimensional model. It would be both interesting and desirable to extend this approach to the multidimensional case.

An important aspect of studying fusion–fission reactions in terms of the stochastic approach is consideration of the temperature dependence of kinetic coefficients. The different theoretical approaches used to calculate kinetic coefficients apply various approximations and parameters, which, however, are determined with insufficient accuracy. For this reason, the obtained temperature dependences of the friction tensor differ dramatically. For example, when the wall formula is derived with the approximations used in [82], it predicts a friction coefficient that is almost temperature-independent. The expression for the wall formula also can be derived within linear-response theory [79, 90], but, in this case, the temperature dependence of the friction coefficient is such that the friction increases with temperature proportionally to T^2. In turn, the two-body viscosity decreases with temperature in accordance with $1/T^2$ [96]. When the temperature dependence of the friction was experimentally investigated [97–99], it was found that the friction coefficient increases with temperature.

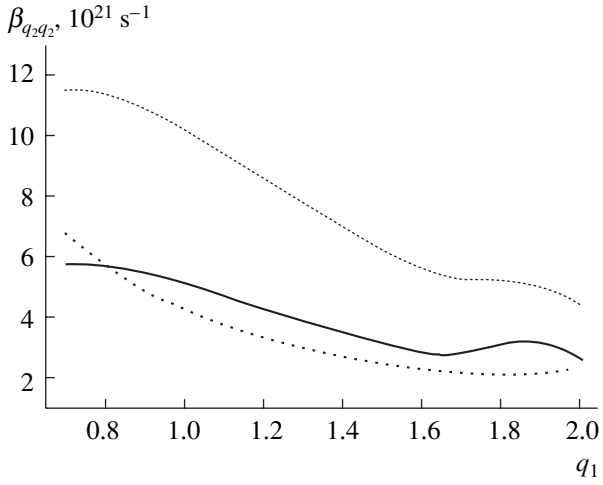

Fig. 6. Reduced viscosity coefficient $\beta_{q_2q_2} = \gamma_{q_2q_2}/m_{q_2q_2}$ calculated at $h = \alpha = 0$ for the ^{224}Th nucleus. The solid and dotted curves correspond to the one-body mechanism of nuclear viscosity with $k_s = 0.25$ and 0.5, respectively. The dotted curve was obtained under the assumption of the two-body mechanism of viscosity with $\nu_0 = 2 \times 10^{-23}$ MeV s fm^{-3}.

The kinetic coefficients can also be calculated within microscopic approaches [79, 90, 100, 101]. Their use makes it possible to remove many of the approximations that are inevitably applied in calculations of the kinetic coefficients within macroscopic models. Nevertheless, performing these calculations within microscopic approaches is extremely cumbersome. In addition, the kinetic coefficients obtained in these calculations and their temperature and deformation dependences depend on the method used, the set of constants, etc., and tend to differ considerably. Therefore, the kinetic coefficients most frequently used in dynamic simulation of reactions involving heavy ions are calculated within macroscopic models.

1.6. Statistical Model of Excited-Nucleus Decay

The decay of excited nuclei can be considered within the statistical fission model proposed by Bohr and Wheeler [7] and Weisskopf [102] and further developed in numerous studies. However, in its conventional form [103], the statistical model is not able to describe experimental data on variances of mass and energy distributions in the heavy-nuclei range with the parameter $Z^2/A > 32$ [104]. This drawback is ultimately associated with the fact that the model does not take into account the dynamics of the fission process.

When performing dynamic calculations, the statistical model is usually used for describing light-particle emission, which both accompanies fission and competes with it. A combination of the dynamic and statistical models makes it possible to bring the theoretical description of nuclear decay and the real process closer together. Such a combination was used for the first time

in [14], where the standard FPE was supplemented with a term describing the continuous-mode emission of light particles. In spite of the fact that, in this study, the authors restricted the analysis to only one collective coordinate and continuous-mode particle emission, they succeeded in reproducing the principal effects produced by the influence of particle emission on the nuclear-fission dynamics. Later, another scheme including the statistical particle-emission model in dynamic calculations was proposed in [105]. In this case, a reduced Langevin equation was considered, and its numerical integration took into account discrete particle emission. Both the continuous [25] and the discrete [18, 19, 26] methods of taking into account particle emission are now widely used.

Within the statistical model, the probability of emission of a certain particle is specified by the nuclear-decay width in the corresponding channel. The decay widths are expressed according to the density of nuclear excited states, which, in turn, depends on the excitation energy, angular momentum, compound-nucleus deformation, and its nucleonic composition.

As a rule, the expression for the nuclear level density is chosen within the Fermi-gas model and has the following form [70, 106]:

$$\rho(E, I, \mathbf{q}) = \frac{(2I+1)a(\mathbf{q})^{1/2}}{12}\left(\frac{\hbar^2}{2J_\perp(\mathbf{q})}\right)^{3/2} \times \frac{\exp[2(a(\mathbf{q})E)^{1/2}]}{E^2}K_{\text{rot}}(E)K_{\text{vib}}(E). \quad (37)$$

Here, A is the mass number, E_{int} is the excitation energy, and I is the spin. The values of K_{vib} and K_{rot} (the collective and rotational enhancements of the level density) are given by the expressions [107]

$$K_{\text{rot(vib)}}(E) = [K^0_{\text{rot(vib)}} - 1]f(E) + 1,$$
$$f(E) = \left[1 + \exp\left(\frac{E - E_{\text{cr}}}{\Delta E}\right)\right]^{-1}. \quad (38)$$

In these expressions, the presence of temperature-related attenuation of collective enhancements of the level density is taken into account in accordance with [107]. The critical energies $E_{\text{cr}} = 40$ MeV and $\Delta E = 10$ MeV are assumed to remain constant. The expressions for K^0_{rot} and K^0_{vib} can be written as

$$K^0_{\text{vib}} = \begin{cases} 1, & \text{for deformed nuclei} \\ \exp(0.0555A^{2/3}T^{4/3}), & \text{for spherical nuclei,} \end{cases} \quad (39)$$

$$K^0_{\text{rot}} = \begin{cases} 1, & \text{for spherical nuclei} \\ J_\perp T, & \text{for deformed nuclei.} \end{cases} \quad (40)$$

The importance of including collective enhancements when calculating the level density, as well as their attenuations under an increase in temperature, was noted, for example, in [107–109]. Nevertheless, collective enhancements were seldom taken into account during the development of the Langevin models. In [67], it was shown that the inclusion of collective enhancements produces a substantial effect on the calculated values of quantities such as the mean prescission neutron multiplicity and the fission probability. Because these characteristics are frequently used to obtain information about, for example, nuclear viscosity, it is necessary to place special emphasis on the accuracy of the level-density calculation when performing such an analysis.

It is well-known that, for deformations that remain close to a spherical nuclear shape, it is possible to introduce only a vibrational enhancement of the level density, while rotational enhancement is absent due to the symmetry effects. In contrast, for strongly deformed nuclei, it is possible to take into account only a rotational enhancement of the level density, while the vibrational enhancement proves to be 10–100 times lower and is usually disregarded. However, for the intermediate region of deformations, it still remains unclear how to pass from vibrational to rotational enhancements as the deformation increases [107]. In this context, an estimation was made in [107] showed that, for quadrupole deformations with $\beta_2 < 0.15$, it is possible to consider a nucleus to be reasonably close to a spherical deformation and that, correspondingly, there is only vibrational enhancement of the level density in this deformation region. For violent deformations, the rotational enhancement sharply increases to the values given by Eq. (40) and becomes predominant in this deformation region.

The partial widths of nuclear decay with the emission of a particle j ($j = n$, p, d, t, ^{3}He, and α particles) can be expressed [106] through the single-particle level density ρ_j of a residual nucleus and the cross section $\sigma^{(j)}_{\text{inv}}$ for the absorption of this particle by the residual nucleus:

$$\Gamma_j = \frac{g_j m_j}{(\pi\hbar)^2}\frac{1}{\rho_0(E^{(0)}_{\text{int}})} \times \int_{V_j}^{E^{(j)}_{\text{int}} - B_j} E\sigma^{(j)}_{\text{inv}}(E)\rho_j(E^{(j)}_{\text{int}} - B_j - E)EdE. \quad (41)$$

Here, g_j, m_j, B_j, and V_j are the statistical factors resulting from the spin of a particle, its mass, the compound-nucleus binding energy, and the Coulomb barrier, respectively, and $E^{(0)}_{\text{int}}$ and $E^{(j)}_{\text{int}}$ are the internal excitation energy of the initial and residual nuclei.

The radiation widths of γ-quanta emission are calculated from the equation

$$\Gamma_\gamma = \frac{1}{(\pi\hbar c)^2}\frac{1}{\rho_0(E_{\rm int}^{(0)})}\int_0^{E_{\rm int}^{(0)}} E\sigma_\gamma(E)\rho_\gamma(E_{\rm int}^{(0)} - E)E^2 dE, \quad (42)$$

where $\sigma_\gamma(E)$ is the inverse cross section for dipole photoabsorption. However, it should be noted that, for a correct description of particle emission when numerically simulating fission within the Langevin models, it is necessary to take into account the deformation dependence of statistical-model parameters such as the emission barriers, binding energies of particles, and cross sections for inverse processes [21, 110]. This necessity is caused by the fact that a compound nucleus most often arises in the region of violent deformations, which fundamentally differ from a spherical state.

The statistical model can be used in dynamic calculations related to description of not only light-particle emission but also nuclear fission. With a decrease in the fissility parameter and/or the excitation energy of a compound nucleus, the mean fission time very quickly increases and the fissility decreases. Therefore, due to the long calculation time needed, the use of a purely dynamic approach becomes virtually impossible for fissile systems with low fissility. If we instead employ a statistical branch of dynamic calculations, where not only light-particle evaporation but also fission is described within the statistical model (this approach was proposed for the first time in [105]), it becomes possible to remove this disadvantage. Such an approach can be used if the following conditions are met: (i) a system is in the ground-state region before the ridge, (ii) the time of calculations exceeds a certain time $t > t_{\rm stat}$, and (iii) the ratio between the nuclear temperature and a fission barrier is $T/B_f < 0.2$. The parameter $t_{\rm stat}$ is selected so that it is certain to satisfy the condition that the particle flux through the fission barrier attains its quasisteady value.

Under the statistical branch of calculations, the fission width can be found in the multidimensional case [11]. Because, as was mentioned above, a nucleus is a thermodynamic system, the quasisteady fission width should be calculated using thermodynamic potentials. Below, we give an expression for the quasisteady value of the fission width in the case of the free-energy potential:

$$\Gamma_f = \omega_{\rm K}\left(\frac{\det\Omega_{ij}^2(\mathbf{q}_{\rm gs})}{\det\left|\Omega_{ij}^2(\mathbf{q}_{\rm sd})\right|}\right)^{\frac{1}{2}}\exp(-(F(\mathbf{q}_{\rm sd}) - F(\mathbf{q}_{\rm gs}))/T). \quad (43)$$

Here, $\Omega_{ij}^2(\mathbf{q}_{\rm gs}) = \mu_{ik}(\mathbf{q}_{\rm gs})\left(\frac{\partial^2 F(\mathbf{q})}{\partial q_k \partial q_j}\right)_{\mathbf{q}=\mathbf{q}_{\rm gs}}$, $\Omega_{ij}^2(\mathbf{q}_{\rm sd}) = \mu_{ik}(\mathbf{q}_{\rm sd})\left(\frac{\partial^2 F(\mathbf{q})}{\partial q_k \partial q_j}\right)_{\mathbf{q}=\mathbf{q}_{\rm sd}}$, and $\omega_{\rm K}$ is the Kramers frequency, which is a unique positive root of the equation

$$\det(E(2\pi\omega_{\rm K}/\hbar)^2 + (2\pi\omega_{\rm K}/\hbar)\mu_{ik}(\mathbf{q}_{\rm sd})\gamma_{kj}(\mathbf{q}_{\rm sd}) + \Omega_{ij}^2(\mathbf{q}_{\rm sd})) = 0. \quad (44)$$

Here, E is the unit matrix, and the coordinates $\mathbf{q}_{\rm sd}$ and $\mathbf{q}_{\rm gs}$ determine the saddle-point and ground-state positions, respectively. In the statistical branch of the program, the probability of system deexcitation due to emission of a particle or fission is calculated using the Monte Carlo method, with the probabilities of each of these events being proportional to the partial decay widths Γ_j and Γ_f. If the system has to be disintegrated, we transfer back from the statistical branch to the dynamic simulation, but, in this case, the calculation proceeds from the ridge surface and the return of a particle to the ground-state region is blocked.

However, it is necessary to note that the choice of the free-energy potential $F(\mathbf{q})$ for calculating the quasisteady fission width is ambiguous. Strictly speaking, Eq. (43) is an approximation of fission. Because fission is not an isothermal process, the accuracy of Eq. (43) depends, correspondingly, on how constant the temperature remains during nuclear fission. Because fission (occurring between evaporations of particles) proceeds with a constant total excitation energy, the use of the entropy instead of the free energy is more justified when calculating the quasisteady value of the fission width. Further discussion of this question and results of dynamic calculations using the entropy can be found, for example, in [26, 27]. However, in our opinion, the use of the entropy for calculating the fission width is not the best solution, since only the behavior of the potential energy near the ground state and at the saddle point is taken into account in Eq. (43) and not the potential-energy landscape. In this sense, a more consistent method of fission-width calculation is based on the concept of a mean first passage time [111, 112] or the alternative concept of mean last passage time [113]. Such a method has been successfully applied for a long time in other fields of physics [8]. Nevertheless, until now, it has been developed only for the nongeneral case of system motion in an overdamped mode. Therefore, the development and improvement of this method is currently one of the important problems to be solved in fission physics.

2. MASS–ENERGY DISTRIBUTION (MED) OF FISSION FRAGMENTS

Mass–energy distributions (MEDs) of fission fragments are conventionally used as a source of information about fission dynamics. They were fully investigated for the first time by Nix and Swiatecki in their zero-viscosity dynamic model [114]. Within the framework of this model, the authors succeeded in describing MED parameters for fission fragments of light fissile nuclei with $Z^2/A \le 31$. For heavier nuclei, the zero-viscosity model [114] regularly results in low values of the variances of mass and energy distributions.

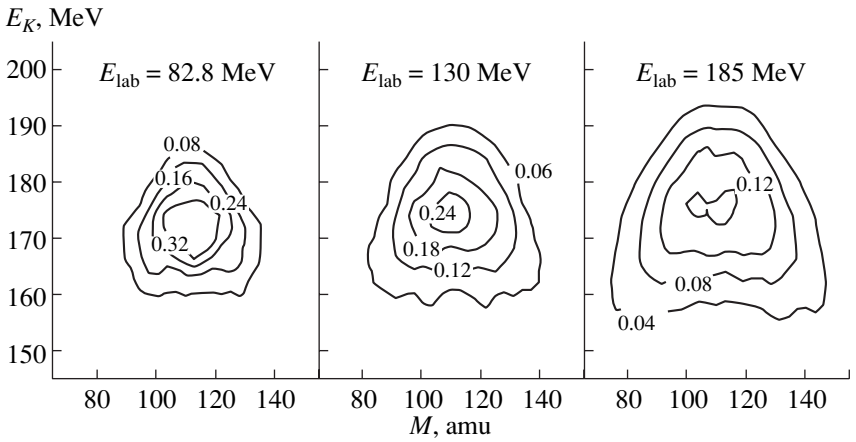

Fig. 7. Mass–energy distributions of the fission fragments obtained from the reaction $^{16}O + ^{208}Pb \longrightarrow ^{224}Th$ at three values of impinging-ion energy. The calculation was performed under the assumption of the one-body mechanism of viscosity with $k_s = 0.25$.

Significant success was attained in relation to description of the MED characteristics of fission fragments and understanding of the role of nuclear dissipation within the diffusion model based on the multidimensional Fokker–Planck equation for the distribution function of collective variables [13, 43]. The important achievement of the diffusion model is that it can offer an explanation for the sharp increase in the variances of mass and energy distributions that is observed as the parameter Z^2/A increases. However, the model still has a number of disadvantages. Its main drawback consists in the fact that it uses approximate methods for solving the Fokker–Planck equation and the fluctuations of collective variables are taken into account in the form of an average. In [45], the variances of energy distributions calculated from the diffusion and two-dimensional Langevin models were compared. As a result, the error, which is due to the approximate nature of the methods used for solving the Fokker–Planck equation, was estimated as being equal to about 30%. In the diffusion model and the Nix model with zero viscosity, compound-nucleus deexcitation due to the emission of prescission particles, which significantly affects the evolution of the collective degrees of freedom and, also, the parameters of the considered distributions of fission fragments were disregarded.

The stochastic approach based on the set of three-dimensional Langevin equations makes it possible to study the MEDs of fission fragments in full. In this chapter, we present the results of regular (in a wide interval of fissility parameters and excitation energies) application of the three-dimensional Langevin equations to studying the MED characteristics of fission fragments.

2.1. Two-Dimensional MEDs of Fission Fragments

The method used for calculation of the observed characteristics is based on the concept of a rupture surface. It is assumed that the distribution of collective variables and their conjugate momenta are formed during the descent of system from a conditional saddle point to a certain scission configuration at which an instantaneous rupture of the nuclear neck takes place without any change in elongation. The further evolution of the collective variables produces only a minor effect on the formed distributions of the reaction products. This method has previously been widely used when studying the MED within the framework of the diffusion model.

When calculating the energy-distribution parameters, it was assumed that the total fission-fragment kinetic energy E_K is the sum of the Coulomb repulsion energy V_C, the nuclear attraction energy V_n of the future fragments, and the kinetic energy of their relative motion (the prescission kinetic energy E_{ps}). All the terms in this sum ($E_K = V_C + V_n + E_{ps}$) were calculated at the instant of scission. The calculated formulas for V_C and V_n in the LDM, taking into account the finite-range nuclear forces and diffuse nuclear surface, are listed in the appendix to [60].

In Fig. 7, calculated fission-fragment MEDs for the ^{224}Th compound nucleus are shown at three impinging-ion energies. It can be seen that the MED of the fragments broadens with an increase in the excitation energy. It should also be noted that the shape of the contour lines of the distributions qualitatively corresponds to the experimentally observed picture. It is more convenient to quantitatively compare the calculated characteristics of the two-dimensional MED of fragments with those observed experimentally in terms of the parameters of one-dimensional mass and energy distributions and the correlation dependences of the MED parameters.

2.2. One-Dimensional Mass and Energy Distributions of Fragments

One-dimensional mass and energy distributions can be obtained by integration of two-dimensional MEDs over the corresponding parameter. They are characterized by single-peak curves at high excitation energies and are usually, both in experimental investigations and theoretical calculations, approximated by Gaussian curves with average values and variances, which are the principal characteristics of these distributions. As a rule, results are discussed in terms of these values. Sometimes, a third γ_3 and fourth γ_4 moment (asymmetry and excess) of the mass and energy distributions are also involved. They characterize the difference between these distributions and normal ones and are defined as

$$\gamma_3 = \langle (X - \langle X \rangle)^3 \rangle / \sigma_X^3, \quad (45)$$

$$\gamma_4 = \langle (X - \langle X \rangle)^4 \rangle / \sigma_X^4 - 3, \quad (46)$$

where X is assumed to be either the kinetic energy E_K of the fragments or the fragment mass M. For a Gaussian distribution, $\gamma_3 = \gamma_4 = 0$.

As is shown by the performed calculations, the first and second moments of the mass and energy distributions are sensitive to the viscosity used in the calculations and the character of the descent of trajectories from the saddle to the scission. The parameters of the energy distribution are also very sensitive to the choice of rupture condition [58, 84].

The energy-distribution parameters have been investigated for various nuclei in a large number of experimental [115–117] and theoretical [44, 45, 118–120] studies. From an analysis of the available experimental data, it was found that $\langle E_K \rangle$ is virtually independent of both angular momentum and excitation energy [115]. In addition, it was shown in [115, 116] that $\langle E_K \rangle$ is not a linear function of the parameter $Z^2/A^{1/3}$, as follows from the Viola systematics [121], and has a break at $Z^2/A^{1/3} \simeq 900$. The break is observed if only the results on strongly heated nuclei are selected from the experimental data and low-energy and spontaneous fission strongly influenced by shell effects, as well as quasifission reactions, are excluded. The systematics proposed in [115, 116] has the form

$$\langle E_K \rangle = \begin{cases} 0.104 Z^2/A^{1/3} + 24.3 \text{ MeV} & (Z^2/A^{1/3} > 900) \\ 0.131 Z^2/A^{1/3} \text{ MeV} & (Z^2/A^{1/3} \le 900). \end{cases} \quad (47)$$

According to the Viola systematics [121], $\langle E_K \rangle$ is given by the expression

$$\langle E_K \rangle = 0.1189 Z^2/A^{1/3} + 7.3 \text{ MeV}. \quad (48)$$

In Fig. 8, we show the mean kinetic energy of fragments as a function of the parameter Z^2/A, which was obtained in three-dimensional Langevin calculations

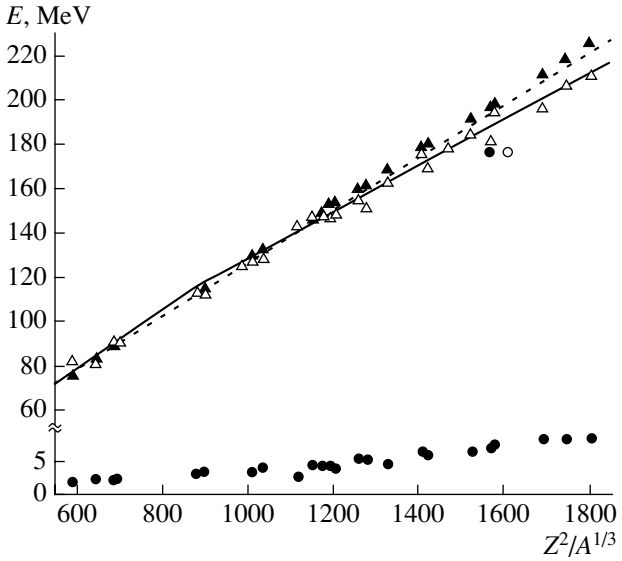

Fig. 8. Dependence of $\langle E_K \rangle$ on the parameter $Z^2/A^{1/3}$. The open triangles show the experimental data, the closed triangles indicate the results of theoretical calculations with $k_s = 0.25$, and the closed circles represent $\langle E_{ps} \rangle$. The solid line shows the following systematics [115, 116]: $0.104Z^2/A^{1/3} + 24.3$ MeV for the region of $Z^2/A^{1/3} > 900$ and $0.131Z^2/A^{1/3}$ for the region of $Z^2/A^{1/3} \le 900$. The dashed curve shows the Viola systematics [121]: $\langle E_K \rangle = 0.1189Z^2/A^{1/3} + 7.3$ MeV.

with a modified variant of the one-body viscosity. From Fig. 8, it can be seen that the calculated values of $\langle E_K \rangle$ agree well with the experimental data and lie closer to the Viola systematics. It is necessary to emphasize that the values we calculated for $\langle E_K \rangle$ [19, 122, 123] decrease with the reduction coefficient k_s. A similar result was obtained in two-dimensional calculations [86] with a neck radius equal to zero taken as the rupture condition. In [86], the best description of the experimental data was attained with k_s approximately equal to 0.3. The values obtained in three-dimensional calculations of $\langle E_K \rangle$ do not appear to be as sensitive to k_s; therefore, it is difficult to make conclusions about the value of viscosity based on them. The fact that $\langle E_K \rangle$ actually ceases to depend on k_s is associated with the inclusion of the evolution of a nucleus in the mass-asymmetry coordinate of the three-dimensional calculations, in contrast to that of the two-dimensional calculations [86]. $\langle E_K \rangle$ is found by integration of $\langle E_K(M) \rangle$ over M. In [25], it is shown that, in the case of high viscosity, when the descent from the saddle to the scission is slow and E_{ps} can be assumed to be equal to zero, the mean kinetic energy $\langle E_K \rangle_{3D}$ of fragments obtained in the three-dimensional calculations is related to the mean kinetic energy $\langle E_K \rangle_{2D}$ of fragments obtained in the two-dimensional calculations in the following way:

$$\langle E_K \rangle_{3D} = (1 - \sigma_{\eta_A}^2) \langle E_K \rangle_{2D}. \quad (49)$$

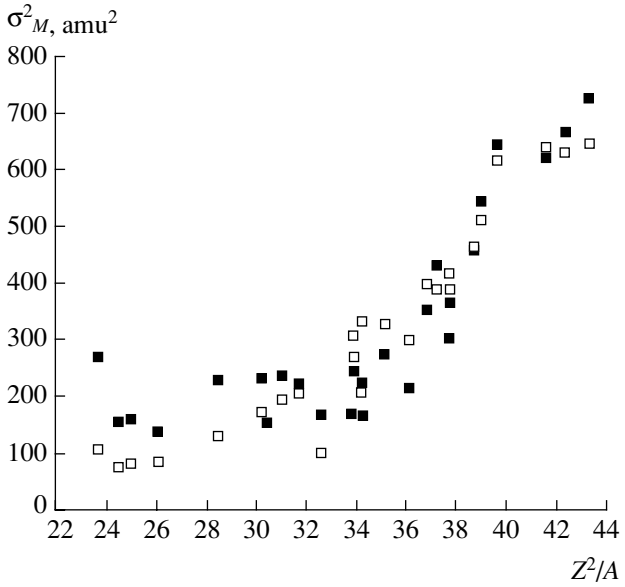

Fig. 9. Variance of the mass distribution as a function of the parameter Z^2/A. The closed squares denote the experimental data and the open squares, the results of theoretical calculations with $k_s = 0.25$.

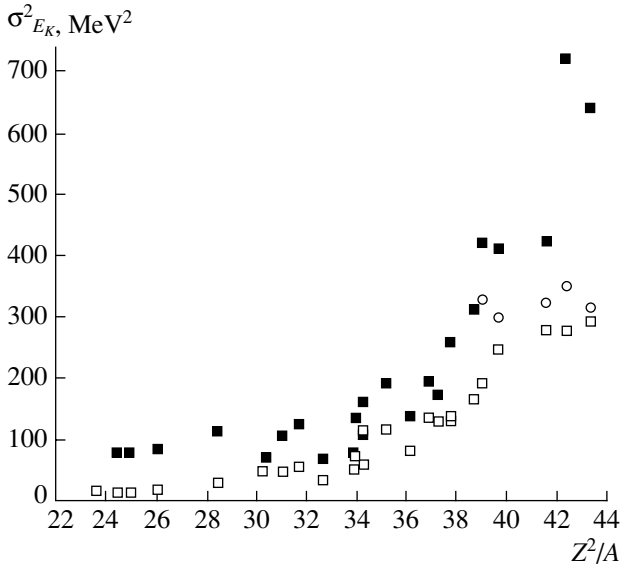

Fig. 10. Variance of the energy distribution as a function of the parameter Z^2/A. The closed squares denote the experimental data and the open squares and circles, the results of theoretical calculations with $k_s = 0.25$ and 0.1, respectively.

Here, $\sigma^2_{\eta_A}$ is the variance of the distribution over the mass-asymmetry coordinate η_A at the instant of scission. As k_s increases, $\sigma^2_{\eta_A}$ decreases. Correspondingly, the expression in brackets increases, while, in contrast, $\langle E_K\rangle_{2D}$ decreases. Thus, the values $\langle E_K\rangle_{3D}$ become less dependent on k_s than $\langle E_K\rangle_{2D}$. As can be seen from Fig. 8, the assumption of the smallness of E_{ps} in calculations with the one-body viscosity is thoroughly justified because, even for the heaviest nuclei, E_{ps} does not exceed 10 MeV. In a wide range of variations of the parameter Z^2/A, E_{ps} contributes less than 2% to E_K.

In Fig. 9, we show the variance of the mass distribution as a function of the parameter Z^2/A. As can be seen from this figure, it is possible to reproduce the sharp increase observed in the experimental values of σ^2_M in the heavy-nuclei range within the stochastic approach and using the modified variant of the one-body viscosity. The results of calculations with $k_s = 1$ [19, 122, 123] virtually coincide with those from the statistical model [103]. The explanation for the increase in σ^2_M as k_s decreases is as follows: On the one hand, the rigidity of the potential energy with respect to the mass-asymmetry coordinate during the descent from the saddle to the scission steadily increases; correspondingly, the mass distribution also narrows. On the other hand, the system retains a "memory" of the former large width of the distribution because the descent proceeds in a finite time. The faster the descent, the larger the "stored" variances. The rate of descent generally depends on the viscosity, whose value depends on the coefficient k_s. A detailed discussion of this mechanism of formation of the mass distribution can be found in [13, 43].

Calculated values of $\sigma^2_{E_K}$ for different k_s are shown in Fig. 10. It can be seen that the calculations in the three-dimensional Langevin dynamics with $k_s \sim 0.1$–0.25 make it possible to adequately reproduce the increase in the experimental variances with Z^2/A. The results of calculations for $k_s = 1$ virtually coincide with those performed in the dynamic zero-viscosity model [114, 124]. As the performed calculations show, the inclusion of the third collective coordinate (the mass-asymmetry coordinate) results in a substantial rise in $\sigma^2_{E_K}$ in comparison with the calculations executed in two-dimensional models [118, 120] for symmetric fission. This result agrees with qualitative estimates [25] that predict an increase in the energy-distribution width obtained in two-dimensional calculations of symmetric fission and taking into account fluctuations in the mass-asymmetry coordinate.

In addition, it is particularly important to note that the energy-distribution parameters are sensitive to the choice of parametrization of fissile-nucleus shape and the rupture condition. For example, in [25], within the two-dimensional Langevin calculations, $\langle E_K\rangle$ and σ_{E_K} were found to be approximately 15% higher for the two-center parametrization [38, 39] with a fixed neck parameter than for a parametrization based on Legendre polynomials [125]. A similar conclusion is reached from comparison of the results given in [44]

and [118, 120], in which the calculations were carried out using the two-body mechanism of nuclear viscosity with approximately identical two-body viscosity coefficients ν_0. However, the authors of [44] used the $\{c, h, \alpha\}$ parametrization [33] and chose a rupture condition with a finite-thickness neck, while the authors of [118, 120] used the Cassini ovaloid parametrization [37] and a rupture condition with a zero neck radius. In these studies, the results of calculations of $\sigma^2_{E_K}$ proved to be very different for close fissile nuclei with almost equal excitation energies.

The asymmetry (γ_3) and excess (γ_4) of mass and energy distributions have also been studied experimentally. In the case of the fission of highly excited nuclei, the condition $\gamma_3 = \gamma_4 = 0$ is satisfied with high accuracy for the mass distribution. The same result is also obtained in theoretical calculations [18, 19, 122]. Experimental investigations [126, 127] into the dependences of γ_3 and γ_4 of the energy distributions of compound nuclei from Os to U at various excitation energies show that the energy distributions are characterized by small and constant values of the coefficients $\gamma_3 \simeq -0.1$ and $\gamma_4 \simeq 0$. The reproduction of these values of γ_3 and γ_4 in theoretical calculations remains to be attained since, as was noted above, the energy-distribution parameters appear to be extremely sensitive to a number of features of the theoretical calculations, such as the rupture condition, viscosity value, and nuclear-shape parametrization. In this context, it is necessary to mention [60], where the influence of the rupture condition on the energy-distribution parameters was studied under the $\{c, h, \alpha\}$ parametrization. It was found that calculated γ_3 and γ_4 move somewhat closer to the experimental data if we use a probabilistic simulation of the scission ($r_N = 0.3R_0$) instead of the rupture condition with a fixed neck thickness. In addition, the use of the probabilistic rupture condition results in smaller values of E_K and in an increase in $\sigma^2_{E_K}$. Thus, the energy-distribution parameters can be used not only for determining the viscosity of nuclear matter during fission but also for investigating the process of disintegration of a nucleus into fragments.

From comparison of the variances calculated for various k_s with the experimental data, it is possible to conclude that, in calculations, it is necessary to use $k_s \sim 0.25$–0.5 in order to obtain a reproduction of the experimental variances in the range of the lightest nuclei considered in this study and $k_s \sim 0.1$ for heavier nuclei.

The statistical model of fission [103] and the dynamic zero-viscosity model [114, 124] cannot even qualitatively describe the sharp increase in the experimental values of $\sigma^2_{E_K}$ and σ^2_M found for heavier fissile nuclei in this range of variation of the parameter Z^2/A. Significant progress has been achieved in relation to description of the dependences of $\sigma^2_{E_K}$ and σ^2_M on the fissility parameter within the diffusion model [13, 43]. However, the diffusion-model calculations were performed without taking into account the evaporation of light prescission particles. This effect has a strong influence on the MED parameters [118, 120], as the evaporating particles carry away a significant part of the excitation energy, and, correspondingly, the variances of both the mass and the energy distributions decrease.

Recently, MEDs have been calculated at low excitation energies. In [21], the results of two-dimensional Langevin calculations of the mass distribution were published for the ^{227}Pa compound nucleus at low excitation energies. Moreover, the shell corrections were taken into account when calculating the potential energy, level-density parameter, and the deformation dependence of the penetrability coefficient in determining the particle-emission widths. In these studies, multimodal fission was obtained in theoretical calculations. In addition, the mass-distribution shape appeared to be extremely sensitive to the nuclear viscosity (to the value of the coefficient k_s). Therefore, the authors of [21] concluded that the mass-distribution parameters are more sensitive to viscosity at low excitation energies than to prescission particle multiplicity. In addition, the authors of [21] stressed the importance of taking into account the temperature dependence of the nuclear viscosity.

2.3. Mechanisms of Nuclear Viscosity and MEDs of Fission Fragments

As was noted above, when describing the dissipation properties of nuclear matter, the one-body and two-body classical mechanisms of nuclear viscosity are conventionally used. The one-body mechanism is, undoubtedly, physically more justified. At the same time, calculations within the diffusion model [13, 43] executed with the two-body viscosity showed good qualitative and quantitative agreement with the experimental data on MED parameters. Therefore, comparison of the results obtained using both mechanisms of viscosity within the three-dimensional Langevin approach is of interest. In [128], the MED parameters of fragments were calculated in the three-dimensional Langevin model for the reaction

$$^{12}\mathrm{C} + {}^{232}\mathrm{Th} \longrightarrow {}^{244}\mathrm{Cm} \quad (E_{\mathrm{lab}} = 97\ \mathrm{MeV}).$$

We chose this reaction because we previously studied it within the framework of the three-dimensional approach and with the one-body viscosity. In [129], the mass distribution, both with one-body and two-body viscosity, was calculated for this reaction within the two-dimensional Langevin approach.

First, we discuss the qualitative side of the comparison of the two mechanisms of nuclear viscosity. In the case of the one-body mechanism of nuclear viscosity ($k_s = 0.25$), the authors of [18] obtained the following

Table 3. MED parameters of fission fragments and mean prescission neutron multiplicities calculated under the assumption of the two-body mechanism of viscosity in comparison with the experimental data [116]

ν_0 (10^{-23} MeV s fm^{-3})	σ_M^2 (amu^2)	$\sigma_{E_K}^2$ (MeV^2)	$\langle E_K \rangle$ (MeV)	$\langle n_{\text{pre}} \rangle$
2	233	122	185	0.8
3.5	270	148	176	1.1
5	304	144	172	1.4
10	302	127	169	2.5
25	261	101	166	3.8
Experiment [116]	366	259	178	3.0

coordinates of the mean scission points: $c_{\text{sc}} = 2.1$ and $h_{\text{sc}} = -0.07$ for the ^{206}Po nucleus, and $c_{\text{sc}} = 2.2$ and $h_{\text{sc}} = -0.11$ for the ^{260}Rf nucleus. It is well known that the two-body mechanism of viscosity results in more prolate scission shapes in comparison with the one-body mechanism. The coordinates of the mean scission point, $c_{\text{sc}} = 2.5$ and $h_{\text{sc}} = -0.25$, calculated in [128] agree well with those previously obtained within the diffusion model under the assumption of two-body viscosity ($\nu_0 = 3.5 \times 10^{-23}$ MeV s fm^{-3}). We also note that the position of the mean scission point weakly varies with the viscosity coefficient (k_s or ν_0) for both mechanisms of nuclear viscosity. This dependence is especially weak in the case of one-body viscosity.

As the calculations in [128] showed, the use of two-body viscosity, in contrast to one-body viscosity, results in nearly Gaussian energy distributions for all the two-body viscosity coefficients ν_0. In this respect, the two-body mechanism of viscosity gives the best qualitative agreement with the experimental data. It should be noted that the mass and mass–energy distributions are also in qualitatively good agreement with the experimental data.

Now, we discuss quantitative characteristics. Calculated MED parameters and $\langle n_{\text{pre}} \rangle$ are listed in Table 3 for a number of two-body viscosity coefficients. This table shows that satisfactory description of the mean prescission neutron multiplicity $\langle n_{\text{pre}} \rangle$ is attained for the two-body viscosity coefficient $\nu_0 = (10\text{–}25) \times 10^{-23}$ MeV s fm^{-3}. The same conclusion was also reached in [129]: to describe the experimental data on $\langle n_{\text{pre}} \rangle$, it is necessary to increase the two-body viscosity coefficient to $\nu_0 = 25 \times 10^{-23}$ MeV s fm^{-3}. At the same time, the data on $\langle E_K \rangle$ are reproduced at $\nu_0 \simeq 3.5 \times 10^{-23}$ MeV s fm^{-3}. Regarding the variances, the variance σ_M^2 of the mass distribution is underestimated by 20%, whereas the variance of the energy distribution differs from the experimental value nearly by a factor of 2.

The behavior of the variance of the mass distribution as a function of the two-body viscosity coefficient can be explained as follows. There are two opposite tendencies: on the one hand, the diffusion-tensor components increase with viscosity, which leads to an increase in the fluctuations in the mass-asymmetry coordinate and, hence, to an increase in σ_M^2; on the other hand, the fission time and, consequently, the prescission neutron emission increases. As a result, the excitation energy decreases as well as σ_M^2. From Table 3, it can be seen that, for $\nu_0 < 5 \times 10^{-23}$ MeV s fm^{-3}, an increase in the fluctuations with ν_0 is of crucial importance and, for $\nu_0 > 10 \times 10^{-23}$ MeV s fm^{-3}, the behavior of the variance depends on the second coefficient.

The mechanism of formation of the energy distribution is more complicated and depends on several factors. It follows from our calculations that an essential difference between the two-body and one-body viscosities is the strong dependence of the mean total kinetic energy on the two-body viscosity coefficient, whereas $\langle E_K \rangle$ is almost independent of k_s for the one-body mechanism of viscosity. As was mentioned above, $\langle E_K \rangle$ is found by summing the average energy $\langle V_{\text{C}} + V_n \rangle$ of the interaction between fragments and the average energy $\langle E_{\text{ps}} \rangle$ of their relative motion at the instant of scission. The calculations showed that $\langle V_{\text{C}} + V_n \rangle$, both for the one-body and two-body mechanisms of viscosity, weakly depends on the value of viscosity because it is generally determined by the coordinates of the mean scission point. In contrast, the behavior of $\langle E_{\text{ps}} \rangle$ is very different for the two mechanisms of viscosity. For this reaction and the excitation energy, the characteristic values of the one-body viscosity are $\langle E_{\text{ps}} \rangle = 4\text{–}7$ MeV, which provides a constant mean kinetic energy of fission fragments in addition to a weak dependence of $\langle V_{\text{C}} + V_n \rangle$ on the dissipative force. Under the assumption of the two-body mechanism of dissipation, the mean prescission energy varies from $\langle E_{\text{ps}} \rangle = 22$ MeV for $\nu_0 = 2 \times 10^{-23}$ MeV s fm^{-3} to $\langle E_{\text{ps}} \rangle = 4$ MeV for $\nu_0 = 25 \times 10^{-23}$ MeV s fm^{-3}. From Table 3, it can be seen that $\langle E_K \rangle$ varies by the same value as $\langle E_{\text{ps}} \rangle$.

In [58, 61], the values of the coefficient ν_0 allowing the authors to describe experimentally observed $\langle E_K \rangle$ were found to be equal to $\nu_0 = 0.9 \pm 0.3 \times 10^{-23}$ MeV s fm^{-3} [61] and $\nu_0 = 1.9 \pm 0.6 \times 10^{-23}$ MeV s fm^{-3} [58] for a wide range of fissility parameters. Study of the MED in the diffusion model [13] gives the following estimate for the two-body viscosity coefficient: $\nu_0 = 1.5 \pm 0.5 \times 10^{-23}$ MeV s fm^{-3}. We obtained $\nu_0 = 3.5 \times 10^{-23}$ MeV s fm^{-3}, for which the calculated energies $\langle E_K \rangle$ agree well with the experimental data but prove to be at least 1.5 times higher than the previously obtained estimates of this value. A similar relation was also obtained in [130]. As in [120, 130], we failed to obtain a value of the two-body viscosity coefficient at which the mean neutron multiplicity and $\langle E_K \rangle$ would both be adequately described. The performed three-dimensional Langevin calculations for the two types of viscosity made it possible to conclude that experimentally observed fission

characteristics such as the mean prescission neutron multiplicity, mean kinetic energy of fission fragments, and variances of the mass and energy distributions can be more satisfactorily reproduced within the one-body mechanism of nuclear viscosity. A similar conclusion was reached concerning the description of $\langle E_K \rangle$ and $\langle n_{\text{pre}} \rangle$ in [130].

2.4. Correlation Dependences of MED Parameters

The correlation dependences of the MED parameters of fission fragments carry additional information about the dynamics of the descent of a fissile system to its last stage immediately before the scission, for example, the dependences $\langle E_K(M) \rangle$ and $\sigma^2_{E_K}(M)$ of the mean kinetic energy and the variance of the energy distribution on the fragment mass, respectively, as well as the dependence $\sigma^2_M(E_K)$ of the variance of the mass distribution on the kinetic energy. In particular, the dependence of the scission configuration on the fragment mass is directly reflected in the correlation of MED parameters of fragments.

In the first approximation, the dependence $\langle E_K(M) \rangle$ can be described by the parabolic law [131]

$$\langle E_K(M) \rangle = \langle E_K(A/2) \rangle \left(1 - \beta \left(1 - \frac{2M}{A}\right)^2\right). \quad (50)$$

The dependence of the mean kinetic energy on the fragment mass generally reflects the dependence of the Coulomb energy on the distance between the centers of mass of future fragments at the instant of scission. We note that an expression similar to Eq. (50) for $\beta = 1$ follows from the Nix dynamic model [114] with zero viscosity and corresponds to the simplest assumption on the independence of the spacing between the centers of mass of fragments. From the experimental data [131], it follows that $\beta < 1$ and depends both on the fissility parameter and the excitation energy of a compound nucleus at the energy $E^* > 20$ MeV for nuclei lighter than ^{213}At. The values of β calculated in our three-dimensional Langevin model vary from $\beta = 0.7$ for ^{198}Pb to $\beta = 0.9$ for ^{248}Cf. For ^{186}Os, the calculated value of $\beta = 0.9$. In the next approximation, it is necessary to take into account the terms containing $(1 - 2M/A)^4$ in Eq. (50). The analysis in [132] showed that the experimentally observed dependences $\langle E_K(M) \rangle$ actually contain the terms $(1 - 2M/A)^4$.

As was observed under experimental conditions, the calculated variances $\sigma^2_{E_K}(M)$ are virtually independent of the fragment mass. The dependence $\sigma^2_M(E_K)$ also qualitatively corresponds to the experiment data (it almost hyperbolically decreases as E_K increases). The dependences $\sigma^2_M(E_K)$ and $\sigma^2_{E_K}(M)$ obtained for fission fragments can be explained from the shape of sections of the MED for $M = \text{const}$ and $E_K = \text{const}$. This problem is considered in detail in [13]. If the energy-distribution width is virtually independent of M, the width, and even the shape, of the mass distribution strongly depend on E_K.

3. NEUTRON MULTIPLICITIES AND FISSION TIMES

3.1. Introduction

Among all the particles that evaporate from a nucleus, neutrons play a special role [133] because, during fission, they evaporate in much greater quantities than charged particles or γ quanta. For this reason, we mainly consider results obtained for prescission (evaporation from a compound nucleus) and postscission (evaporation from fission fragments) neutrons in this review. In the experimental studies of the last 10–15 years, the results obtained in on fission neutron yields, which depend on various compound-nucleus parameters, have been accumulated and systematized [104, 133–135]. Neutrons that evaporate before the compound-nucleus fission into fragments significantly affect the fission process. They reduce the excitation energy and mass of fissile nuclei and, thus, considerably complicate the fission picture. Nevertheless, various characteristics of prescission neutron multiplicity contain valuable information about fission, in particular, the mean prescission neutron multiplicity ($\langle n_{\text{pre}} \rangle$), which represents an original type of "clock" measuring the fission time. In addition, prefission neutron multiplicities can be successfully used, together with other observable quantities, for determining the important characteristic of the viscosity of nuclear matter [25, 45]. It should also be noted that it is not only mean prefission neutron multiplicities that are actively studied in experimental investigations but also their dependences ($\langle n_{\text{pre}}(M) \rangle$) on the mass and ($\langle n_{\text{pre}}(E_K) \rangle$) fission-fragment kinetic energy [133, 134, 136]. Formulating a description of these dependences within the framework of a theoretical approach for a wide range of nuclei is an extremely complicated problem.

The most complete review of experimental results concerning both prescission and postscission neutrons evaporating in fusion–fission reactions is given in [115, 133]. In particular, it was found in these studies, based on experimental investigations for a large number of nuclei, that the number of postscission neutrons increases more slowly than the number of prescission neutrons as the excitation energy increases. As was noted in [133], this result indicates that the fission process is very slow and is accompanied by a significant dissipation of the collective energy into internal energy. Consequently, almost all the initial nuclear excitation energy is transformed into internal energy and, then, is carried away by evaporating particles. Theoretical calculations generally corroborate these conclusions. For example, it was found in [130], using two-dimensional Langevin

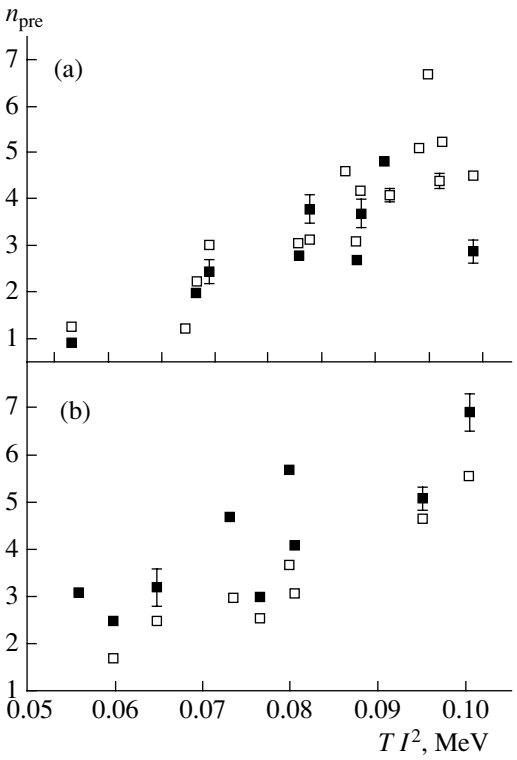

Fig. 11. Mean prescission neutron multiplicity as a function of the parameter TI^2 for nuclei (a) with $A < 224$ and (b) $A > 224$. The closed squares show the experimental data. The open squares show the results of calculations with $k_s = 0.25$.

calculations, that one-body viscosity is more suitable for reproducing the prescission neutron multiplicity while, in the case of the two-body viscosity, it is necessary to use an extraordinary high viscosity coefficient. Specifically, it is 5–10 times higher than the coefficient found in [61, 128] during study of the mean kinetic energy of fission fragments.

3.2. Prescission Neutron Multiplicities and Fission Times

A comparison of the results of calculations of the mean prescission neutron multiplicity in the three-dimensional Langevin model [19, 122] for various k_s with the experimental data are shown in Fig. 11. In this figure, the mean neutron multiplicity is shown separately for (a) light nuclei with $A < 224$ and (b) heavy nuclei. Along the abscissa axis, we plot TI^2, where $I = (N - Z)/A$. As can be seen from this figure, good agreement with the experimental data is attained with $k_s = 0.25$ for reasonably light fissile nuclei with $A < 224$ (Fig. 11a). In the case of heavier nuclei (Fig. 11b), it is necessary to set $k_s > 0.25$ to reproduce calculations of the prescission neutron multiplicity. A similar result was previously obtained in [137], where it was shown, from studying reactions resulting in the formation of heavy nuclei (with mass numbers $A_{CN} > 260$), that it is necessary to use $k_s > 4$ to reproduce experimental values of $\langle n_{pre} \rangle$. It should be noted that the results of calculations of the prescission neutron multiplicity in many respects depend on the parameters used for calculation of nuclear decay width in various channels. For example, calculation with or without consideration of the collective enhancements (and their attenuation with temperature) [107] can strongly influence the level density, and, hence, the nuclear decay width. However, there is no common opinion at present as to whether it is necessary to take into account these enhancements when realizing a dynamic simulation of nuclear decay.

Because neutron multiplicity acts as a type of clock for measuring fission time, it is interesting to compare the obtained theoretical estimates of fission times τ_f and the available experimental data. There are no direct experimental data on fission times. They are conventionally derived from prescission neutron multiplicity using model representations and can differ by an order of magnitude when using different models and sets of parameters [115, 133]. Therefore, at present it is not possible to use fission times for determining the dissipative properties of excited nuclei. However, the majority of experimental and theoretical estimates of the fission time given in [115, 133] show that itamounts to approximately 10^{-20}–10^{-18} s in a wide range of variation of the fissility parameters. As the fissility parameter decreases, the fission time increases. The results of our theoretical investigations [18, 19, 123] agree well with such behavior and values of τ_f. In Fig. 12, we show the mean fission time as a function of the parameter Z^2/A, which we obtained via Langevin calculations with the viscosity coefficient $k_s = 0.25$. In our calculations, the main contribution in τ_f is the time spent by a nucleus before reaching the saddle point, and the time of descent from the saddle point to the scission amounts to less than $(5–8) \times 10^{-21}$ s independently of the fissility parameter. In this review, we selected reactions in which strongly excited nuclei are produced for theoretical investigation. For these nuclei, the influence of shell effects on the decay process can be disregarded, and the contribution of quasifission reactions is much less than that of fusion–fission reactions.

In a recent study [138], it was found, in one-dimensional theoretical calculations, that the dependence of the fission time on the parameter Z^2/A has a peak at $Z^2/A \simeq 33$. However, we observed no such a behavior of τ_f in our calculations.

3.3. Dependence of Prescission Neutron Multiplicity on the Mass and Kinetic Energy of Fragments

The dependences of prescission neutron multiplicity on the mass and the kinetic energy of fission fragments have been experimentally investigated. These dependences provide additional information on fission. In [134], it was shown that many more neutrons are evaporated in symmetric fission events than in asymmetric

ones and that the energy of evaporating neutrons is independent of fragment masses. In addition, this tendency appeared to be almost completely independent of the mass of a fissile compound nucleus. As a result of an analysis of experimental dependences $\langle n_{\text{pre}}(M)\rangle$ taken from [133], it was established that, for the majority of the nuclei under consideration, they can be approximated with good accuracy by the parabolic law

$$\langle n_{\text{pre}}(M)\rangle = \langle n_s\rangle - c_{\text{pre}}(M_s - M)^2, \qquad (51)$$

where M_s is the fragment mass for symmetric nuclear fission and the coefficient c_{pre} characterizes the dependence of prescission neutron multiplicity on the mass asymmetry. As was noted in [133, 134], the mechanism of formation of these dependences cannot be found only from an analysis of experimental data; rather, a combined detailed investigation within the framework of both theoretical models and experimental approaches is required. In [19, 122], we succeeded in reproducing the experimentally observed parabolic dependence $\langle n_{\text{pre}}(M)\rangle$ by applying the three-dimensional Langevin calculations involving the modified variant of one-body nuclear viscosity. Examples of these dependences are shown in Figs. 13a and 14 for the ^{215}Fr and ^{205}Fr nuclei.

When explaining the parabolic shape of the dependence $\langle n_{\text{pre}}(M)\rangle$, the problem of where the neutrons evaporate becomes of fundamental importance. In Fig. 15, we show $\langle n_{\text{pre}}\rangle$ as a function of the elongation coordinate c for the ^{215}Fr and ^{256}Fm nuclei. Our calculations show that a large fraction of the neutrons (as well as other particles) evaporate from the ground-state region. Approximately 50–80% of the total number of evaporating particles are emitted before the saddle point, and approximately 10% are emitted when passing the saddle configurations, independently of the final mass asymmetry. Among all the nuclei under consideration, only in the fission of nuclei heavier than ^{256}Fm does an appreciable fraction of neutrons evaporate at the stage of descent from the saddle point to the scission. A similar result was previously obtained in [139], where it was shown that the number of neutrons evaporating during the descent from the saddle to the scission increases with an increase in excitation energy. Due to the fact that we used the modified variant of one-body nuclear viscosity corresponding to the overdamped mode in our calculations [19, 122], fissile nuclei resided for a significant period of time near the ground state before reaching the saddle-configuration region. Therefore, a large number of prescission neutrons had time to evaporate from the ground-state region before the fissile system reached the fission barrier. The kinetic energy of particles evaporating from the ground-state region is independent of the final mass asymmetry of the fission fragments because the fissile system almost totally "forgets" the dynamic evolution present in the ground-state region after overcoming the saddle-configuration region. How many particles are emitted by a nucleus from the ground-state region is reflected only by the nuclear

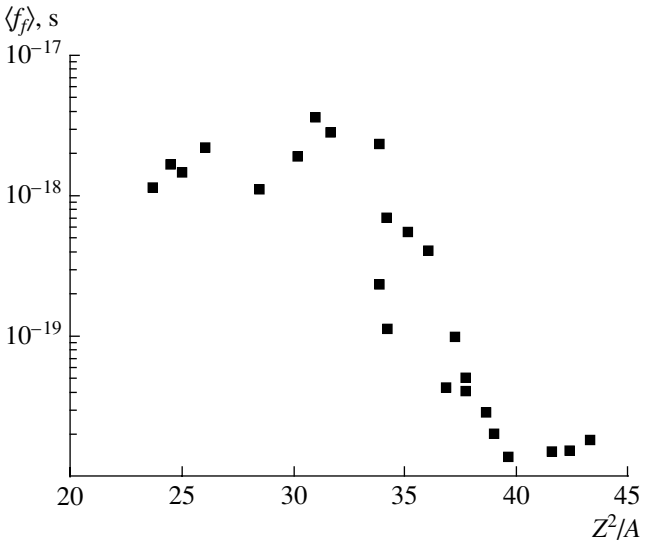

Fig. 12. Mean fission time as a function of the fissility parameter Z^2/A. The dots represent the results of calculations performed with $k_s = 0.25$.

excitation energy. Due to the random movement of Langevin trajectories in the space of collective coordinates, different trajectories reach the ridge surface at different times. Fissile nuclei, which rapidly attain the saddle-configuration region and, thereafter, evaporate a small number of neutrons, retain most of their excitation energy (a large phase volume is accessible to them during the descent from the saddle point to the scission); thus, it is possible for them to quickly reach the rupture surface and possess a high mass asymmetry. In contrast, those nuclei for which, during their evolution, a large number of particles evaporate from the ground-state region lose a significant part of their excitation energy. After passing the ridge surface, for a mass asymmetry approximately equal to zero, they are able only to descend slowly to the bottom of the liquid-drop fission valley and unable to ascend over the potential-energy surface into the large mass-asymmetry region. For such nuclei, the accessible phase volume is smaller during the descent from the saddle to the scission, and the fission time is longer in comparison with that for the nuclei that evaporate a smaller number of neutrons. Thus, it seems that nuclei that evaporate a small number of neutrons during the formation of the dependence $\langle n_{\text{pre}}(M)\rangle$ predominantly fall at the edges of the mass distribution. All nuclei evaporating an arbitrarily large number of prescission particles and, thus, overcoming the ridge surface can fall in a mass-asymmetry region approximately equal to zero. Therefore, it is found that the mean neutron multiplicity is lower at the edges of the mass distribution than it is near the zero mass asymmetry. In Fig. 13b, we show the calculated mean time necessary for fissile nuclei to attain the rupture surface as a function of the fragment mass. Figure 13b shows that the fission times differ by almost a factor of 2 for

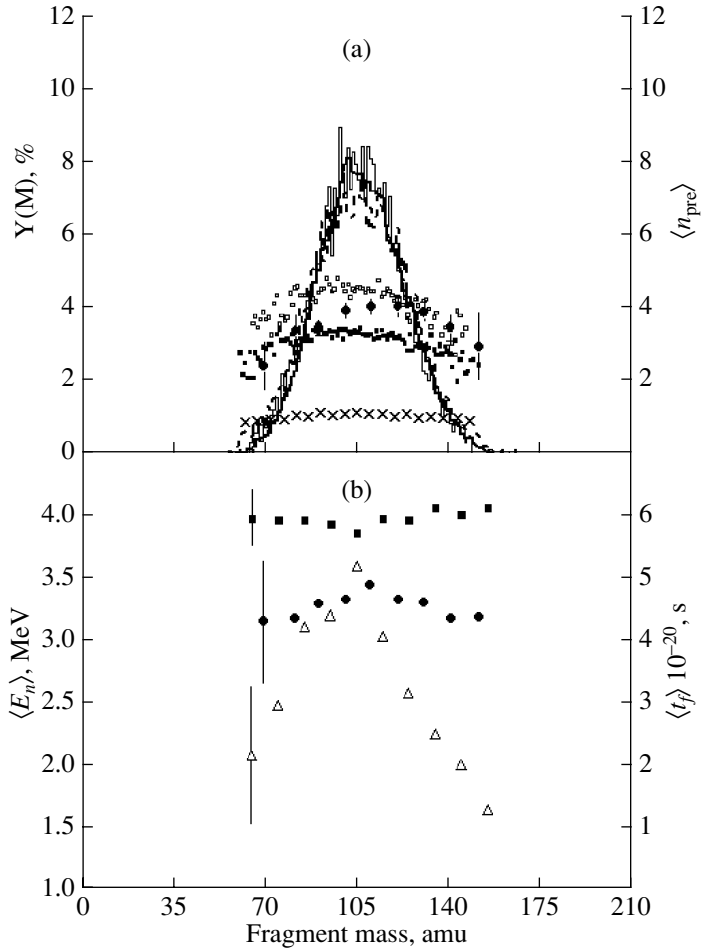

Fig. 13. Experimental data and results of calculations for the reaction $^{18}O + ^{197}Au \longrightarrow ^{215}Fr$ ($E_{l.s}$ = 158.8 MeV) [134]. (a) The mass distribution: the thick solid line shows the experimental data [134] and the thin solid line and dashed lines show the results of calculations with $k_s = 0.5$ and 0.25, respectively. The neutron multiplicity as a function of the fragment mass: the closed circles show the experimental data [134]; the closed squares and open squares show the results of calculations with $k_s = 0.25$ and 0.5, respectively; and the crosses show the results of calculations under the condition that neutron evaporation takes place only during the descent from the saddle to the scission point ($\langle n_{pre}^{gs} \rangle = 0$). (b) The kinetic energy of neutrons as a function of the fragment mass: the closed circles show the experimental data from [134] and the closed squares show the result of calculations with $k_s = 0.5$. The triangles show the fission time calculated with $k_s = 0.5$.

symmetric and asymmetric nuclear fission. Thus, we concluded in [19, 122] that the final mass asymmetry and nuclear fission time depend on the prehistory of the fission's dynamic evolution in the ground-state region. The smaller the number of particles that evaporate from a nucleus in the ground state region, the higher the probability of an event in which a nucleus rapidly reaches the rupture surface for a large mass asymmetry.

It should be noted that the parabolic shape of the dependence $\langle n_{pre}(M) \rangle$ is not characteristic for all the reactions under consideration. For example, in our calculation, we found that the calculated coefficients c_{pre} show a very weak parabolic dependence $\langle n_{pre}(M) \rangle$ for heavy ^{252}Fm and ^{256}Fm nuclei. This result follows from the fact that these nuclei have a very high excitation energy, a small barrier, and are quickly disintegrated. The evaporation of light prescission particles does not for long enough to considerably decrease the excitation energy of these nuclei. Consequently, almost all fissile nuclei have an equally large available phase space during the descent from the saddle to the scission. In this context, the approximately one order of magnitude difference between the experimental data on c_{pre} for ^{252}Fm and ^{256}Fm remains inexplicable in terms of theoretical calculations with $k_s = 0.25$–0.50.

Furthermore, no parabolic dependence $\langle n_{pre}(M) \rangle$ is observed for during fission of the ^{205}Fr nucleus. Because this nucleus is strongly neutron-deficient, one neutron, on average, has time to evaporate before the nucleus decays into fragments. Thus, when simulating ^{205}Fr decay, all the fissile nuclei are assumed to have an approximately identical excitation energy (an identical

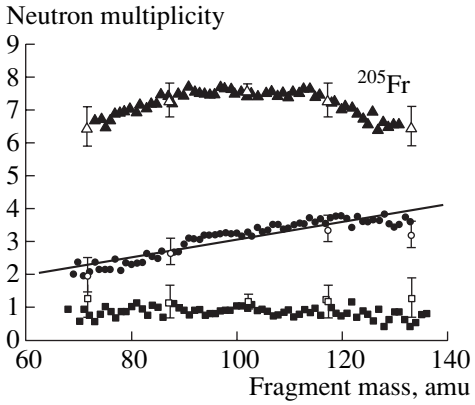

Fig. 14. Experimental data and results of calculations for the reaction ^{36}Ar + ^{169}Tm ⟶ ^{205}Fr ($E_{l.s}$ = 205 MeV) [136]. The open symbols represent the experimental data from [136] and the closed symbols show the results of calculations with k_s = 0.5. The squares represent the prescission neutron multiplicity; the circles, the postscission neutron multiplicity; and the triangles; the total neutron multiplicity.

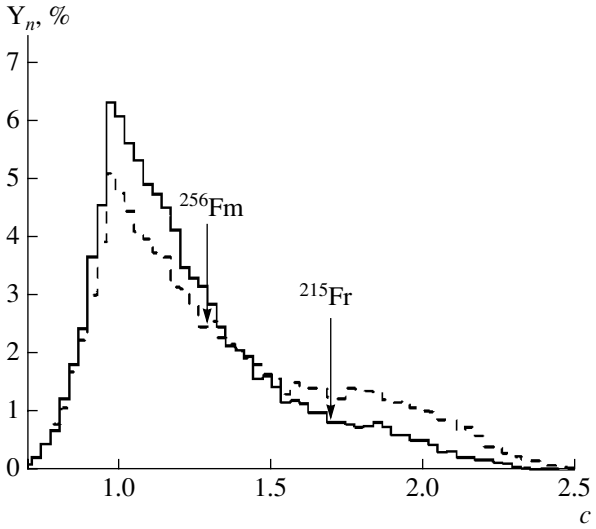

Fig. 15. Calculated prescission neutron yield (as a percentage of the total number) as a function of the elongation coordinate c for the ^{215}Fr (solid curve) and ^{256}Fm (dotted curve) nuclei. The arrows indicate the saddle point position.

available phase space), since the evaporation of prescission particles is the only factor that can change the excitation energy of nuclei. Therefore, there is no parabolic dependence $\langle n_{pre}(M)\rangle$ for ^{205}Fr.

A short time ago, in [140], an attempt to provide a theoretical description of the experimentally observed dependence $\langle n_{pre}(M)\rangle$ was undertaken within the two-dimensional dynamic model based on the classical Euler–Lagrange equations. In the calculations [140], a combination of one-body and two-body viscosities was used. It was ascertained that the viscosity may be dramatically reduced by multiplying the friction-tensor components by $\exp(-K * \alpha * \alpha)$, where $K = 161 \pm 3$, depending on the mass-asymmetry coordinate for the reproduction of the experimentally observed dependence $\langle n_{pre}(M)\rangle$. At the same time, it follows from the calculations in [19, 122] that it is feasible to quantitatively reproduce the dependences $\langle n_{pre}(M)\rangle$ observed under experimental conditions well for many nuclei without introducing additional free parameters in the model. Unfortunately, the calculations in [140] yielded no data on the number of neutrons that evaporate before attaining the saddle point or during the descent from this point to the scission. Therefore, a detailed comparison between the results in [19, 122] and [140] is difficult.

The experimentally observed dependence $\langle n_{pre}(E_K)\rangle$ [136] shows a significant increase with E_K. After applying a recalculation procedure to these results that takes into account recoil effects [134], $\langle n_{pre}(E_K)\rangle$ actually ceases to depend on E_K. In our calculations, $\langle n_{pre}(E_K)\rangle$ and $\langle t_f(E_K)\rangle$ appeared to be almost independent of E_K within the calculation error, and only in the region of low E_K was a small decrease in the dependences $\langle n_{pre}(E_K)\rangle$ and $\langle t_f(E_K)\rangle$ (see Fig. 16) observed. Such a decrease can be explained by the steadily increasing contribution of events with a large mass asymmetry as E_K decreases, which follows from the general character of the two-dimensional MED. It should also be noted that these calculations, which were performed using the modified variant of one-body viscosity, reproduce the shape of the dependence $\langle n_{pre}(E_K)\rangle$ more satisfactorily than calculations within the two-dimensional model [120] including two-body viscosity.

3.4. Postscission and Total Neutron Multiplicities

The evaporation of postscission neutrons weakly affects the observed fission characteristics, for example, the mass–energy distribution of fission fragments. However, postscission particles emitted from fission fragments carry important information about the fission process because the postscission neutron multiplicities provide data on the critical stage of evolution of a fissile nucleus, i.e., on the rupture of a continuous configuration into fragments. At the instant of separation of a continuous shape into fragments, the excitation energy possessed by a compound nucleus before the scission is distributed between the formed fragments. Thus, the postscission particle multiplicities include information about the instant of scission of a compound nucleus and characterize its excitation energy at the instant of fission into fragments. It is also necessary to emphasize that the correlation dependences of the total neutron multiplicity on the mass and kinetic energy of fission fragments can considerably differ from the correlation dependences of prefission neutron multiplicities [133]. This difference is defined by the postscission neutron multiplicity. Therefore, a simultaneous description of

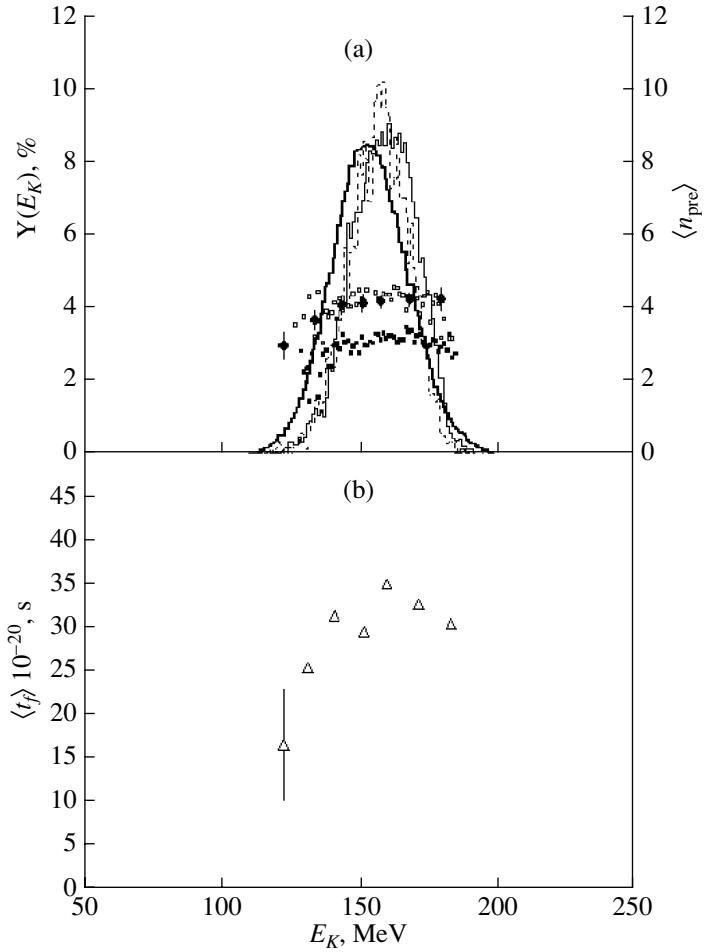

Fig. 16. Experimental data and results of calculations for the reaction $^{18}O + ^{197}Au \longrightarrow ^{215}Fr$ ($E_{l.s}$ = 158.8 MeV) [134]. (a) The energy distribution: the thick solid line shows the experimental data from [134], and the thin solid and dashed lines represent the results of calculations with $k_s = 0.25$ and 0.5, respectively. The neutron multiplicity as a function of the fragment kinetic energy: the closed circles show the experimental data from [134]; the closed squares and open squares show the results of calculations with $k_s = 0.25$ and 0.5, respectively; and (b) the triangles represent the fission time calculated with $k_s = 0.5$.

the correlation dependences of prefission, postscission, and total neutron multiplicities is a serious test for theoretical models. However, a consistent description of these correlation dependences would provide information on how the fission process proceeds, from the stage of compound-nucleus formation to the separation of fragments.

In order to calculate the postscission neutron multiplicity, it is necessary to know the excitation energy of the fragments formed after compound-nucleus fission. In this case, it is usual to assume that the compound-nucleus temperatures before the scission and the fragment temperatures immediately after the scission are equal. In addition, it is conventional to apply the law of conservation of energy, which can be written as [123]

$$Q_f + E_{\rm coll}(t_{\rm sc}) - V(\mathbf{q}_{\rm sc}) - E_K = E^{(1)}_{\rm def} + E^{(2)}_{\rm def}. \qquad (52)$$

Here, Q_f is the reaction energy, which is calculated as the difference between the masses of a compound nucleus and the formed fragments; $E_{\rm coll}(t_{\rm sc})$ and $V(\mathbf{q}_{\rm sc})$ are the collective-motion energy and potential energy at the instant of scission of a nucleus into fragments; E_K is the kinetic energy of motion of the fragments; and $E^{(1)}_{\rm def}$ and $E^{(2)}_{\rm def}$ are the deformation energies of the fragments. The condition that the system maintains a constant temperature before its fission into fragments and the energy conservation law make it possible to determine the internal excitation energy of the formed fragments and their total deformation energy but render it impossible to calculate the deformation energy for each fragment. Therefore, when describing the shape of fragments using several independent parameters, it is necessary to include additional conditions to attain an unambiguous definition of the deformation energy of these fragments. These conditions are as follows: the condition of conservation of the lowest moments of the nuclear-density distribution during fission of an initial compound

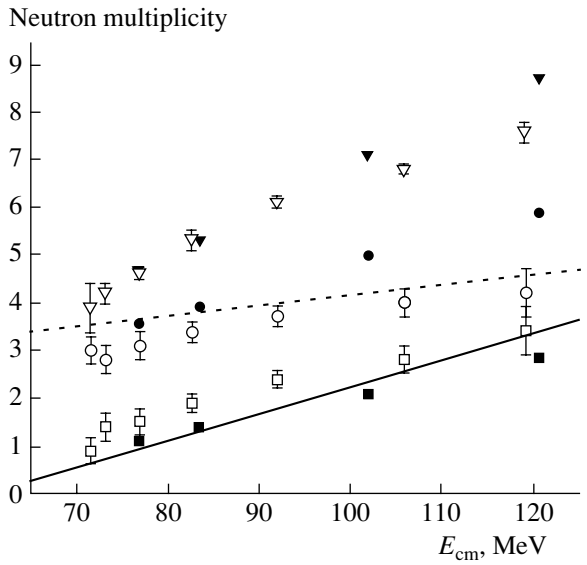

Fig. 17. Mean prefission (squares) and postscission (circles) neutron multiplicities and the total neutron multiplicity (triangles) as functions of the excitation energy for the ^{224}Th nucleus. The open symbols represent the experimental data from [196] and the closed symbols represent the results of calculations with $k_s = 0.5$. The solid and dotted lines show the approximations of prescission and postscission neutron multiplicities proposed in [143, 144].

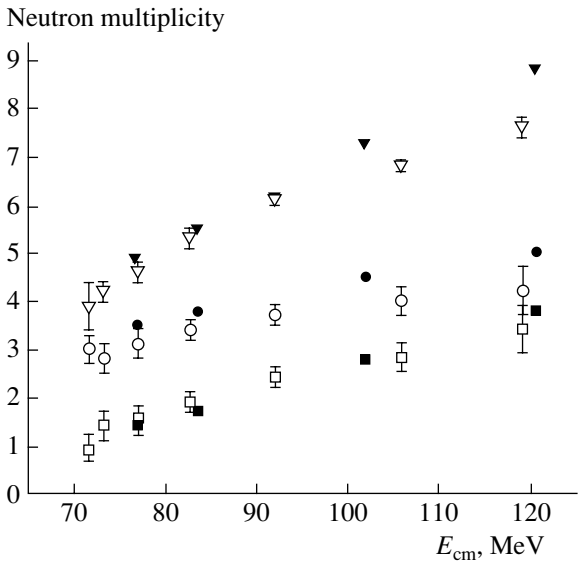

Fig. 18. The same as in Fig. 17. The values are calculated with $k_s = 1$.

nucleus [141] or the condition of maximum entropy of a system consisting of two fragments [142]. Because the energy conservation law in the form of Eq. (52) is satisfied for an arbitrary way of distributing the deformation energy between fragments, the mean postscission neutron multiplicities are virtually identical despite the additional conditions used for finding the deformation energy of each fragment. As a result, calculations [123, 142] performed using various methods of determining the deformation energies of fragments lead to approximately identical results on the mean postscission neutron multiplicities. The use of various conditions for determining the deformation energies of fragments affects only the dependences of postscission neutrons on the mass and kinetic energy of the fragments.

In Figs. 17 and 18, we show the results of calculations of the mean multiplicities for prefission and postscission neutrons and, in addition, the total neutron multiplicity depending on the initial excitation energy of the compound nucleus for the reaction $^{18}O + {}^{208}Pb \longrightarrow {}^{224}Th$ (E_{lab} = 130, 110, 90, and 83 MeV).

In these figures, the solid and dotted lines show the approximation of the prescission and postscission neutron multiplicity proposed in [143, 144]. From a comparison between Figs. 17 and 18, it can be seen that, depending on the value of viscosity, the number of neutrons evaporating from a compound nucleus and its fragments is different; moreover, the results of calculations of the total neutron multiplicity are actually independent of the viscosity, as can be expected for physical reasons. With an increase in the viscosity, the number of particles evaporating from a compound nucleus increases and its internal excitation energy and, consequently, the internal excitation energy of the fragments decreases.

Experimental data and our theoretical calculations [123] performed with the one-body mechanism of nuclear viscosity show that, as the excitation energy increases, the mean postscission neutron multiplicity increases more slowly than the prefission neutron multiplicity. Such a result is valid for $k_s > 0.5$. For $k_s = 1$ (see Fig. 18), the postscission neutron multiplicity depends very weakly on the excitation energy and the calculated values of mean postscission neutron multiplicity are in good agreement with the experimental data. This result confirms the conclusion made in [133], on the basis of an analysis of a large amount of experimental data, that, at the instant of scission, a nucleus is relatively cold; i.e., a significant portion of the excitation energy of a compound nucleus is carried away by prefission neutrons before compound-nucleus fission into fragments.

Investigation of the correlation dependences $\langle n_{post}(M)\rangle$ and $\langle n_{post}(E_K)\rangle$ of the postscission neutron multiplicity on the mass of fragments and their kinetic energy, respectively, is also of interest. The calculated dependences $\langle n_{post}(M)\rangle$ and $\langle n_{post}(E_K)\rangle$ for the ^{205}Fr nucleus are shown in Figs. 14 and 19.

As can be seen from Fig. 14, $\langle n_{post}(M)\rangle$ is a virtually linear dependence on M. This type of dependence is a consequence of the fact that the internal energy E_{int} of a compound nucleus before scission is virtually independent of the mass of the formed fragments and E_{int} is distributed between the fragments proportionally to their masses during the separation of a compound nucleus.

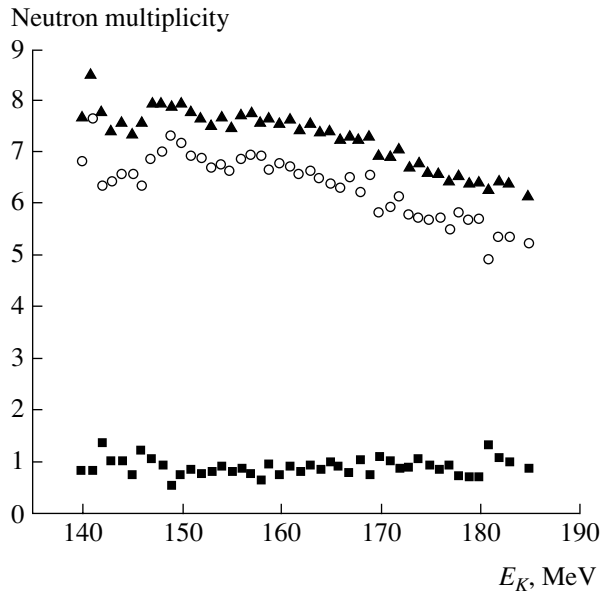

Fig. 19. Neutron multiplicities as functions of the fragment kinetic energy for the ^{205}Fr nucleus calculated with $k_s = 0.5$. The closed squares show the prefission neutron multiplicity, the open circles represent the postscission neutron multiplicity, and the closed triangles refer to the total neutron multiplicity.

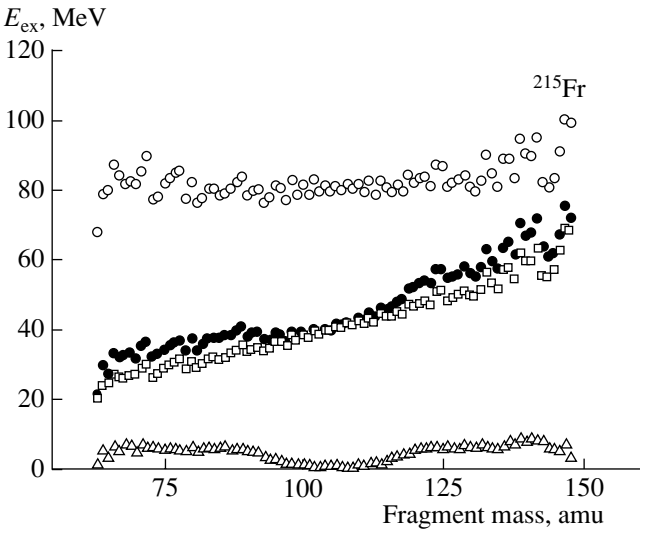

Fig. 20. Fragment excitation energy E_{ex} (closed circles) for the ^{215}Fr nucleus as a function of the fragment mass. The open circles represent the internal excitation energy of a compound nucleus before scission. The open squares and triangles show the internal excitation energy and deformation energy of the fragments, respectively.

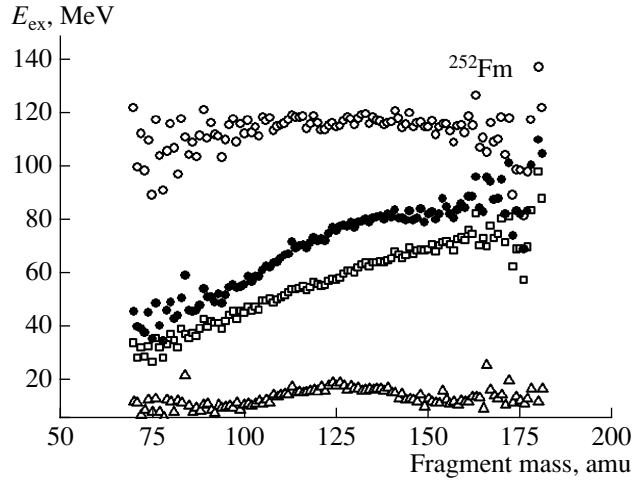

Fig. 21. The same as in Fig. 20 but for the ^{252}Fm nucleus.

As can be seen from Figs. 20 and 21, the internal energy of the fragments considerably exceeds their deformation energy in the case of high viscosity, thus determining the general character of the dependence $\langle n_{post}(M)\rangle$.

In Figs. 20 and 21, it can be also seen that the deformation energy of the fragments nonlinearly depends on their mass. Such a type of dependence is mainly specified by the behavior of Q_f in Eq. (52), for which tabulated values of the nuclear masses [145] were used in the calculation. For fissile nuclei from ^{170}Yb to ^{258}Fm, the filling of a shell with $Z = 50$ and $N = 82$ fundamentally affects $Q_f(M)$. In this case, a pronounced peak reveals itself at $M \simeq 132$ up to At in the dependence $Q_f(M)$. For lighter fissile nuclei, the $Q_f(M)$ peak is shifted to $M \simeq A_{CN}/2$. Correspondingly, as can be seen from Figs. 20 and 21, the peaks of the deformation energy can fall for both symmetric fission, as in the case of ^{256}Fm, and asymmetric fission, as in the case of ^{215}Fr. Thus, the deformation energy of the fragments specifies the deviation of the total fragment excitation energy from linear dependence on M. A similar result was previously obtained in [142] for the reaction ^{4}He + ^{209}Bi $\longrightarrow$ ^{213}At (E_{lab} = 45 MeV), where the deformation energy was calculated using the maximum-entropy condition on the system of fragments.

It is convenient to approximate the dependence of the total neutron multiplicity $\langle n_{tot}(M)\rangle$, as well as $\langle n_{pre}(M)\rangle$, by a parabolic dependence on M with the coefficient c_{tot}. Naturally, the closer the dependence $\langle n_{post}(M)\rangle$ is to a straight line, the less the coefficient c_{tot} differs from c_{pre}. When the dependence $\langle n_{post}(M)\rangle$ is represented by a straight line, c_{tot} should be equal to c_{pre}. As the calculations show, the difference between $\langle n_{post}(M)\rangle$ and a straight line generally depends on the deformation energy, which mainly depends on $Q_f(M)$. Therefore, if $Q_f(M)$ peaks for symmetric fission, $c_{tot} > c_{pre}$; otherwise, $c_{tot} < c_{pre}$. This effect most strongly manifests itself in ^{205}Fr fission (see Fig. 14) for which the prefission neutron multiplicity is actually independent of mass. In this case, the total multiplicity has an explicit parabolic dependence on the fragment mass due to the postscission neutron multiplicity. The dependence $\langle n_{post}(M)\rangle$ produces the opposite effect in ^{215}Fr fission, reducing the coefficient c_{tot} in comparison with c_{pre}.

Table 4. Characteristics of compound-nucleus fission

CN	E^* (MeV)	k_s	c_{pre} 10^{-4}	c_{tot} 10^{-4}	$\frac{dn_{post}}{dM}$ 10^{-2}	$-\frac{dn_{tot}}{dE_K}$ (MeV^{-1})	$\langle n_{pre}\rangle$	$\langle n_{post}\rangle$	$\langle n_{tot}\rangle$
^{162}Yb	114	0.25	8	–1	3.2	0.054	1.8	2.6	7
		0.5	11	–3	2.7	0.058	2.4	2.3	7
Expt. [134]			12	1	3.5	–	2.45	1.7	5.85
^{172}Yb	121	0.25	20	12	3.6	0.038	3.4	3	9.4
		0.5	32	8	2.7	0.052	4.5	2.4	9.3
Expt. [134]			14	10	3.6	0.056	4.4	2	8.4
^{205}Fr	77	0.25	1.3	8	2.6	0.039	0.4	3.4	7.2
		0.5	1.9	11	2.7	0.041	0.9	3.2	7.3
Expt. [136]			0	9.5	1.8	0.046	1.2	–	–
^{215}Fr	111	0.25	5.1	4.8	4.3	0.037	3	3.2	9.4
		0.5	7.1	6	4.1	0.041	4.3	3	10.3
Expt. [134]			6.5	4.4	3.8	0.047	4.1	2.7	9.5
^{256}Fm	101	0.25	1.6	6.6	4.3	0.046	2	6.2	15.5
		0.5	3.6	6.5	4.1	0.066	3.1	5.8	14.7
Expt. [134]			8.2	5.4	4.1	–	5.1	4.25	13.6
^{252}Fm	140	0.25	2.7	2.2	5.4	0.052	2.7	7	16.7
		0.5	3.6	4	4.8	0.061	4.0	6.5	17
Expt. [146]			0	2.4	5	–	6.95	3.83	14.6

Note: The following are the full forms of the notation used in the table: compound nucleus (CN); compound-nucleus excitation energy (E^*); the reduction coefficient (k_s) of the wall-formula contribution; the coefficients (c_{pre}) and (c_{tot}) of the parabolic mass dependence for the prefission and total neutron multiplicities, respectively; the coefficients ($\frac{dn_{post}}{dM}$) and ($-\frac{dn_{tot}}{dE_K}$) of the linear kinetic-energy and mass dependences, respectively, for the postscission neutron multiplicity; the mean prefission, postscission, and total neutron multiplicities ($\langle n_{pre}\rangle$), ($\langle n_{post}\rangle$), and ($\langle n_{tot}\rangle$), respectively.

The calculated and experimental dependences $\langle n_{post}(E_K)\rangle$ for ^{205}Fr are shown in Fig. 19. As can be seen from this figure and Table 4, the multiplicities $\langle n_{post}(E_K)\rangle$ and $\langle n_{tot}(E_K)\rangle$ decrease with an increase in E_K, and such behavior agrees well with the available experimental data. The decrease in the multiplicity $\langle n_{post}(E_K)\rangle$ as E_K increases follows from the law of conservation of energy in the form of Eq. (52). With an increase in E_K, the total excitation energy of the fragments decreases (for a fixed ratio between the fragment masses) and, consequently, the mean postscission neutron multiplicities decrease as well. The total neutron multiplicity also decreases with an increase in E_K because the prefission neutron multiplicity weakly depends on E_K.

3.5. Fission Probability

As was noted above, the evaporation of prescission particles reduces the excitation energy and, thus, competes with the fission process. If the nuclear excitation energy proves to be lower than the fission barrier during particle evaporation, a nucleus becomes an evaporation residue. Along with the prescission particle multiplicities, the cross section for evaporation residues (or fission probability) is an important characteristic, which can be compared with experimental data, and depends on both the parameters used in the statistical model of nuclear decay and the viscosity of nuclear matter.

In dynamic approaches, data on the prescission neutron multiplicity and evaporation probabilities are conventionally used for deriving information about the fission time and nuclear viscosity. Significant successes in describing $\langle n_{pre}\rangle$ and the fission probability P_f were attained in the one-dimensional Langevin model proposed by the Gontchar and Fröbrich group [26]. In order to attain a simultaneous description of the data on $\langle n_{pre}\rangle$ and P_f, it was necessary to introduce the new universal dependence of the reduced friction parameter β on the fission coordinate: $\beta = 2 \times 10^{21}$ s for compact nuclear shapes (such a low value of the parameter β results in a high fission probability). From the instant at which a neck occurs to the instant of scission, β linearly

increases to 30×10^{21} s, which provides a good description of the mean prescission neutron multiplicity.

Further study of the fission probability within the multidimensional Langevin approaches, together with other observed quantities (in particular, the MED parameters of fission fragments), is undoubtedly of interest.

In [47], the two-dimensional Langevin model was used to simultaneously calculate three observed quantities: the prescission neutron multiplicity, fission probability, and variance of the mass distribution. In this study, two sets of coefficients were used for the level-density parameter: those of Ignatyuk *et al.* [69] and those of Töke and Swiatecki [71]. In addition, the potential energy was calculated using two variants of the liquid-drop model: one with a sharp-edge and the other with a diffuse-edge nuclear surface. The influence of the choice of LDM variant and coefficients for calculating the level-density parameter on the obtained values of observed quantities was analyzed. Similarly to the results of [19, 67], it was found in [47] that the use of the level-density parameter proposed by Töke and Swiatecki allowed the authors to better describe the fission probability. In contrast, experimental values of the mean prescission neutron multiplicity were more satisfactorily reproduced with the coefficients of Ignatyuk *et al.*

In [19, 123], on the basis of the three-dimensional Langevin calculations, we showed that the fission probability (the evaporation-residue cross section σ_{ER}) is extremely sensitive to nuclear viscosity, especially in the low-energy range where $\langle n_{pre} \rangle$ weakly depends on the dissipative force. Thus, at low excitation energies, σ_{ER} is an important experimentally observed characteristic that should be included in investigations of the problem of nuclear dissipation. A similar conclusion on the sensitivity of evaporation-residue cross sections was made in [147] on the basis of results of one-dimensional calculations. Furthermore, in [19, 123], we found that good quantitative agreement with the experimental data on σ_{ER} was attained at $k_s = 0.25$–0.50. However, calculations executed with the total one-body viscosity ($k_s = 1$) considerably overestimate the data on evaporation residues.

It is also of interest to gage the influence of the use of the free-energy thermodynamic potential, instead of the potential energy, for determining the conservative force. Our calculations [19] showed that replacement of the driving potential $V(\mathbf{q})$ by $F(\mathbf{q})$ reduces the prescission neutron multiplicity and the fraction of evaporation residues. This result is obtained because the use of free energy makes the fission barrier lower, the mean fission time decrease, and, hence, the mean prescission neutron multiplicity decrease and the fission probability increase.

For superheavy nuclei, theoretical investigation of the fission probability has gained in importance due to recent experiments on the synthesis and study of various characteristics of new superheavy elements. However, the theoretical calculations for reactions resulting in the formation of superheavy elements now face serious problems. Primarily, these problems are associated with large uncertainty in relation to the statistical-model parameters in the heavy-nuclei region. The process of formation of heavy compound nuclei includes various stages such as the fusion of heavy ions and the formation and decay of a compound system. To describe each stage of the process is rather difficult in itself, and the results obtained also strongly depend on the parameters and approximations used. However, significant progress has recently been achieved in this line of research due mainly to the steady development of theoretical approaches and models such as the coupled channel method [148, 149] and the Langevin dynamic models for description of the fusion of ions and the evolution of a compound system [22, 24].

4. CHARGE DISTRIBUTION OF FISSION FRAGMENTS

The charge mode is related to the transfer of nucleons between fragments and strongly differs from the previously considered collective modes of describing variation in nuclear-surface shape. The principal difference between these modes consists in the different ratio between the relaxation times of collective and single-particle modes and between the relaxation times of collective modes and the mean time τ_{ss} of descent of a fissile nucleus from the saddle to the instant of scission. As is known, the charge degree of freedom is very fast in the sense that the relaxation time of a charge is much shorter than τ_{ss} and comparable with the relaxation time of internal degrees of freedom. The relaxation times of the collective modes determining nuclear shape are of the same order of magnitude as the descent time [150].

First, such a ratio between the times makes it possible to consider the charge collective coordinate and nuclear-shape coordinates as independent. Second, because the charge mode is fast, the statistical model should provide a good description of the properties of the charge distribution of fragments. This assumption has been confirmed in a number of theoretical and experimental investigations of the charge distribution in the low-excitation energy range and makes dynamic study of charge fluctuations a valuable source of information on the properties of nuclear matter, in particular, on nuclear viscosity. Indeed, the experimental situation is already understood: at the instant of scission of a nucleus into fragments, an instantaneous statistical limit [20, 151] is established in the charge mode. Finally, because the characteristic times of an internal subsystem and the charge degree of freedom are not very far from each other in the time scale, it is not certain that the Langevin approach (in particular, the Langevin approach used within the Markovian approximation) can be applied to a description of such a fast mode as the charge mode.

4.1. Features of the Model Describing Charge Fluctuations

In order to study the charge distribution of fission fragments within the Langevin approach, it is necessary to introduce a coordinate determining the charge partition between fragments. It is convenient to use the parameter $\eta_Z = (Z_R - Z_L)/(Z_R + Z_L)$, where Z_R and Z_L are the charges of the right-hand and left-hand fragments, respectively, for this coordinate. The coordinate η_Z has frequently been used as the charge coordinate [152, 153] and, in our opinion, is the most convenient. Consideration of asymmetric fission is of minor interest from the standpoint of studying charge fluctuations and, in addition, results in significant complication of the model. For this reason, in [20, 151], we considered the case of symmetric fission, which enabled us to introduce just three collective coordinates: two coordinates to describe nuclear shape in terms of the $\{c, h, \alpha\}$ parametrization (an elongation c and a neck coordinate h) and the charge-asymmetry coordinate η_Z. When restricting the analysis to the case of symmetric fission ($\alpha = 0$), it should be remembered that the model can also be generalized to the case of asymmetric shapes.

In [20, 151], set of three-dimensional Langevin Eqs. (14) serves as a set of equations of motion. At the same time, because the charge mode is a finite mode, it is necessary to use the effective temperature T_Z^* [154], which takes into account quantum vibrations in the charge coordinate, instead of the temperature T for determining random-force amplitude from the coordinate η_Z (see Eqs. (16) and (17)):

$$T_Z^* = \frac{\hbar\omega_Z}{2}\coth\left(\frac{\hbar\omega_Z}{2T}\right). \tag{53}$$

Here, ω_Z is the frequency of vibrations in η_Z. We note that, in contrast to the charge distribution, it is unnecessary to introduce an effective temperature into the mass-asymmetry coordinate when studying the mass distribution (at least at $T > 1$ MeV) due to the smallness of the vibration frequencies for this collective mode in comparison with the thermostat temperature T [13]. In this case ($T \gg \hbar\omega_A/2$, where ω_A is the frequency of vibrations in the mass coordinate), the effective temperature T_A^* is approximately equal to the temperature T.

It is obvious that considering the charge transfer between fragments is meaningful only if it is possible to unambiguously separate one fragment from another. Therefore, in the dynamic calculations described in [20, 151], evolution of the charge degree of freedom began when a neck appeared in a nucleus, while only the coordinates determining nuclear-surface shape evolved for shapes without a neck. For the ^{236}U nucleus, chosen for the calculations, the neck appears after the nucleus passes the ridge separating the ground-state region from the fission valley. Therefore, the question arises as to whether it is expedient to begin dynamic calculations from the ground state instead of, for example, the ridge line. The reason for this choice of initial conditions is obvious. In [19, 122], we showed that an overwhelming prescission neutron fraction (more than half) evaporates in the ground-state region before a nucleus attains the ridge. Thus, for the correct account of neutron evaporation, it is necessary to begin dynamic calculations from the ground state of a compound system. In addition, when discussing methods of calculating the potential energy and the transport coefficients of the charge mode, we assumed that there is a bridge in the nuclear shape.

4.1.1. Potential energy. When calculating the potential energy within the liquid-drop model, the charge density is usually assumed to be constant throughout a nucleus. However, it is obvious that, due to the Coulomb repulsion of protons, the nucleons in a nucleus are redistributed so that the charge density becomes higher at the periphery and lower inside the nucleus. The simplest solution to the problem on the type of charge-density function was proposed in [51, 155], where the charge density was approximated by a linear function of the coordinate z (along the symmetry axis). The problem of the charge distribution in a nucleus was investigated in detail using variational methods in [32, 156], and two liquid-drop models were used in [32]. From the experimental data on the charge distribution [157–159], it is possible to draw the conclusion that the polarizability of nuclear matter is negligible. Therefore, when performing Langevin calculations of the charge distribution in [20, 151], we assumed that the charge density is different but constant inside each future fragment [32, 160]. Such an approximation of the charge density is rather rough, but, at the same time, it meant that we did not have to introduce any additional parameters (for example, the charge-polarization parameter [51, 155]) and, using reasonably simple formulas, it allowed us to describe the charge partition between fragments.

Using the condition of incompressibility of nuclear matter, it is possible to show that the proton densities ρ_R^p and ρ_L^p in the formed fragments are related to the charge coordinate η_Z in the following way:

$$\begin{aligned}\rho_R^p &= \rho_0^p\frac{(k+1)}{2k}(1+\eta_Z),\\ \rho_L^p &= \rho_0^p\frac{(k+1)}{2}(1-\eta_Z).\end{aligned} \tag{54}$$

Here, $\rho_0^p = Z/(4/3\pi R_0^3)$ and $\rho_0^n = N/(4/3\pi R_0^3)$ are the densities of protons and neutrons, respectively, for a uniform charge distribution over the entire nucleus and $k = A_R/A_L$ is the mass ratio for the formed fragments. From Eqs. (54), the corresponding neutron densities ρ_R^n and ρ_L^n are easily expressed.

In the sharp-edge LDM taking the charge degree of freedom into account, the potential energy is formed as a sum of the symmetry energy, the Coulomb and surface energies, and the energy of the rotation of a nucleus as a whole. Calculation of the Coulomb energy is essentially simplified for a homogeneous charge distribution in each fragment and, for the dependence of the potential energy on the charge-asymmetry parameter η_Z, can be expressed as

$$V(\mathbf{q}, \eta_Z) = V(\mathbf{q}, \langle\eta_Z\rangle) + \frac{C_{\eta_Z}(\mathbf{q})}{2}(\eta_Z - \langle\eta_Z\rangle)^2 \quad (55)$$

(here and below, $\mathbf{q} = (c, h)$). The mean value of the charge-asymmetry parameter $\langle\eta_Z(\mathbf{q})\rangle$ is the point of a local minimum of the potential energy for these shape parameters (c, h). In the case of symmetric fission, $\langle\eta_Z\rangle = 0$. The coefficient of rigidity of the potential relative to the parameter η_Z is $C_{\eta_Z}(\mathbf{q}) = (\partial^2 V(\mathbf{q}, \eta_Z)/\partial\eta_Z^2)_{\eta_Z = \langle\eta_Z\rangle}$. The expression for the coefficient of rigidity can be found, for example, in [20, 32, 160, 161]. The coefficient of rigidity of the potential on the charge coordinate weakly depends on the nuclear deformation, since the main contribution is due to the symmetry energy. In its order of magnitude, $C_{\eta_Z} = (7\text{–}8) \times 10^3$ MeV [20, 151].

4.1.2. Inertial parameter of the charge mode. An important problem in nuclear dynamics is calculation of the transport coefficients. For the charge problem, calculation of the transport coefficients is complicated because two collective coordinates describe nuclear-shape variation while the third coordinate (η_Z) describes the charge redistribution in a nucleus and has quite a different physical nature from the shape coordinates. Therefore, different models are necessary when describing the charge component and all the other components of the mass tensor and friction tensor.

We now discuss the method of calculation of the charge-mode mass parameter $m_{\eta_Z\eta_Z}$. In [161], we found the mass parameter from the formula

$$m_{\eta_Z\eta_Z}(\mathbf{q}) = \frac{C_{\eta_Z}(\mathbf{q})}{\omega_1^2(\mathbf{q})}, \quad (56)$$

where ω_1 is the frequency of the longitudinal dipole isovector vibrations obtained from the solution to the Helmholtz equation for charge-density fluctuation [162, 163].

In [164], in the case of a nonviscous-fluid flow through a round aperture of radius r_N connecting two touching spherical fragments, the following expression was obtained for the charge-mode inertial parameter:

$$m_{\eta_Z\eta_Z}(\mathbf{q}) = \frac{\pi}{6} r_0^3 m \frac{ZA^2}{N} \frac{1}{r_N}. \quad (57)$$

Here, m is the nucleon mass.

When deriving Eq. (57), the fact that the neck connecting the fragments has a nonzero length was completely disregarded. In addition, viscosity plays an important role in the Langevin approach. In [165], it was shown that, for the flow of a viscous incompressible fluid through a cylindrical neck of radius r_N and length l_N, the charge-mode mass parameter is described by the expression

$$m_{\eta_Z\eta_Z}(\mathbf{q}) = \frac{m}{3\pi\rho} \frac{ZA^2}{N} \frac{(l_N + 2r_N)}{r_N^2}, \quad (58)$$

where ρ is the nucleon density in a nucleus.

A comparison between the results given by Eqs. (56)–(58) is shown in Fig. 22a for the parameter $h = 0$ (as the line $h = 0$ approximately corresponds to the bottom of the fission valley [33]). The mass-parameter values for Eq. (56) are taken from [161], in which the mass parameter is given as a function of the spacing between the centers of mass of future fragments for several fixed values of the neck parameter h. The mass-parameter values given in this figure correspond to a large value of the elongation parameter c in the nuclear-deformation region from the saddle point to the scission. All three dependences show a characteristic sharp increase in the inertial parameter $m_{\eta_Z\eta_Z}$ when approaching the scission point. From this figure, it can also be seen that Eqs. (56) and (58) yield close values of $m_{\eta_Z\eta_Z}$ while those calculated from Eq. (57) lie much lower.

Equation (56) is the most consistent; however, calculation of the frequencies of dipole isovector vibrations result in a mathematical problem that is rather difficult to realize. From an analysis of the three equations written above, it follows that Eqs. (56) and (58) yield close values of the mass parameter $m_{\eta_Z\eta_Z}$ in the entire region of variation of the nuclear deformation parameters (c, h) that we are interested in. Therefore, it is reasonable to use Eq. (58) in the calculation of the charge-mode mass parameter. To apply this equation, it is necessary to know the neck radius r_N and the neck length l_N for given c and h. To this end, in the region of deformations with a pronounced neck, a nuclear shape can be approximated by two spherical fragments connected by a cylindrical neck of radius r_N. In this case, the centers of the spheres are the centers of mass of the forming fragments and the sphere radii R_R and R_L are found from the condition of conservation of nuclear volume. Then, the neck length is $l_N = R - R_R - R_L$, where R is the spacing between the centers mass of the future fragments.

4.1.3. Friction parameter of the charge mode. In the theoretical studies of the isobaric distribution (see, for example, [161, 166]), the friction coefficient $\gamma_{\eta_Z\eta_Z}$ has frequently been assumed to be a coordinate-independent varied parameter. However, such an assumption is a rough approximation, and it is necessary to take into

account the dependence of the charge-mode friction parameter on nuclear deformation. The coordinate dependence of the friction parameter $\gamma_{\eta_Z\eta_Z}$ was taken into account in [20, 151] in two ways: under the assumption of the one-body and two-body mechanisms of dissipation. The most simple way to estimate the friction parameter is in the hydrodynamic model by studying the energy dissipation in the motion of a viscous incompressible fluid along a pipe (a neck connecting the forming fragments) of length l_N and radius r_N. In this case, the reduced friction coefficient of the charge mode has the form [150, 151, 165]

$$\beta_{\eta_Z\eta_Z}(\mathbf{q}) = \frac{\gamma_{\eta_Z\eta_Z}(\mathbf{q})}{m_{\eta_Z\eta_Z}(\mathbf{q})} = \frac{6\nu}{r_N^2}, \qquad (59)$$

where ν is the kinematic viscosity coefficient. From Eq. (59), it can be seen that, in the hydrodynamic model, the charge-mode friction parameter $\gamma_{\eta_Z\eta_Z}$ depends on the approach used for calculating the inertial parameter $m_{\eta_Z\eta_Z}$. From experimental data on the width of giant dipole resonances [167], it was found that $\nu = 13.5 \times 10^{21}$ fm^2 s^{-1}. Conventionally, the dynamic viscosity coefficient is used in nuclear physics as the two-body viscosity coefficient. Dynamic viscosity is related to kinematic viscosity as follows: $\nu_0 = \rho_0\nu$, where ρ_0 is the nuclear-matter density. For the parameter $r_0 = 1.22$ fm [72], the dynamic viscosity coefficient obtained in [167] amounts to $\nu_0 = 1.8 \times 10^{-23}$ MeV s fm^{-3}. This coefficient ν_0 can be used as the initial value in dynamic calculations with the two-body mechanism of nuclear viscosity, since the dipole isovector vibrations along the nuclear symmetry axis are the basic mechanism of charge redistribution between the fragments.

The application of the one-body viscosity model for calculating the friction parameter of the charge degree of freedom is of particular interest. It should be noted that the one-body viscosity mechanism has been successfully applied to the physics of the fission of excited nuclei when studying the width of giant dipole resonances [168, 169]. In [20, 151], we obtained the following expression for the charge-mode friction parameter when we assumed the one-body mechanism of viscosity:

$$\gamma_{\eta_Z\eta_Z}(\mathbf{q}) = \frac{4m}{9\rho}\frac{AZ}{N}[N\bar{v}_p + Z\bar{v}_n]\frac{1}{\Delta\sigma}. \qquad (60)$$

Here, $\bar{v}_p$ and $\bar{v}_n$ are the mean proton and neutron velocities, respectively.

In Fig. 22b, we show the charge-mode friction parameter as a function of the elongation parameter c for the two-body (the solid curve) and one-body (the dashed curve) mechanisms of viscosity, respectively. From Eq. (60), it can be seen that the parameter $\gamma_{\eta_Z\eta_Z}$ depends only on the neck thickness for the one-body mechanism; hence, $\gamma_{\eta_Z\eta_Z} \sim 1/r_N^2$ for $r_N \longrightarrow 0$ (i.e., when approaching scission). For the two-body mechanism, the inertial parameter calculated from Eq. (58) is proportional to $1/r_N^2$ when the neck radius approaches zero; hence, the friction parameter behaves according to $1/r_N^4$ at $r_N \longrightarrow 0$ for two-body viscosity. From Fig. 22b, it can be seen that the two-body mechanism of nuclear viscosity yields smaller friction parameters than the one-body mechanism for the deformations characteristic at the saddle point. However, $\gamma_{\eta_Z\eta_Z}$ sharply increases when approaching scission under the assumption of two-body viscosity and is twice as high at the scission point than when this parameter is calculated from Eq. (60). We note another important distinction between the two equations for the charge-mode friction parameter: the presence of a varied parameter in the viscosity ν_0 in the equation of two-body viscosity and the absence of varied parameters in the one-body model.

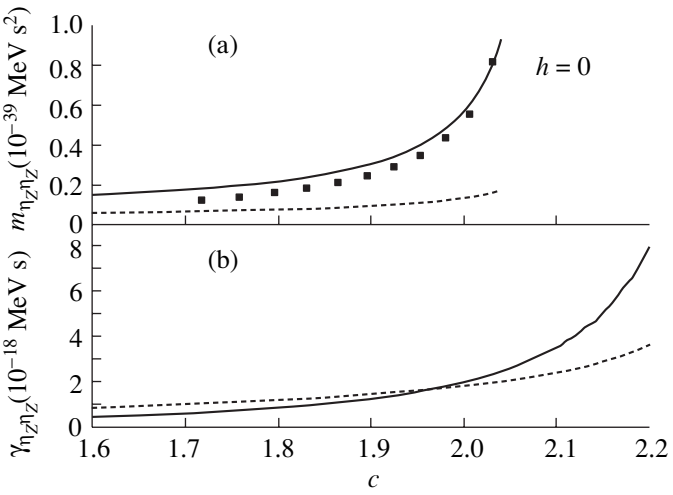

Fig. 22. (a) Comparison between the dependences of the inertial parameter on the coordinate c at the fixed neck parameter $h = 0$: the solid curve shows the mass parameter $m_{\eta_Z\eta_Z}$ calculated from Eq. (58) in [165]; the dashed curve is obtained from Eq. (57) in [164]; and the squares represent the mass parameter calculated from Eq. (56) in [161]. (b) The viscosity parameter of the charge mode as a function of the elongation parameter c along the mean trajectory under the assumption of the two-body mechanism of viscosity $\nu_0 = 1.8 \times 10^{-23}$ MeV s fm^{-3} (solid curve) and the one-body mechanism of viscosity (dashed curve).

4.2. Relaxation Times of the Charge Mode: The Statistical Limit at the Scission Point

The charge distribution for the ^{236}U compound nucleus has been reasonably thoroughly investigated both experimentally and theoretically. The isobaric charge distribution for the nuclear fission of ^{236}U was investigated theoretically using the multidimensional Fokker–Planck equation in [161, 166]. However, in

these studies, the charge-mode friction parameter was chosen independently of the collective coordinates and was a varied parameter. In [20, 151], we performed three-dimensional Langevin calculations for the charge distribution using both the one-body and the two-body mechanisms of viscosity for the charge mode.

There is a large amount of experimental data on variances of the charge distribution for the ^{236}U nucleus at low excitation energies. For example, it is well-known [170, 171] that the charge variance $\sigma_Z^2 = 0.40 \pm 0.05$ in ^{235}U fission induced by thermal neutrons and is independent of the excitation energy. Such behavior of the variance σ_Z^2 indicates the quantum nature of the formation of the charge distribution at low excitation energies. It is also known that the experimental data on σ_Z^2 are described well in this energy range by the following expression for the statistical limit at the mean scission point:

$$\sigma_{Z.\mathrm{st}}^2(E_{\mathrm{int}}) = \frac{T_Z^*(\langle \mathbf{q}_{\mathrm{sc}} \rangle)}{C_Z(\langle \mathbf{q}_{\mathrm{sc}} \rangle)}. \tag{61}$$

Here, $C_Z(\langle \mathbf{q}_{\mathrm{sc}} \rangle) = 4C_{\eta_z}(\langle \mathbf{q}_{\mathrm{sc}} \rangle)/Z^2$ and $\langle \mathbf{q}_{\mathrm{sc}} \rangle$ are the coordinates of the mean scission point. If $T \ll \hbar\omega_Z/2$, $T_Z^* \simeq \hbar\omega_Z/2$, which explains the constancy of the charge variance at low energies. The dynamic model, which disregards shell effects in calculation of the transport coefficients and the potential energy, cannot be used to describe low-energy fission. Nevertheless, it is possible to calculate $\sigma_{Z.\mathrm{st}}^2$ and to compare the resulting value with experimental data. For an excitation energy of 6.4 MeV (corresponding to ^{235}U thermal-neutron fission), it was found in [20, 151] that $\sigma_{Z.\mathrm{st}}^2 = 0.35$, which agrees well with the experimental data.

We now consider the results of dynamic calculations. Most importantly, we discuss the characteristic times for the nuclear charge mode. In a system with dissipation, the characteristic time is the relaxation time [150] in the corresponding collective mode:

$$\tau_{\eta_z} = \begin{cases} 2\tilde{\beta}_{\eta_z}^{-1}, & \omega_{\eta_z} \geq \tilde{\beta}_{\eta_z}/2 \\ [\tilde{\beta}_{\eta_z}/2 - (\tilde{\beta}_{\eta_z}^2/4 - \omega_{\eta_z}^2)^{1/2}]^{-1}, & \omega_{\eta_z} < \tilde{\beta}_{\eta_z}/2. \end{cases} \tag{62}$$

Here, $\tilde{\beta}_{\eta_z} = \beta_{\eta_z} + \dot{m}_{\eta_z\eta_z}/m_{\eta_z\eta_z}$ is the generalized damping coefficient for the charge mode. In Eq. (62), the first case ($\omega_{\eta_z} \geq \tilde{\beta}_{\eta_z}/2$) corresponds to the mode of damped vibrations and the case $\omega_{\eta_z} < \tilde{\beta}_{\eta_z}/2$ corresponds to the mode of aperiodic damping. The results of calculations of τ_{η_z} are shown in Fig. 23 for both mechanisms of viscosity. We now discuss relaxation times calculated under the assumption of the two-body mechanism of nuclear viscosity. It is possible to see that the coordinate dependence of τ_{η_z} is essentially determined by two-body viscosity. In particular, τ_{η_z} decreases with an increase in the deformation when the charge oscillator is in the damping mode (Figs. 23a and 23b) and, in contrast, τ_{η_z} increases in the overdamped mode (Figs. 23e and 23f). The case shown in Figs. 23c and 23d corresponds to the damped-vibration mode at the beginning of charge-mode evolution, and the system passes into the aperiodic-damping mode at $c \simeq 2.1$ for $\nu_0 = 1.8 \times 10^{-23}$ MeV s fm^{-3} and $c \simeq 1.75$ for $\nu_0 = 5.7 \times 10^{-23}$ MeV s fm^{-3}. Furthermore, Fig. 23c shows that the charge-mode relaxation time, $\tau_{\eta_z} \simeq 0.4 \times 10^{-21}$ s, remains virtually constant in the entire interval of motion of the system from the saddle point to the scission point under the assumption of one-body viscosity, which is not the case for two-body viscosity. This is associated with the fact that the inertial and friction coefficients of the charge mode for the one-body mechanism of friction are proportional to $1/r_N^2$. Hence, the generalized damping coefficient $\tilde{\beta}_{\eta_z}$ does not vary along a mean trajectory (the ratio $\dot{m}_{\eta_z\eta_z}/m_{\eta_z\eta_z}$ is small in comparison with β_{η_z}). In the two-body mechanism, this friction coefficient [see Eq. (59)] depends on the neck thickness; therefore, τ_{η_z} also appreciably depends on the coordinate involving two-body viscosity for the charge mode.

Another important problem arising in connection with the discussion of relaxation times for the charge mode is the applicability of the Langevin equations for describing charge fluctuations. The use of the Langevin equations in the Markovian approximation assumes that the relaxation times τ_{int} of the internal degrees of freedom are much shorter than the relaxation times of the collective mode under consideration. In [172], it was shown that τ_{int} amounts to about 0.2×10^{-21} s. We can consider the Markovian limit to be valid if the relaxation time of the charge degree of freedom is at least two to three times as long as τ_{int} (i.e., $\tau_{\eta_z} > (0.4\text{–}0.6) \times 10^{-21}$ s). As was noted above, $\tau_{\eta_z} \simeq 0.4 \times 10^{-21}$ s in the case of the one-body mechanism of dissipation, which is at the boundary of the validity range of the Markovian approximation. In the case of two-body viscosity for $\nu_0 < 0.57 \times 10^{-23}$ MeV s fm^{-3} and $\nu_0 > 1.8 \times 10^{-23}$ MeV s fm^{-3}, the Markovian description is valid. The most problematic case from all those considered above is the case shown in Fig. 23c. The minimal value that can be attained by the charge relaxation time is about 0.3×10^{-21} s, and the condition of the Markovian case is not met. However, in the region determining the

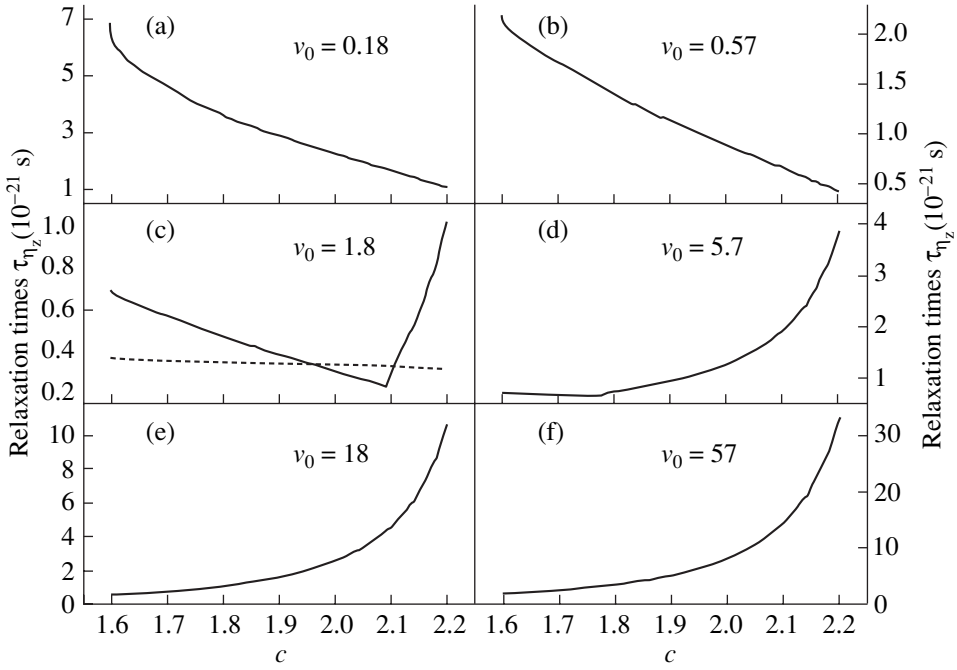

Fig. 23. Relaxation times τ_{η_z} for the charge mode as functions of the elongation coordinate c along the mean trajectory. The solid curves are obtained under the assumption of the two-body mechanism of viscosity in the charge coordinate for various viscosity coefficients. The magnitudes of the viscosity coefficients are indicated in the figures in units of (10^{-23} MeV s fm^{-3}). The dotted curve shows the results of the calculation for the one-body mechanism of viscosity. The figure is taken from [20].

parameters of the charge distribution (near the instant of scission), $\tau_{\eta_z} = (0.7–0.9) \times 10^{-21}$ s. This value is at least three times higher than τ_{int}. Thus, the above arguments provide evidence that the charge-distribution parameters calculated from the Langevin equations in the Markovian approximation are correct. In our opinion, the use of the Langevin approach in the Markovian limit is the first necessary step in solving the problem of evolution of the charge degree of freedom. However, if the Markovian description is unsuitable for studying charge fluctuations, it is still possible to use the Langevin equations, but with so-called "delayed" friction (see [173] or review [25]). It is necessary to note that the charge mode is interesting in relation to studying the memory effects caused by small relaxation times.

4.3. Variance of the Charge Distribution

Studying the behavior of the variance of the charge distribution with the excitation energy is of great interest. Most importantly, it is necessary to compare the results obtained for both mechanisms of viscosity. As is shown by the calculations, the relaxation times for the charge coordinate are much shorter than the characteristic times for the other modes associated with a variation in nuclear-surface shape (see, for example, [32]). Because of this circumstance, it is possible to predict that statistical equilibrium is established for the charge mode not only at low excitation energies but also at high ones. In Fig. 24a, we show the variance of the charge distribution as a function of the internal nuclear excitation energy at the scission point. The curve in Fig. 24a shows the variance $\sigma^2_{Z.\text{st}}$ as a function of E_{int}. When plotting this curve, we took into account that the neck length is virtually independent of the nuclear deformation, as is shown in our calculations and the results presented in [174].

On the basis of the data shown in Fig. 24a, it is possible to draw the following conclusions. First, the calculated variance of the isobaric distribution shows a characteristic increase as the excitation energy increases. Second, the calculations performed with the different mechanisms of viscosity result in identical values of variance within the statistical error associated with the limited number (about 10^4) of Langevin trajectories. Thus, we can state that, within the Langevin model developed in [20, 151], the variance of the charge distribution is insensitive to the mechanism of nuclear viscosity selected. It is noteworthy that charge distribution was investigated in [175] for the same ^{232}Th fission reaction induced by helium ions in an excitation-energy range from 20 to 57 MeV. It was found that the charge distribution can be described with a Gaussian curve and that the variance is independent of the excitation energy below 39 MeV. The dynamic calculations performed in [20, 151] at an excitation energy of 39 MeV yield $\sigma^2_Z = 0.46$, which is in agreement with

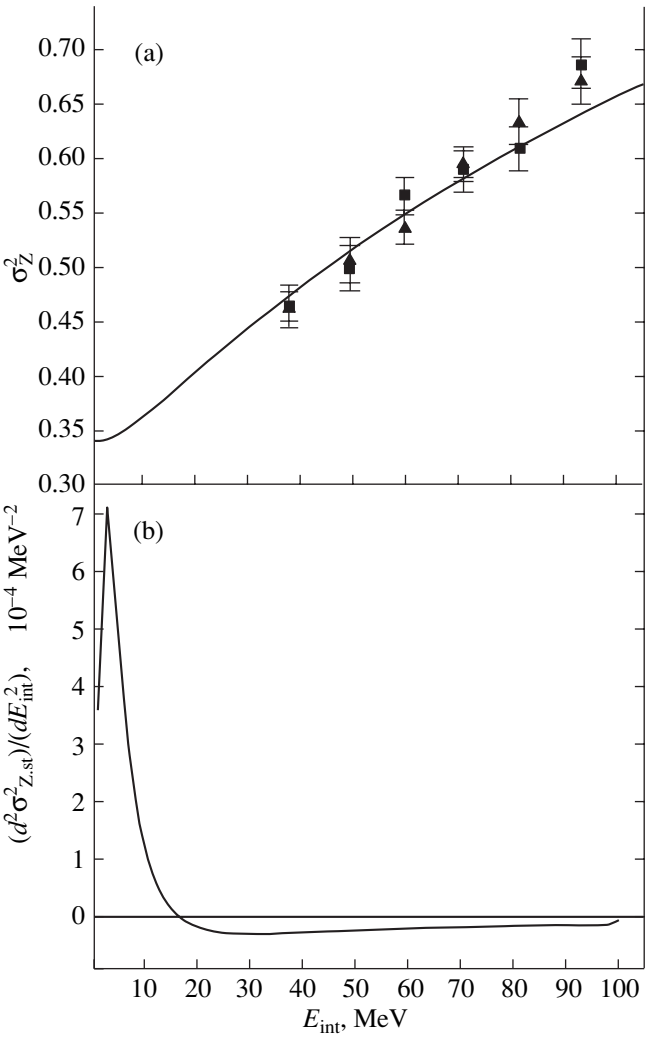

Fig. 24. (a) Variance σ_Z^2 of the isobaric distribution as a function of the internal excitation energy of a compound nucleus at the scission point: the squares represent the calculations with the two-body mechanism of viscosity for the charge mode ($\nu_0 = 1.8 \times 10^{-23}$ MeV s fm^{-3}); and the triangles represent the calculations with the one-body mechanism of viscosity. The solid curve shows the statistical limit at the mean scission point (see Eq. (61) and comments related to it). (b) The second derivative $(d^2\sigma_{Z.st}^2)/(dE_{int}^2)$ as a function of the internal excitation energy E_{int} at the mean scission point.

the results given in [175], where $\sigma_Z^2 = 0.45$–0.50 was obtained for the entire energy range under investigation. Third, as can be seen from Fig. 24a, the variance σ_Z^2 obtained in dynamic calculations lies almost at the statistical-limit curve, which passes through the presented experimental data on the charge variance at the excitation energies $E^* = 6.4$ and 39 MeV. Therefore, it is possible to conclude that statistical equilibrium for the charge coordinate is established both at low and high energies.

Figure 24b shows the second derivative $(d^2\sigma_{Z.st}^2)/(dE_{int}^2)$, which includes important information on the mechanism of formation of the charge distribution as a function of the internal excitation energy at the mean scission point. It can be seen that the energy axis can be divided into two intervals: $E_{int} < 20$ MeV and $E_{int} > 20$ MeV. In the first interval, $(d^2\sigma_{Z.st}^2)/(dE_{int}^2) > 0$; i.e., quantum fluctuations play the predominant role in formation of the charge distribution. In the second interval, $(d^2\sigma_{Z.st}^2)/(dE_{int}^2) < 0$ and fluctuations of the charge mode generally have a thermal nature.

4.4. Determination of the Two-Body Viscosity Coefficient from Study of Charge Mode Fluctuations

In our discussion on calculation of the friction tensor, we mentioned the different behavior of the friction parameter in relation to the charge coordinate for the two mechanisms of viscosity. This difference manifests itself especially distinctly when a nucleus approaches scission. However, Langevin calculations show that the mechanism of nuclear viscosity exerts almost no influence on the charge-distribution width. Therefore, we should expect a weak dependence of σ_Z^2 on the only free parameter of the model—the dynamic viscosity ν_0. In order to investigate this problem, we calculated the variance of the charge distribution in a wide range of $\nu_0 = (0.18$–$57) \times 10^{-23}$ MeV s fm^{-3} [20]. The results of these calculations are shown in Fig. 25 in the logarithmic scale. Figure 25 shows that when σ_Z^2 is calculated dynamically in the interval $(0.6 \le \nu_0 \le 1.8) \times 10^{-23}$ MeV s fm^{-3}, it agrees well with the statistical limit at the mean scission point and the experimental data on σ_Z^2. This interval represents an estimate of the two-body viscosity coefficient obtained from studying fluctuations of the charge mode.

The coordinate dependence and relaxation times τ_{η_Z} shown in Fig. 23 for all the considered values of viscosity provide the key to understanding the behavior of σ_Z^2. Statistical equilibrium is established for the charge mode if τ_{η_Z} is much shorter than the time τ_{ss} ($\tau_{ss} \simeq (5$–$10) \times 10^{-21}$ s) taken for descent of a fissile system from the ridge to the scission. Figure 23b shows that $\tau_{\eta_Z} \simeq 0.5 \times 10^{-21}$ s $\ll \tau_{ss}$ near the scission, which is the most significant (for the charge-distribution parameters of fission fragments) deformation region. In the case shown in Fig. 23c, $\tau_{\eta_Z} < 10^{-21}$ s for the entire descent from the saddle to the scission. A sharp

increase in the charge-mode relaxation time at the final stage of the descent cannot lead to a significant deviation of the dynamically calculated charge variance from the statistical limit. Hence, it is possible to conclude that the behavior and the relaxation times τ_{η_Z} in the interval $(0.6 \le \nu_0 \le 1.8) \times 10^{-23}$ MeV s fm^{-3} are such that the statistical description of the charge variance should be valid. However, the relaxation times τ_{η_Z} are comparable for $\nu_0 < 0.57 \times 10^{-23}$ MeV s fm^{-3} (Fig. 23a) and $\nu_0 > 1.8 \times 10^{-23}$ MeV s fm^{-3} (Figs. 23d–23f) and even exceed τ_{ss}. Therefore, no statistical equilibrium is established at the instant of scission.

The mechanism determining an increase in the charge variance for $\nu_0 > 1.8 \times 10^{-23}$ MeV s fm^{-3} can be called a "memory effect." Its essence can be explained as follows. A weak coordinate dependence of the rigidity factor C_{η_Z} and an increase in the charge-mode mass parameter as the deformation of a fissile nucleus increases lead to a decrease in the effective temperature T_Z^*. In turn, this leads to a decrease in charge fluctuations during the descent of a nucleus to scission and to a narrowing of the equilibrium charge distribution (determined by the ratio T_Z^*/C_Z). In contrast, a fast increase in the friction parameter $\gamma_{\eta_Z\eta_Z}$ results in the charge degree of freedom being frozen, and σ_Z^2 no longer varies in arbitrary way during the further descent of the system towards scission. The charge mode is frozen at a high two-body viscosity coefficient $\nu_0 > 1.8 \times 10^{-23}$ MeV s fm^{-3}, which corresponds to the overdamped mode. In addition, the higher the coefficient ν_0, the earlier the charge degree of freedom is frozen and, hence, the broader the charge distribution of fission fragments. This mechanism qualitatively explains the increase in charge variance as ν_0 increases.

The mechanism of two-body viscosity has previously been widely used to study the mass–energy distribution of fission fragments, and certain conclusions have been formulated about the value of the friction coefficient. In [58, 61], the mean kinetic energy of fission fragments was calculated in a wide interval of $Z^2/A^{1/3}$, and the following values of this coefficient were found from fitting the obtained results to experimental data: $\nu_0 = (0.9 \pm 0.3) \times 10^{-23}$ MeV s fm^{-3} [61] and $\nu_0 = (1.9 \pm 0.6) \times 10^{-23}$ MeV s fm^{-3} [58]. In [13], we investigated the MED of fission fragments with the aid of the multidimensional Fokker–Planck equation and showed that the results of dynamic calculations agreed most closely with the experimental data for $\nu_0 = (1.5 \pm 0.5) \times 10^{-23}$ MeV s fm^{-3}. In [176], various types of collective nuclear motion (in particular, the fission of a nucleus into fragments and giant dipole resonances) were considered. Based on the obtained results, the authors assumed that the two-body viscosity coefficient was universal for all types of collective nuclear motion

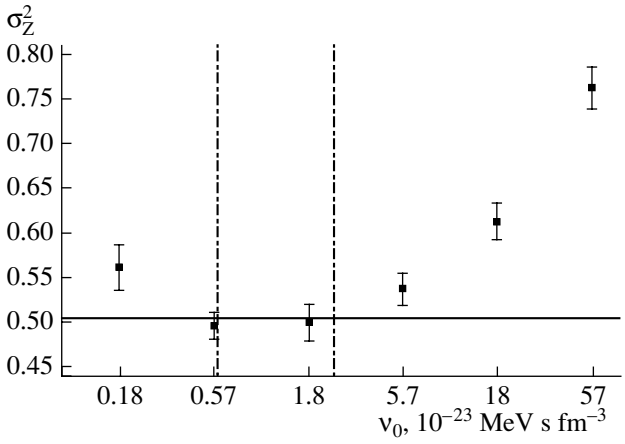

Fig. 25. Variance σ_Z^2 of the charge distribution as a function of the two-body viscosity coefficient ν_0 at the excitation energy E^* = 50 MeV. The solid line shows the statistical limit at the mean scission point. The vertical dashed–dotted lines restrict the interval of values of the two-body viscosity coefficient obtained in [13, 58, 61, 176]. The figure is taken from [20].

and had the value $\nu_0 \simeq 10^{-23}$ MeV s fm^{-3}. It is easy to see that the interval of the coefficient ν_0 found by us for the charge mode agrees well with the former estimates.

In summary, we note once again that, at present, Langevin calculations of the charge distribution are performed only for symmetric nuclear fission into fragments. Study of the mass–charge distribution is of particular interest, and, in order to calculate it, it is necessary either to introduce a fourth coordinate (of mass asymmetry) into the model or, in the three-dimensional model, to select the mass-asymmetry coordinate, the charge-asymmetry coordinate, and a third coordinate responsible for nuclear elongation and, eventually, for fission into fragments as the collective coordinates.

5. ANGULAR DISTRIBUTION (AD) OF FISSION FRAGMENTS

Statistical theory describes the anisotropy of the angular distribution (AD) of fission fragments well for many nucleus-target–impinging-particle combinations in a wide excitation-energy range. At early the stages of experimental research into the ADs of fission fragments, reactions in which neutrons, ^{3}He ions, and α particles were used as impinging particles were considered [157, 177]. The compound nuclei formed in such reactions have a temperature of about 1 MeV and low angular momenta. For these reactions, the fission-barrier height is much higher than the nuclear temperature, and the conventional saddle-point transition-state (SPTS) model [157, 178, 179] gives a reasonably exact reproduction of the experimental data on the AD anisotropy of fragments.

Later, ADs were studied with more massive impinging ions of carbon, oxygen, and heavier ions [177]. The study of the ADs of fragments produced in the fission of heavier nuclei with much higher temperatures and angular momenta became possible. For such systems, it was found that the standard SPTS model regularly predicted low values of AD anisotropy in comparison with the experimental data.

The challenges arising in the theoretical description of ADs in reactions with heavy ions can be conditionally separated into two problems (for more details, see, for example, review [180] and the references therein):

(1) At impinging-ion energies much higher than the Coulomb barrier, theoretical models based on the SPTS model usually predict a decrease in AD anisotropy in response to an increase in the impinging-ion energy, whereas an increase or the approximate constancy of this value is observed under experimental conditions (see, for example, [181]). In this section, we mainly consider this problem. Several hypotheses have been proposed to explaining the high values of AD anisotropy observed in this energy range:

(i) The transition state for compound nuclei with a high fissility and momentum is located not at the saddle point but at a more deformed scission point [182, 183]. Thus, the scission-point transition-state (SCTS) model was proposed. Great success in describing the AD in reactions with heavy ions was achieved with the version of the SCTS model developed in [184]. The authors of this study proposed a model which more accurately (in comparison with the first variants of the SCTS model [182, 183]) took into account the spin (twisting and wriggling) modes of formed fission fragments.

(ii) At the same time, it was shown in [185] that the experimentally observed AD anisotropy cannot be described by either the SPTS or SCTS models. Therefore, it was assumed, in the general case, that the transition state determining the AD of fission fragments is located somewhere between the saddle point and the scission point.

(iii) Abnormal values of AD anisotropy for a number of reactions can be explained by the presence of a significant fraction of events, which are not fusion–fission events, proceeding without the formation of a compound nucleus in the total fission cross section. To such reactions, we assign quasifission [88, 186–190], fast fission [188, 191, 192], and pre-equilibrium fission [193].

(2) For deformed actinide target nuclei, a sharp increase in the AD anisotropy is experimentally observed at energies close to and below the Coulomb barrier (in reactions such as ^{16}O, ^{19}F + Th, U, Np) when the impinging-ion energy is decreased. No such increase is observed if the Bi and Pb nuclei, which are lighter and spherical in the ground state, are used as the target. This abnormal behavior of the AD anisotropy is associated either with a sharp increase in the second moment of the total momentum distribution of nuclei [194] (as a result of the Coulomb-barrier influence) or with an increase in the contribution made by quasifission events [195] (for head-on collisions).

Detailed study of ADs shows that the AD anisotropy is extremely sensitive to an entrance-channel asymmetry $\alpha = (A_t - A_p)/(A_t + A_p)$, where A_t and A_p are the masses of a target nucleus and impinging particle, respectively.

The value of the Businaro–Gallone parameter α_{BG} defines the validity range of the standard SPTS model: for $\alpha > \alpha_{BG}$, the theoretical calculations are in accordance with the experimental data; for $\alpha < \alpha_{BG}$, experimental methods give considerably higher values of anisotropy than are predicted by theoretical calculations with the saddle point as the transition state.

However, even in the "safe" range of $\alpha > \alpha_{BG}$, where the SPTS model gives a satisfactory description of AD anisotropy, calculations executed in statistical models without taking into account the dynamic features of nuclear fission encounter serious difficulties in determining the saddle configuration of a fissile nucleus (temperature and surface shape).

Primarily, these difficulties are caused by the fact that the statistical models predict a decrease in the mean prescission neutron multiplicity $\langle n_{pre} \rangle$ in response to increasing excitation energy [104]. Consequently, they give an underestimated value of $\langle n_{pre} \rangle$ and, therefore, an overestimated value of the temperature T_{sd} of a nucleus at the saddle point at high excitation energies. In addition, the fraction of neutrons evaporating after the system passes the saddle increases with the excitation energy and mass number of a fissile nucleus. Therefore, even if the calculations in the statistical model reproduce the experimental value of the total prescission neutron multiplicity, the presence of neutrons emitted at the stage of evolution between the saddle and the instant of scission results in an incorrect value of T_{sd}. In the dynamic models including an evaporation branch, no problems associated with definition of the nuclear configuration arise because the nuclear configuration is obtained as the solution to equations of motion. A secondary factor causing difficulties in determination of the saddle configuration is that the multidimensional nature of the fission barrier is disregarded in the statistical SPTS models when determining the transition-state position, which leads to seriously underestimated calculated values of the AD anisotropy in the range of high excitation energies (for more details, see Section 5.1.2). In this context, a promising approach would seem to be to actively use multidimensional dynamic models in the theory of angular distributions of fission fragments.

In the analysis of an AD, it is usually assumed that fission fragments are emitted in the direction of the nuclear symmetry axis. In this case, the AD is specified by three quantum numbers: I, K, and M, where I is the total momentum of a compound nucleus, K is the projection of I towards the nuclear symmetry axis, and M is the projection of the total moment in the direction

of the impinging-ion beam. In the case of fusion of spinless ions, the value of $M = 0$; hence, the total moment I coincides with the orbital momentum l. Then, the AD for fixed values of I and K has the form

$$W(\theta, I, K) = \frac{I + 1/2}{\pi}\left|d^I_{0,K}(\theta)\right|^2, \quad (63)$$

where $d^I_{M,K}(\theta)$ is the Wigner rotation function and θ is the angle between the nuclear symmetry axis and the axis of the impinging-ion beam. For large values of I, the following expression is valid:

$$W(\theta, I, K) \simeq \frac{I + 1/2}{\pi}[(I + 1/2)^2 \sin^2\theta - K^2]^{-\frac{1}{2}}. \quad (64)$$

The angular distribution of fission fragments observed in experiments can be obtained by averaging Eq. (63) over the quantum numbers I and K:

$$W(\theta) = \sum_{I=0}^{\infty}\sigma_I \sum_{K=-I}^{I}\rho(K)W(\theta, I, K). \quad (65)$$

From Eq. (65), it can be seen that, for calculation of ADs, it is necessary to specify the type of distributions $[\sigma_I]$ and $[\rho(K)]$ of compound nuclei over I and K, respectively. We described the problems associated with calculation of the distribution σ_I over the total nuclear momentum in Section 1.3. Therefore, we now discuss the problem of finding the distribution $\rho(K)$.

5.1. Transition-State Model

The transition-state model [157, 178, 179] is conventionally used in theoretical analysis of the data on ADs of fission fragments. The essence of this model consists in the assumption that there is a certain chosen (transition) configuration of a fissile system that determines the AD of the fission fragments. Thus, there are two limiting assumptions on the position of the transition state and, correspondingly, two variants of the transition-state model: the saddle-point transition-state (SPTS) model and the scission-point transition-state (SCTS) model.

When developing the classical SPTS model, certain key assumptions are made: (i) The mean residence time of a nucleus in the saddle-point region is sufficiently long for an equilibrium distribution over K to be established at the saddle point. In other words, the time τ_{gs} of the motion of the system from the ground state to the saddle point is much longer than the relaxation time of the K degree of freedom ($\tau_{gs} \gg \tau_K$). (ii) The mean time τ_{ss} of descent of a nucleus from the saddle to the instant of scission is short in comparison with τ_K. In this case, the K distribution formed at the saddle point is retained at the scission point. (iii) The type of K distribution depends on the factor $\exp(-E_{rot}/T)$ [179],

$$E_{rot} = \frac{\hbar^2 K^2}{2J_\parallel} + \frac{\hbar^2(I^2 - K^2)}{2J_\perp}. \quad (66)$$

Thus, the K equilibrium distribution is

$$\rho(K) = \frac{\exp\left[-\frac{K^2}{2K_0^2}\right]}{\sum_{K=-I}^{I}\exp\left[-\frac{K^2}{2K_0^2}\right]}. \quad (67)$$

The parameter K_0 determines the width of this distribution:

$$K_0^2 = \frac{T}{\hbar^2}J_{eff}, \quad J_{eff} = \frac{J_\parallel J_\perp}{J_\perp - J_\parallel}. \quad (68)$$

Here, T is the temperature of a nucleus in the transition state, J_{eff} is the effective moment of inertia, $J_\parallel$ and $J_\perp$ are the solid-state moments of inertia of a nucleus with respect to the symmetry axis and to the axis perpendicular the symmetry axis, respectively.

By averaging Eqs. (63) and (64) over $\rho(K)$, we obtain an expression for the angular distribution with a fixed I and given K_0:

$$W(\theta, I) = \frac{(I + 1/2)}{\pi}\frac{\sum_{K=-I}^{K=I}\left|d^I_{0,K}(\theta)\right|^2\exp(-K^2/2K_0^2)}{\sum_{K=-I}^{K=I}\exp(-K^2/2K_0^2)}, \quad (69)$$

$$W(\theta, I) \simeq \sqrt{\frac{2p}{\pi}}\frac{\exp[-p\sin^2\theta]J_0[-p\sin 2\theta]}{\mathrm{erf}[\sqrt{2p}]}. \quad (70)$$

Here, J_0 is the zero-order Bessel function and $p = \left(I + \frac{1}{2}\right)^2/(4K_0^2)$. Equation (70) is known as the Halpern–Strutinsky equation [157, 179].

If $p \gg 1$, it is possible to show that the AD anisotropy is given by the approximate relation

$$\frac{W(0°)}{W(90°)} \simeq 1 + \frac{\langle I^2\rangle}{4K_0^2}. \quad (71)$$

Equation (71) is pictorial and, consequently, convenient for revealing qualitative features in the behavior of the AD anisotropy. Equations (69) or (70) are used for quantitative analysis. It is necessary to note that both these expressions give identical probabilities $W(\theta, I)$ [186] to a good level of accuracy.

In addition to the initial spin distribution of compound nuclei, it is possible to select two more factors determining angular-distribution anisotropy in the SCTS model: the effective nuclear moment of inertia (or the deformation) in the transition state and the

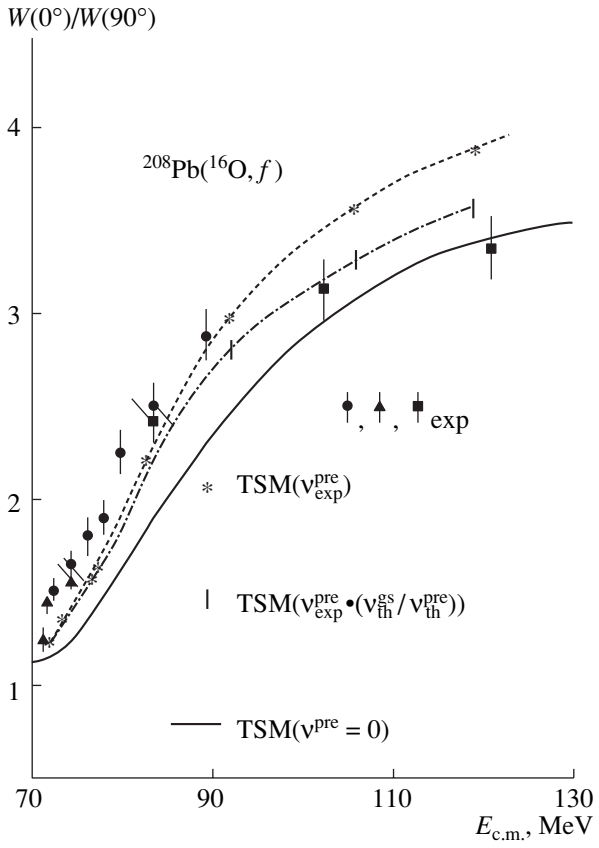

Fig. 26. Comparison of experimental data on the AD anisotropy (closed circles, squares, and triangles) with the results of theoretical analysis within the SPTS model. The results of the calculations are obtained using various methods of taking into account evaporation of prescission neutrons: the solid curve is obtained without taking into account neutron evaporation [196]; the asterisks connected by the dotted curve correspond to a situation in which all the neutrons evaporate before a nucleus reaches the saddle configuration [196]; the rectangles connected by the dashed and dotted curve refer to the evaporation occurring at the stage of descent of the system from the saddle point to the scission point. The figure is taken from [199].

temperature in this state. The following two sections are devoted to discussing the new features that arise when studying the AD of fission fragments within the Langevin approach in comparison with the statistical models.

5.1.1. The effect of prescission neutron evaporation on AD anisotropy. The nuclear temperature $T = T_{sd}$ in the transition state is closely related to the prescission neutron multiplicity and, therefore, to dissipation of the collective energy into an internal form. The influence of prescission neutron evaporation on the calculated fragment ADs was studied in [19, 196–200]. An improvement in the agreement between the calculated values of the AD anisotropy and the experimental data was observed in all these studies if we take into account neutron evaporation. The typical results obtained both with and without inclusion of the neutron evaporation are shown in Fig. 26. As can be seen, with an increase in the excitation energy, the prescission neutron multiplicity increases, and, hence, the difference between the curves obtained with and without inclusion of the neutron evaporation increases as well.

In [196–198], the temperature in the transition state was determined under the assumption that all the neutrons evaporate before a nucleus attains the saddle point. In [19, 199, 200], the results of one-dimensional [199, 200] and three-dimensional [19] Langevin calculations were used, and it was concluded that only the presaddle fraction of neutrons affects the transition-state temperature. An obvious advantage of the dynamic models is that they can be used to determine the fraction of neutrons that evaporate before attaining the saddle configuration, which is impossible in pure statistical models. The temperature T_{sd} of a nucleus at the saddle point depends on the mean presaddle neutron multiplicity $\langle n_{pre}^{gs} \rangle$, i.e., on the fraction of neutrons that evaporate before the nucleus attains a conditional saddle point. The mean prescission neutron multiplicity depends on the mean nuclear dissipation, while the ratio $\langle n_{pre}^{gs} \rangle / \langle n_{pre} \rangle$ is determined mainly by the coordinate dependence of the friction-tensor components. Therefore, ADs can be considered as a source of information on the magnitude and mechanism of nuclear viscosity. It should be noted that we investigated AD anisotropy as a function of a value of the one-body viscosity in [19]. We showed that, although the variation in viscosity affects the ADs under consideration, this characteristic is less sensitive to nuclear viscosity in the quantitative sense than the prescission neutron multiplicity.

As was shown in [19, 199], the ratio $\langle n_{pre}^{gs} \rangle / \langle n_{pre} \rangle$ increases in response to an increase in the excitation energy. Therefore, as can be seen from Fig. 26, the angular distributions obtained under the assumption that all the neutrons are evaporated before reaching the saddle point differ appreciably from the results of calculations taking into account only the presaddle neutron fraction when determining T_{sd} under the effect of increasing excitation energy.

We note that the energy dependence of $\langle n_{pre}^{gs} \rangle / \langle n_{pre} \rangle$ obtained in [19] qualitatively agrees with the dependence obtained in [199] for the same reaction. The results of [199] enabled the authors to demonstrate that quantitative agreement with the experimental data on AD anisotropy for high excitation energies is possible only when a significant prescission neutron fraction evaporates during the descent from the saddle point to the scission point. The predicted ratio $\langle n_{pre}^{gs} \rangle / \langle n_{pre} \rangle$ is 3–5 times higher than that obtained in [19] at the same excitation energies. However, good quantitative agreement was achieved with experimental data in both studies. The disparity can be explained by the fact that dif-

ferent models and, in particular, a different number of collective coordinates were used.

5.1.2. The effect of model dimension on AD. The set of all the accessible transition states is determined by the potential energy landscape and, hence, by the number of collective coordinates. At the same time, the particular ensemble of transition points strongly depends on the fission dynamics and, consequently, is sensitive virtually to all the components of the model used: the conservative force, nuclear-viscosity mechanism, method of calculation of the mass tensor, etc. It should be noted that there is only one transition state, the saddle point, in the one-dimensional models for each angular momentum, while the entire ensemble of conditional saddle points forms the set of transition states in the multidimensional models. The multidimensional dynamic models, in comparison with the one-dimensional ones, take into account the multidimensional nature of the fission barrier. This circumstance can strongly influence the AD anisotropy predicted in models with a different number of collective coordinates.

In [19], we assumed that the model dimension influences the calculated AD anisotropy. In addition, this influence should increase with an increase in the nuclear fissility and excitation energy. In fact, under these conditions, the fission barrier lowers and the rigidity of the potential-energy trough decreases. Hence, a greater number of transition states are allowed for a fissile nucleus. An increase in the nuclear excitation energy also results in an increase in the phase-space volume accessible to a nucleus at the ridge.

In [123], we considered the reaction $^{16}O + ^{232}Th \longrightarrow ^{248}Cf$ in the three-dimensional Langevin model and compared our results with the results of calculations for the same reaction [200] obtained in the one-dimensional model. In [200], the AD anisotropy was calculated for the reaction $^{16}O + ^{232}Th \longrightarrow ^{248}Cf$ and for certain systems of impinging-ion–target combinations close to $^{16}O + ^{208}Pb$. When calculating the AD anisotropy of the fragments, corrections were made to the emission of presaddle neutrons according to [196]. The authors of [200] obtained good agreement with the experimental data on AD anisotropy for systems of the $^{16}O + ^{208}Pb$ type. In contrast, for the heavier system of $^{16}O + ^{232}Th$, the calculated values of the anisotropy drastically differ from the experimental data. Thus, the disagreement between theoretical calculations and experimental data increases as the excitation energy decreases, which qualitatively agrees with the calculations in [123]. Generally, the results obtained in the three-dimensional approach are in better agreement with the experimental data. If the excitation energy increases, the difference between theoretical and experimental values decreases faster than in the one-dimensional calculations. In [123], this result was interpreted as being due to the effect of inclusion of several collective coordinates.

In order to study the dependence of the calculated AD of fragments on the number of collective coordinates included in the model in more detail, we calculated the AD anisotropy in the one-dimensional and three-dimensional Langevin models for two reactions: $^{16}O + ^{208}Pb \longrightarrow ^{224}Th$ and $^{16}O + ^{232}Th \longrightarrow ^{248}Cf$. To rule out the influence of the temperature and angular-momentum variation resulting from prescission particle evaporation, we disregarded evaporation in the calculations. Figure 27 shows that, although the AD anisotropy almost coincides in the one-dimensional and three-dimensional calculations at low excitation energies, the three-dimensional model predicts considerably higher values of the AD anisotropy than the one-dimensional model as the excitation energy increases. The greatest difference is found at the highest considered energy $E^* \simeq 150$ MeV. It can be seen that the AD anisotropy obtained in the three-dimensional calculations for the reaction resulting in the formation of the lighter compound nucleus ^{224}Th at $E^* \simeq 150$ MeV is a third higher than that obtained in the one-dimensional calculations. For the reaction resulting in the formation of the heavier compound nucleus ^{248}Cf, this difference reaches almost 40%, which agrees with the assumption that the influence of model dimension should be stronger for heavier nuclei.

In order to understand why the multidimensional calculations give higher values of anisotropy than the one-dimensional ones, we should consider Fig. 28. As can be seen, the saddle point is located at $h \simeq 0$ and $\alpha = 0$. A weak dependence of the effective moment of inertia on the mass-asymmetry parameter and a stronger dependence on the parameter h are shown. In this case, the values of J_{eff} decrease if the parameter h deviates from zero either on the positive or the negative sides of the figure. In the multidimensional model for calculation of the AD anisotropy, averaging over the ensemble of transition points takes place, while, in the one-dimensional model, only one transition state, the saddle point, is realized. Therefore, the values of K_0 obtained in the three-dimensional calculations are lower on average than in the one-dimensional case both due to an increase in the effective moment of inertia and a decrease in the transition-state temperature for a deviation from the saddle point. Lower values of the parameter K_0 correspond to a narrower AD.

It should be noted that both the calculations in [181] and the one-dimensional calculations described above show a decrease in the AD anisotropy at high excitation energies, whereas this value is observed to increase in experiments. In [181], it was shown that the reason for this decrease in the anisotropy is a sharp increase in J_{eff}, calculated at the saddle point in the diffuse-edge LDM, if the compound-nucleus spin increases. The authors of [181] therefore concluded that fission events proceeding without the formation of a compound nucleus amount to a significant fraction of the total for high momenta (which are realized at high excitation energies), which results in a desirable decrease in J_{eff}. How-

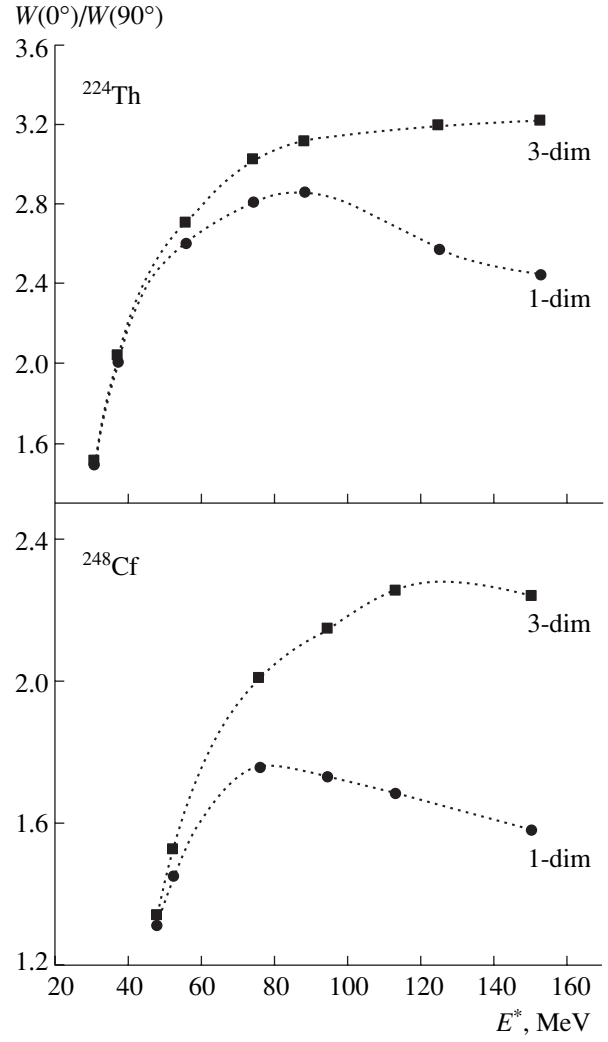

Fig. 27. Angular-distribution anisotropy obtained in one-dimensional (circles) and three-dimensional (squares) Langevin calculations for the one-body mechanism of nuclear viscosity with $k_s = 0.25$ for ^{224}Th and ^{248}Cf nuclei.

ever, it can be seen from the results shown above that the problem can be solved if all the events are considered as true fusion–fission events and the multidimensional nature of the fission barrier is taken into account.

5.2. K-Mode Relaxation Time

In recent years, evidence has appeared indicating that it is necessary to take into account the dynamic features of AD formation. In the most general case, the K mode should be considered as an independent collective coordinate, and its evolution can be studied using, for example, the multidimensional Langevin approach. Such a completely dynamic approach makes it possible to determine, in the most general form, the desired distribution $\rho(K)$. However, in this case, the problem of calculating the conservative force for the K mode, as well as the inertial and friction parameters, must be

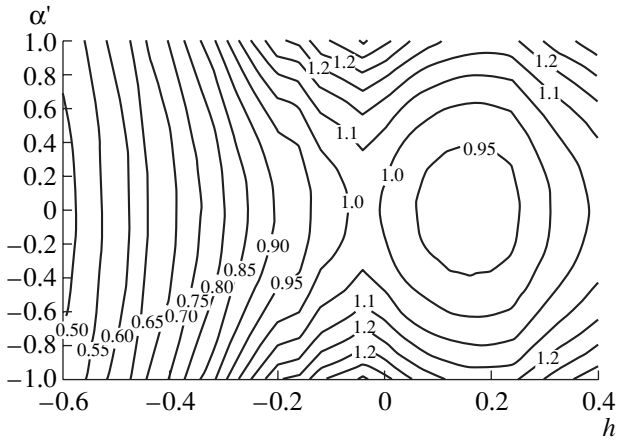

Fig. 28. Effective moment of inertia $J_{\text{eff}}/J_{\text{sph}}$ of a nucleus in units of the moment of inertia of an equivalent spherical nucleus on a ridge surface. The calculations are performed in the coordinates (h, α') for a ^{224}Th nucleus with the spin $I = 20\hbar$.

dealt with. From the known dependence of the rotational energy on K in Eq. (66), it is easy to determine the desired conservative-force component. At the same time, a method for use in calculation of the friction parameter for the K mode has not been described in previous publications. Therefore, a fully dynamic consideration of the evolution of the K degree of freedom is still difficult.

However, the dynamic aspects of AD formation can be contained within a characteristic named the K-mode relaxation time τ_K. In [201], it was proposed that K-mode evolution be considered using the Monte Carlo method. In [201], compound-nucleus fission was characterized by two collective degrees of freedom: the nuclear elongation and K. The initial K distribution was assumed to be uniform in the nuclear ground state. At each step in the process of solving the Langevin equations for the elongation coordinate, there was a variation of K under fulfillment the condition $\xi < \tau/\tau_K$, where ξ is a random number uniformly distributed in the interval [0, 1] and τ is the integration step of the solution to the Langevin equations. A new value of K was sampled based on the following distribution:

$$P(K) \sim \exp(\Delta F/T). \qquad (72)$$

Here, ΔF is the free-energy increment resulting from variation in K. It is necessary to note that the method used by the authors of [201] is reasonably general in the sense that it allows us to consider the evolution of an arbitrary finite collective mode in a similar way.

The described algorithm was applied in [201] to calculating the AD of the fission fragments for the systems ^{16}O + ^{232}Th, ^{16}O + ^{238}U, and ^{16}O + ^{248}Cm at impinging oxygen ion energies ranging from 80 to 160 MeV. From an analysis of the obtained results and experimental data, the authors succeeded in deriving a K-mode relaxation time of $\tau_K = 21 \times 10^{-21}$ s.

It is more often assumed that the K-mode relaxation time is constant. The obtained estimates of τ_K lie in the interval $(5–8) \times 10^{-21}$ s [104, 193, 202, 203] to 60×10^{-21} s [204]. We note that the relaxation time τ_K was determined in [203] within the one-dimensional Langevin model, while, in other studies, the calculations were performed within statistical models.

At the same time, it follows from [205] that there is a dependence of τ_K on the nuclear rotation velocity; i.e., considering the K-mode relaxation time as constant is only an approximation. Until now, there have been no dynamic calculations performed using this result. The results of [205] were applied in an analysis of an AD within the framework of the statistical model proposed in [206]. The authors of these studies achieved reasonably good agreement with the experimental data in the region of near-barrier and sub-barrier fusion–fission.

In summarizing this subsection, it is necessary to note that clarification of the role of dynamic coefficients in formation of the ADs of fission fragments is still at an early stage. The use of the multidimensional Langevin models, which consider the K mode as an independent collective degree of freedom, seems to be promising. In this case, during the calculation of an AD, it is extremely important to consider the reaction from the instant of contact of colliding ions.

CONCLUSIONS

In recent years, a stochastic approach based on multidimensional Langevin equations has been widely used for describing the dynamics of induced fission and heavy-ion fusion. In this review, we showed potential of this approach with regard to description of the large number of different quantities observed in fusion–fission reactions. In our opinion, the results obtained in recent years with the use of the multidimensional stochastic approach are impressive. In particular, calculations in the three-dimensional stochastic approach naturally reproduce the large variances and significant increase observed in the mass–energy distribution of fragments with the compound-nucleus fissility parameter. These characteristic pronounced features of the distribution cannot be explained within the framework of the fission models conventionally used for analysis of fragment distributions and the previously favoured two-dimensional Langevin calculations. In addition, within the developed multidimensional stochastic approach, it is possible to satisfactorily describe quantitatively fine correlation characteristics of the mass–energy distribution of fragments and the correlation of evaporated neutrons with the mass and kinetic energy of fragments. A consistent description of the correlation dependences for the prefission, postscission, and total neutron multiplicities makes it possible to obtain information on the time taken at all the stages of the fission process from compound-nucleus formation to the deexcitation of fragments.

Now, there is evidently no doubt that the stochastic approach based on multidimensional Langevin equations in combination with the evaporation of light particles and gamma quanta provides the most adequate dynamic description of the investigated fusion–fission reactions. At the same time, considerably poorer agreement is observed among researchers with respect to the components representing the physical basis of the stochastic approach. As before, it primarily concerns the choice of the dependence of the friction parameter (the tensor) on the collective coordinates and (or) temperatures.

In summary, it would also be desirable to emphasize that the regular calculations of the mass–energy distribution of fragments and prescission neutron multiplicities performed within the three-dimensional stochastic approach have made it possible to unambiguously choose, after much discussion, which nuclear-viscosity mechanism (two-body or one-body) is realized during nuclear fission. A simultaneous description of the parameters of the mass–energy distribution of fragments and the mean prescission neutron multiplicities is attained for the one-body mechanism of viscosity in its modified variant with the reduction coefficient k_s = 0.25–0.5 for the contribution from the wall formula. At the same time, it is necessary to mention that, for more substantiated conclusions concerning both the deformation and the temperature dependences of nuclear viscosity, more realistic variants have to be used to statistically describe particle emission in dynamic calculations, particularly in relation to the deformation dependence of the particle-emission barriers and the binding energy. As an example, we note the study of Pomorski *et al.* [21, 207] in which the influence of nuclear deformation was shown for a partial nuclear-decay width. In addition, as supplementary observed quantities, experimental data on the emission of charged particles can be employed for deeper analysis of nuclear dissipative properties.

The attenuation of the dissipation relative to the wall-formula predictions for a fissile nucleus with a highly symmetric configuration (such as a sphere or weakly deformed ellipsoid) is now understood well both from the use quantum-mechanical calculations and from the ideas of chaos theory. However, the abnormally sharp increase in the dissipation for strongly deformed configurations close to scission, which was introduced in the calculations of Fröbrich and Gontchar, has yet to receive a proper theoretical explanation despite the good agreement of their calculations with the data from numerous experimental studies. Therefore, the character of the mechanism of dissipation realized in fission requires both further theoretical and further experimental study. Finally, in dynamic simulation of a fusion–fission reaction, the calculations should begin from the point of contact between fusing ions instead of an arbitrary initial configuration corresponding to a statistically equilibrium compound nucleus. The first of such calculations have now been performed.

ACKNOWLEDGMENTS

We are grateful to A.Ya. Rusanov for his part in numerous interesting discussions and useful consultations on the experimental data, which formed the basis of this review, throughout the entire period in which the review was being formulated. We also thank H.J. Krappe, P. Fröbrich, K.Kh. Schmidt, M.G. Itkis, V.A. Rubchenya, A.S. Il'inov, G.I. Kosenko, and M.V. Mebel' for discussing certain chapters of the review, their constructive suggestions, and their attention to this paper.

REFERENCES

1. S. Chandrasekhar, Rev. Mod. Phys. **15**, 1 (1943).
2. H. Risken, *The Fokker-Plank Equation* (Springer, Berlin, 1989).
3. C. W. Gardiner, *Handbook of Stochastic Methods for Physics, Chemistry, and the Natural Sciences* (Mir, Moscow, 1986; Springer-Verlag, Berlin, 1985).
4. N. G. Van-Kampen, *Stochastic Processes in Physics and Chemistry* (Vysshaya Shkola, Moscow, 1990) [in Russian].
5. V. V. Volkov, Phys. Rep, **44**, 93 (1978); V. V. Volkov, *Nuclear Reactions of High-Inelastic Transfers* (Energoizdat, Moscow, 1982) [in Russian].
6. H. A. Kramers, Physica A **7**, 284 (1940).
7. N. Bohr and J. A. Wheeler, Phys. Rev. **56**, 426 (1939).
8. P. Hängi, P. Talkner, and M. Borcovec, Rev. Mod. Phys. **62**, 251 (1990).
9. V. I. Melnikov, Phys. Rep. **209**, 1 (1991).
10. H. Feldmeier, Rep. Prog. Phys. **50**, 915 (1987).
11. P. Grangé, Li. Jung-Qing, and H. A. Weidenmüller, Phys. Rev C **27**, 2063 (1983); Z. Jing-Shang and H. A. Weidenmüller, Phys. Rev. C **28**, 2190 (1983).
12. P. Grangé, Nucl. Phys. A. **428**, 37 (1984).
13. G. D. Adeev, I. I. Gonchar, V. V. Pashkevich, *et al.*, Fiz. Elem. Chastits At. Yadra **19**, 1229 (1988) [Sov. J. Part. Nucl. **19**, 529 (1988)]; G. D. Adeev and V. V. Pashkevich, Nucl. Phys. A **502**, 405 (1989).
14. H. Delagrange, C. Grégoire, F. Scheuter, and Y. Abe, Z. Phys. A **323**, 437 (1986); E. Strumberger, K. Ditrich, and K. Pomorski, Nucl. Phys. A. **529**, 522 (1991).
15. T. Wada, in *Proceedings of the 2nd Tours Symposium on Nuclear Physics, Tours, 1994*, Ed. by H. Utsunomiya, M. Ohta, J. Galin, and G. Munzenberg (World Sci., Singapore, 1995).
16. J. Blocki, O. Mazonka, J. Wilczynski, *et al.*, Acta Phys. Pol. **31**, 1513 (2000).
17. P. N. Nadtochii, A. V. Karpov, D. V. Vanin, and G. D. Adeev, Yad. Fiz. **64** (5), 926 (2001) [Phys. At. Nucl. **64**, 861 (2001)].
18. A. V. Karpov, P. N. Nadtochy, D. V. Vanin, and G. D. Adeev, Phys. Rev. C **63**, 054610 (2001).
19. P. N. Nadtochy, G. D. Adeev, and A. V. Karpov, Phys. Rev. C **65**, 064615 (2002).
20. A. V. Karpov and G. D. Adeev, Eur. Phys. J. A **14**, 169 (2002).
21. C. Schmitt, J. Bartel, K. Pomorski, and A. Surowiec, Acta Phys. Pol. B **34**, 1651 (2003); C. Schmitt, J. Bartel, A. Surowiec, and K. Pomorski, Acta Phys. Pol. B **34**, 2135 (2003).
22. Y. Aritomo, J. Nucl. Radiochem. Sci. **3**, 17 (2002).
23. T. Ichikawa, T. Asano, T. Wada, and M. Ohta, J. Nucl. Radiochem. Sci. **3**, 67 (2002).
24. G. I. Kosenko, F. A. Ivanyuk, and V. V. Pashkevich, Yad. Fiz. **65**, 1629 (2002) [Phys. At. Nucl. **65**, 1588 (2002)]; G. I. Kosenko, F. A. Ivanyuk, and V. V. Pashkevich, J. Nucl. Radiochem. Sci. **3**, 71 (2002); C. Shen, G. I. Kosenko, and Y. Abe, Phys. Rev. C **66**, 061602 (R) (2002).
25. Y. Abe, S. Ayik, P.-G. Reinhard, and E. Suraud, Phys. Rep. **275**, 49 (1996).
26. P. Fröbrich and I. I. Gontchar, Phys. Rep. **292**, 131 (1998).
27. I. I. Gonchar, Fiz. Elem. Chastits At. Yadra **26**, 932 (1995) [Phys. Part. Nucl. **26** (4), 394 (1995)].
28. P. Fröebrich and R. Lipperheide, *Theory of Nuclear Reactions. Studies in Nuclear Physics* (Oxford Univ. Press, Oxford, 1996), Vol. 18.
29. H. J. Krappe, in *Proceedings of International Workshop on Dynamical Aspects of Nuclear Fission, Smolenice 1991*, Ed. by J. Kristiak and B. I. Pustylnik (Joint Institute for Nuclear Research, Dubna, 1992), p. 51.
30. H. Hofmann, Phys. Rep. **284**, 137 (1997).
31. F. A. Ivanyuk, H. Hofmann, V. V. Pashkevich, and S. Yamaji, Phys. Rev. C **55**, 1730 (1997).
32. G. D. Adeev, Fiz. Elem. Chastits At. Yadra **23**, 1572 (1992) [Sov. J. Part. Nucl. **23**, 684 (1992)].
33. M. Brack, J. Damgaard, A. S. Jensen, *et al.*, Rev. Mod. Phys. **44**, 320 (1972).
34. S. Trentalange, S. E. Koonin, and A. J. Sierk, Phys. Rev. C **22**, 1159 (1980).
35. V. S. Stavinskii, N. S. Rabotnov, and A. A. Seregin, Yad. Fiz. **7**, 1051 (1968) [Sov. J. Nucl. Phys. **7**, 631 (1968)].
36. G. D. Adeev, I. A. Gamalya, and P. A. Cherdantsev, Phys. Lett. B **35**, 125 (1971); G. D. Adeev and P. A. Cherdantsev, Phys. Lett. B **39**, 485 (1972).
37. V. V. Pashkevich, Nucl. Phys. A **169**, 275 (1971); **477**, 1 (1988); Xu. Shuwei and W. Zhengda, Phys. Rev. C **37**, 1968 (1988).
38. J. Maruhn and W. Greiner, Z. Phys. A **251**, 431 (1972).
39. K. Sato *et al.*, Z. Phys. A **288**, 383 (1978).
40. H. C. Pauli, Phys. Rep. **7**, 35 (1973).
41. V. M. Strutinsky, N. Ya. Lyashchenko, and N. A. Popov, Nucl. Phys. A. **46**, 639 (1963).
42. V. M. Strutinskii, N. Ya. Lyashchenko, and N. A. Popov, Zh. Eksp. Teor. Fiz. **43**, 584 (1962) [Sov. Phys. JETP **16**, 418 (1963)].
43. O. I. Serdyuk, G. D. Adeev, I. I. Gonchar, *et al.*, Yad. Fiz. **46**, 710 (1987) [Sov. J. Nucl. Phys. **46**, 399 (1987)].

44. J. Bao, Y. Zhuo, and X. Wu, Z. Phys. A **352**, 321 (1995).
45. G. I. Kosenko, I. I. Gonchar, O. I. Serdyuk, and N. I. Pischasov, Yad. Fiz. **55**, 920 (1992) [Sov. J. Nucl. Phys. **55**, 514 (1992)].
46. G. I. Kosenko, I. G. Kolyari, and G. D. Adeev, Yad. Fiz. **60**, 404 (1997) [Phys. At. Nucl. **60**, 334 (1997)].
47. I. I. Gonchar, A. E. Gettinger, L. V. Gur'yan, and V. Vagner, Yad. Fiz. **63**, 1778 (2000) [Phys. At. Nucl. **63**, 1688 (2000)].
48. G. I. Kosenko, D. V. Vanin, and G. D. Adeev, Yad. Fiz. **61**, 2142 (1998) [Phys. At. Nucl. **61**, 2031 (1998)].
49. A. Mamdouh, J. M. Pearson, M. Rayet, and F. Tondeur, Nucl. Phys. A **644**, 389 (1998).
50. V. M. Strutinskii, Zh. Eksp. Teor. Fiz. **45**, 1900 (1963) [Sov. Phys. JETP **18**, 1305 (1964)].
51. J. N. P. Lawrence, Phys. Rev. B **139**, 1277 (1965); R. W. Hasse and W. D. Myers, *Geometrical Relationships of Macroscopic Nuclear Physics* (Springer, Berlin, 1988).
52. T. Ledergerber, H. C. Pauli, and Y. Yariv, Nucl. Phys. A **280**, 241 (1977).
53. H. J. Krappe, in *Proceedings of XIII Meeting on Physics of Nuclear Fission in the Memory of Professor Smirenkin G.N, Obninsk, 1995,* Ed. by B. D. Kuzminov (SSCRF-IPPE, Obninsk, 1995), p. 134.
54. J. Marten and P. Fröbrich, Nucl. Phys. A **545**, 854 (1992).
55. P. Fröbrich, Phys. Rep. **116**, 337 (1984).
56. A. S. Iljinov, M. V. Kazarnovsky, and E. Ya. Paryev, *Intermediate Energy Nuclear Physics* (CRC, Boca Raton, 1994).
57. U. Brosa, S. Grossmann, and A. Müller, Phys. Rep. **194**, 167 (1990).
58. K. T. R. Davies, R. A. Managan, J. R. Nix, and A. J. Sierk, Phys. Rev. C **16**, 1890 (1977).
59. A. I. Startsev, in *Proceedings of XIII Meeting on Physics of Nuclear Fission in the Memory of Professor Smirenkin G.N., Obninsk 1995*, Ed. by B. D. Kuzminov (SSCRF-IPPE, Obninsk, 1995), p. 94.
60. G. D. Adeev and P. N. Nadtochii, Yad. Fiz. **66**, 647 (2003) [Phys. At. Nucl. **66**, 618 (2003)].
61. K. T. R. Davies, A. J. Sierk, and J. R. Nix, Phys. Rev. C **13**, 2385 (1976).
62. H. J. Krappe, Phys. Rev. C **59**, 2640 (1999).
63. H. J. Krappe, J. R. Nix, and A. J. Sierk, Phys. Rev. C **20**, 992 (1979).
64. A. J. Sierk, Phys. Rev. C **33**, 2039 (1986).
65. M. Brack, C. Guet, and H. B. Häkansson, Phys. Rep. **123**, 275 (1985).
66. C. Guet, E. Strumberger, and M. Brack, Phys. Lett. B **205**, 427 (1988).
67. A. V. Karpov, P. N. Nadtochy, E. C. Ryabov, and G. D. Adeev, J. Phys. G.: Nucl. Phys **29**, 2365 (2003).
68. R. Balian and C. Bloch, Ann. Phys. (N.Y.) **60**, 401 (1970).
69. A. V. Ignatyuk, M. G. Itkis, V. N. Okolovich, *et al.*, Yad. Fiz. **21**, 1185 (1975) [Sov. J. Nucl. Phys. **21**, 612 (1975)].
70. A. V. Ignatyuk, *Statistical Properties of Excited Atomic Nuclei* (Energoatomizdat, Moscow, 1983) [in Russian].
71. J. Töke and W. J. Swiatecki, Nucl. Phys. A **372**, 141 (1981).
72. W. D. Myers and W. J. Swiatecki, Ark. Phys. **36**, 343 (1967).
73. A. E. S. Green, *Nuclear Physics* (McGraw-Hill, New York, 1955), pp. 185, 250.
74. J. Bartel, K. Mahboub, J. Richert, and K. Pomorski, Z. Phys. A **354**, 59 (1996).
75. B. Nerlo-Pomorska, K. Pomorski, J. Bartel, and K. Dietrich, Phys. Rev. C **66**, 051302(R) (2002).
76. I. Kelson, Phys. Rev. B **136**, 1667 (1964).
77. V. S. Stavinskii, N. S. Rabotnov, and A. A. Seregin, Yad. Fiz. **9**, 779 (1969) [Sov. J. Nucl. Phys. **9**, 454 (1969)].
78. A. A. Seregin, Yad. Fiz. **55**, 2639 (1992) [Sov. J. Nucl. Phys. **55**, 1473 (1992)].
79. F. A. Ivanyuk, V. M. Kolomietz, and A. G. Magner, Phys. Rev. C **52**, 678 (1995); S. V. Radionov, F. A. Ivanyuk, V. M. Kolomietz, and A. G. Magner, Yad. Fiz. **65**, 856 (2002) [Phys. At. Nucl. **65**, 824 (2002)].
80. H. Jeffreys and B. Swirles, *Methods of Mathematical Physics*, 3rd ed. (Cambridge Univ. Press, Cambridge, 1966; Mir, Moscow, 1969).
81. S. L. Sobolev, *Equations of Mathematical Physics* (Nauka, Moscow, 1996) [in Russian].
82. J. Blocki, Y. Boneh, J. R. Nix, *et al.*, Ann. Phys. (N.Y.) **113**, 330 (1978).
83. J. Randrup and W. J. Świątecki, Ann. Phys. (N.Y.) **125**, 193 (1980).
84. A. J. Sierk and J. R. Nix, Phys. Rev. C **21**, 982 (1980).
85. J. J. Griffin and M. Dvorzecka, Nucl. Phys. A **455**, 61 (1986).
86. J. R. Nix and A. J. Sierk, in *Proceedings of the International School-Seminar on Heavy Ion Physics, Dubna, 1986,* Ed. by M. I. Zarubina and E. V. Ivashkevich (Joint Institute for Nuclear Research, Dubna, 1987), p. 453; in *Proceedings of the 6th Adriatic Conference on Nuclear Physics: Frontiers of Heavy Ion Physics, Dubrovnik, 1987*, Ed. by N. Cindro *et al.* (World Sci., Singapore, 1990), p. 333.
87. G. Abal, R. Donangelo, and C. O. Dorso, Phys. Rev. C **46**, 380 (1992).
88. W. J. Swiätecki, Phys. Scr. **24**, 113 (1981).
89. R. Donangelo and L. F. Canto, Nucl. Phys. A **451**, 349 (1986).
90. S. E. Koonin, R. L. Hatch, and J. Randrup, Nucl. Phys. A **283**, 87 (1977).
91. S. E. Koonin and J. Randrup, Nucl. Phys. A **289**, 475 (1977).
92. J. Blocki, J.-J. Shi, and W. J. Swiatecki, Nucl. Phys. A **554**, 387 (1993).

93. S. Pal and T. Mukhopadhyay, Phys. Rev. C **54**, 1333 (1996); T. Mukhopadhyay and S. Pal, Phys. Rev. C **56**, 296 (1997); S. Pal and T. Mukhopadhyay, Phys. Rev. C **57**, 210 (1998).
94. G. Chauduri and S. Pal, Phys. Rev. C **63**, 064603 (2001); Phys. Rev. C **65**, 054612 (2002); Eur. Phys. J. A **18**, 9 (2003).
95. J. Blocki, F. Brut, T. Srokowski, and W. J. Swiatecki, Nucl. Phys. A **545**, 511 (1992).
96. G. Wegmann, Phys. Lett. B **50**, 327 (1974).
97. P. Paul and M. Thoennessen, Ann. Rev. Part Nucl. Sci. **44**, 65 (1994).
98. D. J. Hofman, B. B. Back, I. Dioszegi, *et al.*, Phys. Rev. Lett. **72**, 470 (1994).
99. G. Rudolf and A. Kelic, Nucl. Phys. A **679**, 251 (2001).
100. S. Yamaji, H. Hofmann, and R. Samhammer, Nucl. Phys. A **475**, 487 (1988).
101. H. Hofmann, S. Yamaji, and A. S. Jensen, Phys. Lett. B **286**, 1 (1992).
102. V. Weisskopf, Phys. Rev. **52**, 295 (1937).
103. P. Fong, *Statistical Theory of Nuclear Fisson* (Gordon and Breach, New York, 1969).
104. Dzh. O. N'yuton, Fiz. Elem. Chastits At. Yadra **21**, 821 (1990) [Sov. J. Nucl. Phys. **21**, 349 (1990)]; Yu. Ts. Oganessian and Yu. A. Lazarev, "Heavy Ions and Nuclear Fission," in *Treatise on Heavy Ion Science*, Ed. by D. A. Bromley (Plenum, New York, 1985), Vol. 4, p. 1.
105. N. D. Mavlitov, P. Fröbrich, and I. I. Gontchar, Z. Phys. A **342**, 195 (1992).
106. A. S. Iljinov, M. V. Mebel, N. Bianchi, *et al.*, Nucl. Phys. A **543**, 517 (1992).
107. A. R. Junghans, M. de Jong, H.-G. Clerc, *et al.*, Nucl. Phys. A **629**, 635 (1998).
108. S. Björnholm, A. Bohr, and B. R. Mottelson, in *Proceedings of the Third IAEA Symposium on Physics and Chemistry of Fission, Rochester, 1973* (IAEA, Vienna, 1974).
109. G. Hansen and A. S. Jensen, Nucl. Phys. A **406**, 236 (1983).
110. G. La Rana *et al.*, Phys. Rev. C **35**, 373 (1987).
111. I. I. Gontchar, P. Fröebrich, and N. I. Pischasov, Phys. Rev. C **47**, 2228 (1993).
112. H. Hofmann and F. A. Ivanyuk, Phys. Rev. Lett. **90**, 132701 (2003); H. Hofmann and A. G. Magner, Phys. Rev. C **68**, 014606 (2003).
113. J. D. Bao and Y. Jia, Phys. Rev. C **69**, 027607 (2004).
114. J. R. Nix and W. J. Swiatecki, Nucl. Phys. **71**, 1 (1965); J. R. Nix, Nucl. Phys. A **130**, 241 (1969).
115. M. G. Itkis and A. Ya. Rusanov, Fiz. Elem. Chastits At. Yadra **29**, 389 (1998) [Phys. Part. Nucl. **29**, 160 (1998)].
116. M. G. Itkis, S. M. Luk'yanov, V. N. Okolovich, *et al.*, Yad. Fiz. **52**, 23 (1990) [Sov. J. Nucl. Phys. **52**, 15 (1990)].
117. M. G. Itkis, V. N. Okolovich, and G. N. Smirenkin, Nucl. Phys. A **502**, 243 (1989).
118. G.-R. Tillack, Phys. Lett. B **278**, 403 (1992).
119. T. Wada, N. Carjan, and Y. Abe, Nucl. Phys. A **538**, 283 (1992).
120. G.-R. Tillack, R. Reif, A. Schülke, *et al.*, Phys. Lett. B **296**, 296 (1992).
121. V. E. Viola, K. Kwiatkowski, and M. Walker, Phys. Rev. C **31**, 1550 (1985).
122. P. N. Nadtochii, A. V. Karpov, and G. D. Adeev, Yad. Fiz. **65**, 832 (2002) [Phys. At. Nucl. **65**, 799 (2002)].
123. P. N. Nadtochy, A. V. Karpov, D. V. Vanin, and G. D. Addev, Yad. Fiz. **66**, 1240 (2003) [Phys. At. Nucl. **66**, 1203 (2003)].
124. J. R. Nix, Nucl. Phys. A **130**, 241 (1969).
125. N. Carjan, A. J. Sierk, and J. R. Nix, Nucl. Phys. A **452**, 381 (1986).
126. S. V. Zhdanov, M. G. Itkis, S. M. Mul'gin, *et al.*, Yad. Fiz. **55**, 3169 (1992) [Sov. J. Nucl. Phys. **55**, 1766 (1992)].
127. S. V. Zhdanov, M. G. Itkis, S. M. Mul'gin, *et al.*, Yad. Fiz. **56**, 55 (1993) [Phys. At. Nucl. **56**, 175 (1993)].
128. A. V. Karpov, Candidate's Dissertation (Omsk. Gos. Univ., Omsk, 2002).
129. D. V. Vanin, P. N. Nadtochii, G. I. Kosenko, and G. D. Adeev, Yad. Fiz. **63**, 1957 (2000) [Phys. At. Nucl. **63**, 1865 (2000)].
130. T. Wada, Y. Abe, and N. Carjan, Phys. Rev. Lett. **70**, 3538 (1993).
131. M. G. Itkis, V. N. Okolovich, A. Ya. Rusanov, and G. N. Smirenkin, Fiz. Elem. Chastits At. Yadra **19**, 701 (1988) [Sov. J. Part. Nucl. **19**, 301 (1988)].
132. M. G. Itkis, V. N. Okolovich, A. Ya. Rusanov, and G. N. Smirenkin, Yad. Fiz. **41**, 1109 (1985) [Sov. J. Nucl. Phys. **41**, 709 (1985)].
133. D. Hilscher and H. Rossner, Ann. Phys. (Paris) **17**, 471 (1992).
134. D. J. Hinde, D. Hilscher, H. Rossner, *et al.*, Phys. Rev. C **45**, 1229 (1992).
135. D. Hilscher, I. I. Gontchar, and H. Rossner, Yad. Fiz. **57**, 1255 (1994) [Phys. At. Nucl. **57**, 1187 (1994)].
136. H. Rossner, D. Hilscher, D. J. Hinde, *et al.*, Phys. Rev. C **40**, 2629 (1989).
137. J. Wilczynski, K. Siwek-Wilczynska, and H. W. Wilschut, Phys. Rev. C **54**, 325 (1996).
138. I. I. Gontchar, N. A. Ponomorenko, V. V. Turkin, and L. A. Litnevsky, Nucl. Phys. A **734**, 229 (2004).
139. P. Fröbrich, I. I. Gontchar, and N. D. Mavlitov, Nucl. Phys. A **556**, 281 (1993).
140. A. K. Dhara, K. Krishan, C. Bhattacharya, and S. Bhattacharya, Phys. Rev. C **57**, 2453 (1996).
141. V. A. Rubchenya and S. G. Yavshits, Yad. Fiz. **40**, 649 (1984) [Sov. J. Nucl. Phys. **40**, 416 (1984)]; V. A. Rubshenya and S. G. Yavshits, Z. Phys. A **329**, 217 (1988).
142. G. I. Kosenko, D. V. Vanin, and G. D. Adeev, Yad. Fiz. **61**, 416 (1998) [Phys. At. Nucl. **61**, 356 (1998)].

143. M. G. Itkis, Yu. A. Muzychka, Yu. Ts. Oganesyan, *et al.*, Yad. Fiz. **58**, 2140 (1995) [Phys. At. Nucl. **58**, 2026 (1995)].

144. E. M. Kozulin, A. Ya. Rusanov, and G. N. Smirenkin, Yad. Fiz. **56**, 37 (1993) [Phys. At. Nucl. **56**, 166 (1993)].

145. P. Möller and J. R. Nix, Atom. Data Nucl. Data Tables **39**, 213 (1988).

146. D. J. Hinde, H. Ogata, M. Tanaka, *et al.*, Phys. Rev. C **39**, 2268 (1989).

147. P. Fröbrich and I. I. Gontchar, Nucl. Phys. A **563**, 326 (1993).

148. K. Hagino, N. Rowley, and A. T. Kruppa, Comput. Phys. Commun. **123**, 143 (1999).

149. V. I. Zagrebaev and V. V. Samarin, Yad. Fiz. **67**, 1488 (2004) [Phys. At. Nucl. **67**, 1462 (2004)].

150. G. D. Adeev, I. I. Gonchar, V. V. Pashkevich, and O. I. Serdyuk, Yad. Fiz. **50**, 1242 (1989) [Sov. J. Nucl. Phys. **50**, 774 (1989)].

151. A. V. Karpov and G. D. Adeev, Yad. Fiz. **65** (9), 1637 (2002) [Phys. At. Nucl. **65**, 1596 (2002)].

152. R. K. Gupta, W. Scheid, and W. Greiner, Phys. Rev. Lett. **35**, 353 (1975); Gupta, R.K., Fiz. Elem. Chastits At. Yadra **8**, 717 (1977) [Sov. J. Part. Nucl. **8**, 289 (1977)].

153. U. Brosa and H. J. Krappe, Nukleonika **24**, 389 (1979).

154. L. D. Landau and E. M. Lifshitz, *Statistical Physics*, (Nauka, Moscow, 1976; Pergamon, Oxford, 1980).

155. R. W. Hasse, Pramana **11**, 441 (1978).

156. M. G. Mustafa, H. W. Schmitt, and U. Mosel, Nucl. Phys. A **178**, 9 (1971).

157. R. Vandenbosch and J. R. Huizenga, *Nuclear Fission* (Academic, New York, 1973).

158. E. K. Hyde, I. Perlman, and G. T. Seaborg, *The Nuclear Properties of the Heavy Elements*, Vol. 5: *Nuclear Fission* (Prentice-Hall, Englewood Cliffs, N.J., 1964; Atomizdat, Moscow, 1969).

159. D. C. Hofman and M. H. Hofman, Ann. Rev. Nucl. Sci. **24**, 151 (1974).

160. G. D. Adeev, L. A. Filipenko, and P. A. Cherdantsev, Yad. Fiz. **23**, 30 (1976) [Sov. J. Nucl. Phys. **23**, 15 (1976)]; G. D. Adeev and T. Dossing, Phys. Lett. B **66**, 11 (1977).

161. G. D. Adeev, I. I. Gonchar, and L. A. Marchenko, Yad. Fiz. **42**, 42 (1985) [Sov. J. Nucl. Phys. **42**, 25 (1985)].

162. I. Aizenberg and V. Grainer, *Nucleus Model. One-Particle and Collective Phenomena* (Atomizdat, Moscow, 1975) [in Russian].

163. W. E. Undegraff and D. S. Onley, Nucl. Phys. A **161**, 191 (1971).

164. U. Brosa and H. J. Krappe, Z. Phys. A **287**, 65 (1978); U. Brosa and D. H. E. Gross, Z. Phys. A **294**, 217 (1980).

165. E. S. Hernandez, W. D. Myers, J. Randrup, and B. Remaud, Nucl. Phys. A **361**, 483 (1981).

166. B. Martschew and K. Pomorski, Acta Phys. Pol. B **13**, 747 (1982).

167. R. W. Hasse and P. Nerud, J. Phys. G.: Nucl. Phys **2**, L101 (1976).

168. B. Bush and Y. Alhassid, Nucl. Phys. A **531**, 27 (1991).

169. W. D. Myers, W. J. Swiatecki, T. Kodama, *et al.*, Phys. Rev. C **15**, 2032 (1977).

170. F. Gönnenwein, in *Nuclear Fission Process*, Ed. by C. Wagemans (CRC, Boca Raton, 1991).

171. H.-G. Clerc, W. Lang, H. Wohlfarth, *et al.*, in *Proceedings of the Forth Symposium on the Physics and Chemistry of Fission, Jülich, 1979*, Ed. by J. W. Weil (IAEA, Vienna, 1980), Vol. 2, p. 65; W. Lang, H. -G. Clerc, H. Wohlfarth, *et al.*, Nucl. Phys. A **345**, 34 (1980).

172. H. Hofmann, A. S. Jensen, and F. Scheuter, in *Proceedings of the 12th International Symposium on Nuclear Physics, Gaussing, 1982*, Report NISSN 0138-2950, p. 96.

173. S. Ayik, E. Suraud, J. Stryjewski, and M. Belkacem, Z. Phys. A **337**, 413 (1990).

174. M. Asghar, Z. Phys. A **296**, 79 (1980).

175. J. A. McHugh and M. C. Michel, Phys. Rev **172**, 1160 (1968).

176. R. Wieczorec, R. W. Hasse, and G. Süssmann, in *Proceedings of the Third Symposium on the Physics and Chemistry of Fission, Rochester, 1973*, Ed. by F. M. Markhof (IAEA, Vienna, 1974), Vol. 97, p. 1.

177. L. C. Vaz and J. M. Alexander, Phys. Rep. **97**, 1 (1983).

178. A. Bohr, in *Proceedings of the United Nations International Conference on the Peaceful Uses of Atomic Energy, Geneva, 1955* (United Nations, New York, 1956), Vol. 2, p. 151.

179. I. Halpern and V. M. Strutinsky, in *Proceedings of the Second United Nations International Conference on the Peaceful Uses of Atomic Energy, Geneva, 1957* (United Nations, Geneva, 1958).

180. S. Kailas, Phys. Rep. **284**, 381 (1997).

181. D. J. Hinde, A. C. Berriman, M. Dasgupta, *et al.*, Phys. Rev. C **60**, 054602 (1999).

182. P. D. Bond, Phys. Rev. Lett. **52**, 414 (1984); Phys. Rev. C **32**, 471 (1985); Phys. Rev. C **32**, 483 (1985).

183. H. H. Rossner, J. R. Huizenga, and W. U. Schröder, Phys. Rev. Lett. **53**, 38 (1984); Phys. Rev. **33**, 560 (1986).

184. B. John and S. K. Kataria, Phys. Rev. **57**, 1337 (1998).

185. R. Freifelder, M. Prakash, and J. M. Alexander, Phys. Rep. **133**, 315 (1986).

186. B. B. Back, R. R. Betts, J. E. Gindler, *et al.*, Phys. Rev. C **32**, 195 (1985).

187. S. Björnholm and W. J. Swiatecki, Nucl. Phys. A **391**, 471 (1982).

188. C. Ngo, Prog. Part. Nucl. Phys. **16**, 139 (1986).

189. W. Q. Shen, J. Albinski, A. Gobbi, *et al.*, Phys. Rev. C **36**, 115 (1987).

190. J. Töke, R. Bock, DaiGuang-Xi, *et al.*, Nucl. Phys. A **440**, 327 (1985).

191. C. Lebrun, F. Hanappe, J. F. Lecolley, *et al.*, Nucl. Phys. A **321**, 207 (1979).

192. B. Borderie, M. Berlanger, D. Gardes, *et al.*, Z. Phys. **299**, 263 (1981).

193. V. S. Ramamurthy and S. S. Kapoor, Phys. Rev. Lett. **54**, 178 (1985).

194. R. Vandenbosch, T. Murakami, C.-C. Sahm, *et al.*, Phys. Rev. Lett. **56**, 1234 (1986); T. Murakami, C.-C. Sahm, R. Vandenbosch, *et al.*, Phys. Rev. C **34**, 1353 (1986).

195. D. J. Hinde, M. Dasgupta, J. R. Leigh, *et al.*, Phys. Rev. C **53**, 1290 (1996).

196. H. Rossner, D. J. Hinde, J. R. Leigh, *et al.*, Phys. Rev. C **45**, 719 (1992).

197. A. Saxena, S. Kailas, A. Karnik, and S. S. Kapoor, Phys. Rev. C **47**, 403 (1993).

198. S. Kailas and P. Singh, Z. Phys. A **347**, 267 (1994).

199. P. Fröbrich and H. Rossner, Z. Phys. A **349**, 99 (1994).

200. A. M. Samant, S. Kailas, A. Chatterjee, *et al.*, Eur. Phys. J. A **7**, 59 (2000).

201. V. A. Drozdov, D. O. Eremenko, O. V. Fotina, *et al.*, Nucl. Phys. A **734**, 225 (2004).

202. M. A. Butler, S. S. Datta, R. T. de Souza, *et al.*, Phys. Rev. C **34**, 2016 (1986).

203. V. A. Drozdov, D. O. Eremenko, S. Yu. Platonov, *et al.*, Yad. Fiz. **64**, 221 (2001) [Phys. At. Nucl. **64**, 179 (2001)].

204. R. G. Thomas, R. K. Choudhury, A. K. Mohanty, *et al.*, Phys. Rev. C **67**, 041601 (2003).

205. T. Dössing and J. Randrup, Nucl. Phys. A **433**, 215 (1985).

206. Z. Liu, H. Zhang, J. Xu, *et al.*, Phys. Lett. B **353**, 173 (1995); H. Zhang, Z. Liu, J. Xu, *et al.*, J. Nucl. Radiochem. Sci. **3**, 99 (2002).

207. K. Pomorski, J. Bartel, J. Richert, and K. Dietrich, Nucl. Phys. A **605**, 87 (1996).